Atmos. Chem. Phys. Discuss., 8, 11149–11292, 2008
www.atmos-chem-phys-discuss.net/8/11149/2008/

Atmospheric Chemistry and Physics Discussions

Tropical cyclogenesis in a tropical wave critical layer: easterly waves

T. J. Dunkerton[1,2], **M. T. Montgomery**[2], **and Z. Wang**[2]

[1]NorthWest Research Associates, Bellevue WA, USA
[2]Naval Postgraduate School, Monterey CA, USA

Received: 3 January 2008 – Accepted: 28 January 2008 – Published: 9 June 2008

Correspondence to: T. J. Dunkerton (tim@nwra.com)

Published by Copernicus Publications on behalf of the European Geosciences Union.

Abstract

The development of tropical depressions within tropical waves over the Atlantic and eastern Pacific is usually preceded by a "surface low along the wave" as if to suggest a hybrid wave-vortex structure in which flow streamlines not only undulate with the waves, but form a closed circulation in the lower troposphere surrounding the low. This structure, equatorward of the easterly jet axis, resembles the familiar critical layer of waves in shear flow, a flow configuration which arguably provides the simplest conceptual framework for tropical cyclogenesis resulting from tropical waves, their interaction with the mean flow, and with diabatic processes associated with deep moist convection. The critical layer represents a sweet spot for tropical cyclogenesis in which a proto-vortex may form and grow within its parent wave. A common location for storm development within the critical layer is given by the intersection of the wave's critical latitude and trough axis, with analyzed vorticity centroid nearby. The wave and vortex live together for a time, and initially propagate at approximately the same speed. In most cases this coupled propagation continues for a few days after a tropical depression is identified. For easterly waves, as the name suggests, the propagation is westward. It is shown that in order to visualize optimally this "marsupial paradigm" one should view the flow streamlines, or stream function, in a frame of reference translating horizontally with the phase propagation of the parent wave. This translation requires an appropriate "gauge" that renders translating streamlines and isopleths of translating stream function approximately equivalent to flow trajectories. In the translating frame, the closed circulation is stationary, and a dividing streamline effectively separates air within the critical layer from air outside. The critical layer equatorward of the easterly jet axis is important to tropical cyclogenesis because it provides (i) a region of cyclonic vorticity and weak deformation by the resolved flow, (ii) containment of moisture entrained by the gyre and/or lofted by deep convection therein, (iii) confinement of mesoscale vortex aggregation, (iv) a predominantly convective type of heating profile, and (v) maintenance or enhancement of the parent wave until the vortex becomes

a self-sustaining entity and emerges from the wave as a tropical depression. These ideas are formulated in three new hypotheses describing the flow kinematics and dynamics, moist thermodynamics and wave/vortex interactions comprising the marsupial paradigm. A survey of 55 named tropical storms in 1998–2001 reveals that actual critical layers sometimes resemble the ideal east-west train of cat's eyes, but are usually less regular, with one or more recirculation regions in the translating frame. It is shown that a "wave gauge" given by the translation speed of the parent wave is the appropriate choice, as well, for isolated proto-vortices carried by the wave. Some implications for entrainment/containment of vorticity and moisture in the cat's eye are discussed from this perspective, based on the observational survey.

1 Introduction

The genesis of tropical cyclones, hurricanes and typhoons is one of the most important unsolved problems in dynamical meteorology (Emanuel, 2005) and climate (Gore, 2006). As for why the problem remains unsolved, after decades of research, it is unfortunately true that in situ observations of genesis are mostly lacking over remote tropical oceans, that field campaigns are too few while operational efforts generally target mature storms, that critically important processes and their multi-scale interactions are challenging to model and observe. Nature in some cases provides little advance warning of these storms and prediction of genesis beyond 48 h is generally too uncertain to be useful. Funding and technological resources are needed to remedy these deficiencies, to the extent they can be remedied, but – to be honest – it is unlikely that fundamental progress will be made without a quantum leap in theoretical understanding as well. As will be demonstrated in this paper and the sequels, available observations on the synoptic scale need to be analyzed in a manner that is consistent with the Lagrangian nature of tropical cyclogenesis. As a moist diabatic vortex, the tropical cyclone, through its lifecycle from genesis to intensification, represents a coherent interaction between potential vorticity (PV) and moist entropy, both of which are

adiabatic invariants, i.e., material properties of a conservative flow. In the earliest stage of genesis, the fluid motion is mostly horizontal and quasi-conservative, punctuated by intermittent deep convection, a strongly diabatic and turbulent process, to be sure. In order to fully appreciate the transport of PV and moist entropy by the flow, their interaction with one another, the impacts of deep convective transport and protection of the proto-vortex from hostile influences requires, among other things, an understanding of material surfaces and Lagrangian boundaries in the horizontal plane. This viewpoint, although used subconsciously by forecasters[1], is invisible to researchers working with standard meteorological products in an Eulerian framework. For tropical cyclogenesis it is necessary to understand the morphology of Lagrangian transport, and it is desir-

[1]The elusive but sometimes exposed "low cloud swirls" and other stratiform cloud or water vapor anomalies represent *Lagrangian entities* to the extent that these features are passively advected by the flow. Feature-tracking provides instantaneous Eulerian winds (e.g., Velden et al., 1997, 2005), while animation of the accumulated horizontal displacement of cloud or water vapor anomalies (away from their sources and sinks: viz., deep convection and other regions of moist ascent) effectively provides a Lagrangian view. So the geostationary imagery are helpful in this respect, whereas standard meteorological charts in the Earth-relative frame and infrequent snapshots from polar orbiting satellites are not. Surface winds from scatterometry are indisputably valuable, but it is unnecessary for such images (as from QuikSCAT or ASCAT) to display a closed circulation in order for a closed circulation to exist in a Lagrangian sense (see Appendix A). A morphed animation of total precipitable water from microwave imagery (beginning in 2006) is proving very helpful for analysis and prediction of moist tropical waves in the lower troposphere (http://cimss.ssec.wisc.edu/tropic2). Forecasters are now using this product to detect, locate and extrapolate the position of wave troughs. By viewing the sequence of frames, the viewer obtains a sense of Lagrangian horizontal motions weighted by the vertical profile of moisture, together with the impacts of convective moistening and horizontal entrainment. Extraction of quantitative Lagrangian information from sequential imagery is far from trivial, but a worthwhile goal. When it comes to closed circulations in propagating waves, the difference between Eulerian and Lagrangian flow is critically important, as will become clear in this paper. Forecasters deal simultaneously with both viewpoints in their arsenal of observations, yet (to our knowledge) without a clear differentiation between them.

able to know whether, and how, suitable information for this purpose can be obtained from an intelligent manipulation of Eulerian data.

Compounding the problem is that multiple pathways to genesis exist. Four plausible pathways identify one or more of the following as key ingredients: (i) tropical waves, (ii) monsoon troughs, (iii) extratropical disturbances and (iv) topographic flows[2]. For each pathway we can imagine a theoretical paradigm that provides conceptual stepping stones along the path. In tropical waves, a sweet spot for development evidently exists along the wave, associated with a region of low pressure in the lower troposphere. Having such a sweet spot does not guarantee genesis, of course, because other environmental factors also play in important role in deciding whether or not a storm may form. Many individual wave-troughs occur in a single hurricane season but only a fraction – approximately 10% in the eastern and central Atlantic (Simpson et al., 1968) – contribute to the formation of a tropical depression-strength vortex (defined hereafter as "genesis"). Among those disturbances that produce depressions almost all have a "surface low along the wave" in the forecaster's familiar parlance. Few are thought to have a mid-level cyclonic vortex without the surface signature, a negligible fraction of the original wave count. Mid-level vortices without a discernable surface circulation are indeed observed in the tropics, increasingly so as satellite remote sensing improves, and in regions of frequent deep convection, such as the ITCZ. Some have suggested that tropical mesoscale convective systems produce mesoscale convective vortices initially without a cyclonic circulation near the surface (Bister and Emanuel,

[2]The third and fourth pathways do not represent TC genesis in the pure sense of the term. The third pathway is not entirely tropical, and the fourth pathway is not entirely oceanic. Therefore if one is interested in pure tropical cyclogenesis, the problem reduces to (i) a *tropical-wave* pathway and (ii) a *geophysical turbulence* pathway. The latter may be subdivided into *quasi-2-D* and *rotating 3-D-convective* pathways to highlight the role of horizontal circulations and deep moist convection in a rotating environment, respectively. One can then appreciate the fuzzy nature of the classification scheme, as waves and turbulence generally coexist (Lilly, 1983; McWilliams, 1984; McIntyre, 2003). Genesis is not a question about which of these mechanisms is acting in a particular situation, but rather, how much of each, and how they interact.

1997; Ritchie and Holland, 1997) and that this may be a reason why only a small fraction of disturbances become tropical depressions (E. Zipser, personal communication; Harr and Elsberry, 1996). It will be shown here that for storms originating in tropical waves, the synoptic wave itself plays a vital role in the near-surface circulation. In our proposed tropical-wave scenario the relevant theoretical paradigm is the formation of a closed proto-vortex within the wave in the *lower* troposphere and subsequent eddy shedding whereby the vortex, energized further by deep convective heating, becomes detached from the wave and begins to control its own destiny. In what follows we refer to this sequence of events as the *marsupial paradigm*. Central to our presentation of the marsupial paradigm is a rudimentary understanding of the Lagrangian flow and its dynamical and thermodynamical properties in the neighborhood of the developing storm.

Our series on TC genesis, of which this paper is the first, addresses the tropical wave pathway and variations thereof (easterly wave propagation, tropical depression disturbances, instability of the ITCZ, and trapped equatorial modes) and the ability of these disturbances to create a closed gyre or "pouch" and subsequently within the pouch, a proto-vortex or "embryo" favorable for hurricane formation[3]. We are concerned also with the monsoon trough pathway (e.g., Harr and Elsberry, 1996; Simpson et al., 1997). But for TC genesis, environmental conditions in the monsoon trough (McBride and Zehr, 1981) appear favorable over a larger area, providing a diverse set of flow configurations in the lower troposphere (shear line, confluence, gyre; Ritchie

[3]The "embryo" is borrowed from other authors (Emanuel, 1993, 2007; M06) so to be consistent with the marsupial paradigm we might refer to the proto-vortex as a "joey". Extending the analogy, a female joey provides a second "baby pouch" for convective organization at smaller scales. Observations sometimes suggest multiple low-level circulation centers in systems that are still becoming organized. Forecasters and scientists alike want to know more about these proto-structures; e.g., their role in Ekman pumping and convective triggering. For now and the foreseeable future, the LT in developing environments remains a mysterious realm frequently obscured by patches of deep convective cloud and stratiform anvils. Geostationary microwave technology, needed to penetrate this environment continuously, is ∼20 years away.

and Holland, 1999) and making the role of tropical waves (with their sweet spot) more challenging to ascertain – although precursor waves of one type or another can be seen in many of these cases. Genesis by spontaneous aggregation (now a popular subject of research: e.g., Emanuel and Nolan, 2004; Nolan et al., 2006; Held, 2007; Borth, 2007; Schecter and Dunkerton, 2007, 2008[4]) may be regarded as a limiting case of the monsoon trough pathway in which no particular region is favored, but conditions are rendered more favorable, e.g., by cranking up the underlying SST. In the real world, spontaneous aggregation is likely nature's last resort[5]. En route to storm formation, the tropical atmosphere almost always provides a sweet spot or more extensive region favorable to genesis. We believe this fact has important implications for the study of tropical cyclogenesis in climate change. Whereas an increase of SST is expected naively to increase the intensity of mature tropical cyclones, the effects of climate change on tropical cyclogenesis will be felt more immediately by modulation of *local environments that are already favorable for genesis in the current climate*; effects that will be manifested, for instance, in a changed morphology of tropical waves, monsoon troughs and their favorable regions, as well as changes of large-scale circulation and ITCZ that affect storm tracks and ambient environment (Frank and Young, 2007; Vecchi and Soden, 2007; Ventham and Wang, 2007; Vimont and Kossin, 2007; Wing et al., 2007) possibly directing storms into regions of warmer SST[6].

[4]Schecter, D. A. and Dunkerton, T. J.: Hurricane formation in diabatic Ekman turbulence, Q. J. Roy. Meteor. Soc., submitted, 2008.

[5]As also the case in the "real world" of 3-km simulations performed on Earth Simulator (Matsuno, 2006, 2007) which indicate a crucial role of tropical easterly waves for TC genesis in the present climate.

[6]The role of off-equatorial circulations as a link between *hurricanes* and *climate change* is recognized in the papers cited. These two topics, along with *air quality*, are the most important in contemporary atmospheric science and their relationship deserves scrutiny at a dynamical, not merely statistical, level of understanding. The effect of climate change on hurricanes is not simply to increase the potential intensity (PI) of a hurricane and thereby increase hurricane intensity ipso facto. Leaving aside frontier matters concerning the formulation and accuracy of

In the study by Montgomery et al. (2006b; hereafter M06) the TC genesis problem was posed as the metamorphosis of a mid-level mesoscale convective vortex (MCV)

current PI theory (Emanuel, 2005; Montgomery et al., 2006a; Smith et al., 2007) actual hurricane intensities form a continuous probability distribution function (PDF) bounded above by a limiting intensity. SST is but one of several factors explaining the PDF and its variation (DeMaria et al., 2005) so it is not merely a question of how PI varies with SST. Nor can we ignore the number of storms reaching tropical depression status and how this might change in the future; the percentage of developers versus wave-troughs is small in the present climate – nowhere near saturation. Though little attention has been given to the issue, perhaps for lack of evidence, the *number of storms generated* is an integral part of the climate-change question. We consider it unlikely that nature will somehow produce more storms of high intensity without producing more storms at all levels of intensity (although this point was disputed by Held, 2007, based on results obtained with a simple GCM; see also Benggston et al., 2007; Knutson, 2007; Knutson et al., 2007, 2008). Two reasons underlying this "common sense" viewpoint are (i) it is likely for physical *and* statistical reasons that if more storms are generated, the number of intense storms will increase; and (ii) regions of genesis and highest intensity are (for the most part) well separated spatially, thanks to the zonal motion of storms, restricting the ability of intense storms to suppress new storms in their wake. In this respect, storms of the real world differ from those of a horizontally periodic geometry, in which the suppression can be significant. Genesis depends on the spatial pattern as well as amplitude of underlying SST, and most SST variations are contained in coupled patterns of atmosphere-ocean variability that oscillate with time. Even if one could somehow isolate a simple-pattern/secular-trend of SST variation and study its effect on the general circulation (as done by Magnusdottir, 2001, for the NH winter season) the effect on genesis is non-trivial. Consider the following: a horizontally uniform change in underlying SST, e.g., the simplest of all changes in an altered world, would be superposed on the existing distribution that is a strong function of latitude (responsible, among other things, for the latitude of the ITCZ). The impact of a uniform change is therefore also a function of latitude owing to the strong nonlinearity of the Clausius-Clapeyron relation. With changes in SST and ITCZ come changes in the tropical waves and instabilities (hence, hurricanes) that depend, directly or indirectly, on the structure and stability of circulations associated with the ITCZ. Such changes impact the hydrological cycle on a global scale, with regional consequences (IPCC, 2007).

with weak cyclonic circulation at the ocean surface into a self sustaining warm-core tropical depression vortex. The initial MCV embryo was assumed to be a by-product (e.g., Emanuel, 1993; Bister and Emanuel, 1997; Raymond et al., 1998) of one or more mesoscale convective systems (MCSs) that form and evolve within the trough region of an African easterly wave in the Atlantic basin, or monsoon trough in the western Pacific basin. The hurricane embryo problem was examined using a non-hydrostatic full physics cloud model (RAMS) at 2 km and 3 km horizontal grid spacing for realistic sea surface temperatures (SSTs) and thermodynamic vertical profiles of moist static energy within the low pressure region of a tropical disturbance. M06 obtained new insight on convective and mesoscale processes operating within such an idealized pre-genesis environment. In the absence of hostile influences, such as strong vertical wind shear or dry air intrusions, M06's high-resolution simulations demonstrated an upscale cloud/mesoscale mechanism for building the incipient tropical storm vortex. This mechanism was shown to operate on realistic time scales and, equally important, to *precede* the wind-speed/evaporation feedback believed to govern the intensification of an already formed tropical depression strength surface vortex (Rotunno and Emanuel, 1987; Emanuel, 1989).

Within the convectively unstable and cyclonic-vorticity rich environment of the initial MCV embryo, horizontally small-scale warm-core updrafts possessing intense cyclonic vorticity in their cores ("vortical hot towers"; VHTs) emerged spontaneously as the dominant coherent structures. As often observed in real developing storms, the most prominent VHTs were triggered at a finite radius from the proto-circulation center, consistent with the expected radial dependence of Ekman-like pumping in a geophysical vortex boundary layer (Smith, 1968; Eliassen and Lystad, 1977). Concurrent with this low-level vortex spin-up process are localized downdrafts and spreading gust front boundaries. Minima in equivalent potential temperature occur in association with localized downdrafts that import low equivalent potential temperature from the middle troposphere into the surface boundary layer. Unlike warm season continental or maritime mesoscale convection that often favors linear propagating structures (squall lines), the

spreading gust front boundaries were confined laterally, to some extent, by the near-surface cyclonic circulation and the low-level inflow generated by the mean latent heating in the vortex towers. M06 showed that this low level inflow was reasonably well captured by the axisymmetric Eliassen balanced circulation (Shapiro and Willoughby, 1982; Wirth and Dunkerton, 2006) driven primarily by the mean (temporally and azimuthally averaged) heating rate of the vortex towers. The rotational confinement of these gust front boundaries appears important for *sustained* deep convective activity within the MCV embryo and surface spin-up.

The numerical experiments of M06 demonstrated a plausible vortex assembly process that can occur within a local MCV environment possessing a small but finite amplitude cyclonic surface circulation. Yet to be answered, however, is how this embryonic circulation is created in the first place and whether it can survive long enough in realistic environments (e.g., with vertical shear or dry air intrusions) to enable the transition to a self-sustaining warm-core vortex. Because of the strongly helical nature of the VHTs, another aspect not yet investigated concerns the role of helicity (Moffat, 1969) in stabilizing the upscale cascade (Lilly, 1986a, b; Herring and McWilliams, 1989; Weisman and Rotunno, 2000; Kurgansky, 2006), a process that occurs generically within the MCV, parent synoptic wave, or monsoon trough. A major objective of our series on TC genesis is to explain the generation and maintenance of the hurricane embryo within its parent synoptic-scale wave or monsoon trough environment. Another is to advance beyond M06 and understand more completely the role of moist convective (helical) turbulence that operates within the embryo.

The first three papers of the series are concerned exclusively with the tropical wave pathway to genesis, a pathway that involves

(i) the familiar easterly waves of the Atlantic (e.g., Carlson, 1969; Burpee, 1974; Reed et al., 1977; Thorncroft and Hodges, 2001) and Pacific basins (Chang et al., 1970; Raymond et al., 1998);

(ii) the less familiar (mixed) Rossby-gravity waves of the central and far eastern Pacific Oceans (Hendon and Liebmann, 1991; Dunkerton, 1993; Dunkerton and Baldwin,

1995; Molinari, 2004); and

(iii) the so-called "tropical depression" disturbances of the western tropical Pacific (Liebmann and Hendon, 1990; Lau and Lau, 1990; Takayabu and Nitta, 1993; Dunkerton, 1993; Dunkerton and Baldwin, 1995; Wheeler and Kiladis, 1999; Sobel and Bretherton, 1999; Wheeler et al., 2000).

These wave types comprise a range of ground-based periods from 2.5–9 days. Slower waves such as moist Kelvin waves (Dunkerton and Crum, 1995; Wheeler et al., 2000), equatorial Rossby waves (Molinari et al., 2006) and Madden-Julian oscillation (Maloney and Hartmann, 2000) also modulate tropical cyclogenesis and TD disturbances (Maloney and Dickinson, 2003). Tropical waves in the 2.5–9 day band may originate from convective coupling (Hayashi, 1970; Lindzen, 1974), lateral forcing (Wilson and Mak, 1984; Randel, 1992; Zhang and Webster, 1992), hydrodynamic instability of the ITCZ (Hack et al., 1989; Schubert et al., 1991; Wang and Magnusdottir, 2005, 2006) or fully developed TCs and their associated "Rossby wave wakes" (McWilliams and Flierl, 1979; Montgomery et al., 1999; Ritchie and Holland, 1999). The role of equatorially trapped waves in tropical cyclogenesis requires knowledge of their latitudinal structure and cross-equatorial symmetry, while that of TD disturbances requires that we account for a significant meridional component of propagation. These wave types are examined separately. Excluded from consideration in our first three papers are

(iv) tropical storms originating from extratropical upper-level PV anomalies in a moist baroclinic environment (Montgomery and Farrell, 1993) and/or stalled frontal zones in the subtropics (the so-called *tropical transition* pathway: e.g., Davis and Bosart, 2004) and topographic effects (Zehnder et al., 1999; Chang et al., 2003).

Neither of these pathways (TT or topography) are purely tropical *and* oceanic. We note, however, that a key ingredient of TC genesis (formation of a closed recirculation region) also pertains to many examples of subtropical development in the central and western Pacific that we have encountered in our preliminary survey. A fourth paper will examine these cases.

Local instability of the ITCZ as a direct pathway to genesis is possible, although more commonly, the waves produced thereby propagate downstream into regions more favorable to genesis: e.g., with warmer water or larger absolute vorticity. Storms generally do not originate within the locus of ITCZ convection, but cause a significant poleward distortion or obliteration of the ambient ITCZ (Dunkerton, 2006). Significant storms in the historical record affecting coastal regions of the southeastern US and Gulf states have originated from within tropical waves in the eastern and central Atlantic (the "main development region" or MDR) notwithstanding a few spectacular storms originating in the western Atlantic monsoon trough and the Gulf of Mexico. Owing to their quasi-monochromatic nature and relative simplicity, we begin our genesis study in the context of Atlantic easterly waves (Kiladis et al., 2006; Hall et al., 2006) and their eastern Pacific extension, although the papers to follow will extend this line of research to other types of tropical waves and instabilities relevant to other ocean basins (Bessafi and Wheeler, 2006; Frank and Roundy, 2006; Molinari et al., 2006). To isolate key elements of the various sub-types of tropical-wave cyclogenesis cited above, we begin our discussion in Sect. 2 with a conceptually simple scenario in which hydrodynamically neutral waves emerge from an unstable source region upstream, propagate westward into the domain of interest, and create regions favorable for genesis; regions which may, in turn, maintain or enhance the neutral waves via convective heating against dissipation while propagating across the basin. This scenario is most relevant to the Atlantic sector, wherein easterly waves generated by moist hydrodynamic instability over Africa (that is, over land, where TCs cannot form owing to surface friction and absence of sustained latent heat fluxes) or by other means propagate westward into a warm ocean, providing seedlings for possible genesis. It is also relevant to other basins, such as the eastern tropical Pacific or mid-Atlantic, but we recognize that in such regions (over ocean, where surface friction is relatively small and latent heat is plentiful), instability of the ITCZ may sometimes lead directly to genesis (Hack et al., 1989; Schubert et al., 1991; Wang and Magnusdottir, 2005, 2006). Some of the events occurring in our time period of interest may belong to this category; they are more akin

to instability than the neutral wave propagation imagined in our ideal scenario.

Section 2 outlines the basic theoretical concepts underlying our analysis, while Sect. 3 describes the datasets used and analysis methods. Section 4 illustrates the morphology of waves and convection in relation to the mean flow and embedded critical layers, in various representative cases, while Sect. 5 affords a closer look at the 3-D structure and evolution of the critical layer, closed material contours, and diabatic vortices in one of these cases. The time period of interest encompasses the peak hurricane seasons of 1998–2001 the years when the two primary datasets used in our study (ERA-40 and TRMM) overlap.

2 Conceptual fundamentals of the marsupial paradigm

Whether hydrodynamic instability plays an immediate role in TC genesis (as sometimes observed in the eastern Pacific and mid-Atlantic) or excites waves that later become instrumental in genesis downstream (as in the African/Atlantic sector) there is a fluid dynamical situation arising in both scenarios that is relevant to genesis for reasons to be enumerated below. This situation involves the familiar *critical layer* of waves in shear flow, wherein parcels experience irreversible displacements and trapping about the wave's *critical level*, viz., the location where mean flow and wave phase speeds are equal[7]. In the so-called "cat's-eye" of the critical layer where trapping of parcels takes place, the fluid becomes isolated from its surroundings on either side of the critical layer as parcels outside this layer are advected in opposite directions. The Lagrangian mean flow is asymptotically discontinuous on the edges of the critical layer and its horizontal profile consists of three components: two are in opposite directions outside the layer on either side, while the middle is stationary with respect to the cat's-eye pattern (Andrews and McIntyre, 1978). The latter is equivalent to a statement that the Lagrangian mean

[7]The critical level is generally a *surface* in three dimensions, but the word *level* or *line* has been used in the literature to represent any of these dimensions, e.g., latitude or altitude.

flow in the critical layer is zero in a frame of reference moving with the critical layer itself: i.e., at the phase speed of the wave. Here we take the Lagrangian mean to be a spatial average in the direction of the Eulerian mean flow, which we also assume to be the direction of wave propagation, as shown in Fig. 1. This simplifying assumption will motivate our discussion of the role of the critical layer in TC genesis, but it should be borne in mind we are always concerned with the actual direction of wave propagation in relation to the mean flow, regardless of their azimuthal directions, and will define the critical level generally in terms of the locus of points where the wave intrinsic frequency goes to zero.

2.1 An idealized easterly jet

To fix ideas, consider a zonally uniform easterly jet at tropical latitudes off the equator. For simplicity, assume a barotropic jet structure as depicted in Fig. 2. There is cyclonic shear equatorward of the easterly jet maximum, and anticyclonic shear poleward of the jet maximum. Equatorward of the jet core the cyclonic shear vorticity is enhanced by the planetary vorticity, while poleward of the jet core, the anticyclonic shear vorticity and the planetary vorticity tend to compensate. The absolute vorticity poleward of the jet core is therefore weakly negative or close to zero. Since the meridional gradient of the absolute vorticity changes sign both poleward and equatorward of the jet core, the mean flow satisfies one of the necessary (Rayleigh) conditions for barotropic instability. It has been long recognized in the literature that the African easterly jet is unstable to disturbances which might be described as a moist barotropic instability or mixed barotropic/baroclinic instability[8]. More recently it has been suggested that

[8]The critical level plays a central role in such instabilities, enabling phase-locking of counter-propagating Rossby waves in adjacent regions of opposite meridional PV gradient (Hoskins et al., 1985; Heifetz et al., 1999) or, in linear ray theory, as the locus of wave overreflection (Lindzen and Tung, 1978; Lindzen et al., 1983). Either of these mechanisms leads to wave growth if certain conditions are met. One of these conditions is the existence of a critical level within the zone of reversed PV gradient.

synoptic-scale instability by itself may be too slow to explain easterly wave disturbances in the African sector (Hall et al., 2006). In either event, if we assume that the locus of wave instability or excitation lies upstream, i.e., that the region of interest is stable with respect to exponential growth, it may be inferred that the phase speed of waves generated upstream lies *outside* the range of mean flow speeds in the region of reversed PV gradient, as depicted in Fig. 2. The alternative – a critical level *within* the zone of reversed gradient – would likely cause unstable growth. For an easterly jet north of the equator, the critical level (hereafter, critical "latitude") therefore resides a bit south of the southernmost latitude where the effective beta is zero.

A second critical latitude also exists north of the jet axis, north of the northernmost latitude where the effective beta is zero again, on the opposite side of the jet. As already noted, however, the shear vorticity of the mean flow is *cyclonic* south of the jet and *anticyclonic* to the north. If a critical layer of finite width were to form at the location of either critical latitude as a result of wave propagation into the region of interest, the sense of rotation in the cat's eye would be the same as that of the mean relative vorticity. For TC genesis we are obviously interested in cyclonic rather than anticyclonic vorticity in the lower troposphere and therefore regard the southern, not northern, critical layer as a possible locus of TC formation. Moreover, we should not imagine that actual wave disturbances and the critical layers they generate are exactly symmetric or antisymmetric about the jet axis[9]. For the case of an idealized unstable easterly jet, Thorncroft and Hoskins (1994a) showed that the most unstable wave disturbance south of the jet is centered equatorward of the southernmost latitude where the effective beta changes sign. Their maximum amplitude is near the critical latitude, in accord with our propagating-wave scenario (as might be expected from consideration of linear parcel displacements, which maximize at the critical latitude or level). This asymmetry of wave amplitude about the axis of the jet, favoring the southern or equatorward

[9]The north-south symmetry of the basic state about the jet axis is broken by mean absolute vorticity, which is asymmetric, and a meridional gradient of moisture, if one exists. Further asymmetry may arise from wave sources upstream.

side, also emphasizes the cyclonic critical layer at the expense of the anticyclonic one. For the case of an exponentially stable jet flow, discrete neutral or slowly decaying "quasi-mode" wave packets (Reasor and Montgomery, 2001; Schecter et al., 2002) – stimulated, perhaps, by mesoscale processes within the trough region of the wave envelope (Berry and Thorncroft, 2005; Hall et al., 2006) – should possess similar phase speed and wave maxima characteristics as their unstable counterparts. Our immediate concern is not with wave sources, which lie outside the scope of this paper, but with downstream propagation of neutral waves on an easterly jet as depicted in Fig. 2. We simply consider the consequences of wave propagation for TC genesis.

2.2 Three new hypotheses regarding the wave-vortex hybrid

One of these consequences was noted above: cyclonic roll-up of mean vorticity in the southern critical layer favors TC genesis in the sense that this "synoptic" concentration[10] of cyclonic vorticity provides a seedling for amplification by mesoscale convective processes (M06) which, as we now argue, might occur preferentially in the critical layer. As shown in Fig. 1, the longitudinal center of the cat's eye corresponds to the trough of the wave, a region favorable for deep moist convection in observations. Concentration of cyclonic vorticity by (i) critical layer development on the synoptic scale, and (ii) convective enhancement and up-scale aggregation of cyclonic vorticity on the mesoscale, is a plausible outcome of the neutral wave propagation depicted in Fig. 2. Important to this sequence of events is that the easterly jet is located in the lower, not middle, troposphere and that *lower* tropospheric vorticity is immediately amplified. In real life the waves and their effects are more complicated than in our ideal scenario; actual waves are local, episodic, and vary from one trough to the next. This variability, in fact, is so important to genesis that NHC/TPC forecasters (for better or worse) in

[10]Following convention, 2.5–9 day moist tropical waves relevant to TC genesis occur on *synoptic* spatial scales (2000–8000 km or so) while cat's eyes and closed recirculation regions develop at meso-α (200–2000 km). Proto-vortex development occurs at meso-β (20–200 km), involving deep moist convection at meso-γ (2–20 km).

their online discussion regard each individual trough as a "tropical wave". We do not expect a uniform train of cyclonic cat's eyes but rather a zonally nonuniform pattern of cyclonic eddies – eddies which, in some sense, are "shed" from the AEJ as a result of the wave propagation and interaction with the mean flow at the critical latitude. Our first hypothesis concerning the role of the tropical wave critical layer in TC genesis is therefore

H1. Proto-vortex cyclonic eddies instrumental in TC formation are intimately associated with the parent wave's critical latitude in the *lower troposphere*. The critical layer, formed as a result of the wave's finite-amplitude interaction with its own critical latitude, is a region of cyclonic rotation and weak straining/shearing deformation in which synoptic and mesoscale anomalies move together and amplify on a nearly zero relative mean flow. This multi-scale interaction provides a dynamical pathway to "bottom-up" development of the proto-vortex from below.

The notion of bottom-up development (Halverson et al., 2007) is advanced as a counterpart to the more familiar "top-down" scenario advocated by Bister and Emanuel (1997) and Ritchie and Holland (1997), respectively; see also Ritchie et al. (2003). (This perspective was in vogue when M06 was written. The two scenarios are not mutually exclusive, as emphasized by Halverson et al., 2007) The top-down pathway begins with a recognition of the "top-heavy" nature of moist convective heating profiles in the presence of combined convective and stratiform precipitation processes. A top-heavy heating profile in a rotating environment necessarily leads to the conclusion that cyclonic vorticity is first concentrated in the *middle* troposphere by the induced vertical profile of convergence and must therefore find a way subsequently to burrow downward into the lower troposphere in order to provide the surface development needed for warm-core TC genesis. This pathway is inefficient (Tory and Montgomery, 2006) and invites a more direct route to genesis if one could be found, particularly in sectors where development is marginal to begin with. Observational findings of the top-down school were biased to the western Pacific warm pool, but in light of forecaster's experience we are inclined to regard this pathway as largely irrelevant to the Atlantic and eastern

Pacific sectors outside the ITCZ[11]. The genesis of depressions in this region of the world is almost always associated with a surface low along the wave (see Reasor et al., 2005, for a case study); examples of mid-level cyclonic vortices in developing tropical systems, without a corresponding cyclonic signature near the surface, are evidently rare. Bottom-up development is inextricably linked to column moistening, which favors convective over stratiform heating as the leading contribution to the vertical heating profile. Column moistening, in turn, is naturally favored in a cyclonic critical layer. Our next hypothesis expands on this theme:

H2. The critical layer of the parent wave provides a set of quasi-closed material contours inside of which air is repeatedly moistened by convection, protected to some degree from lateral intrusion of dry air and impinging vertical shear, and (thanks to its location near the critical latitude) able to keep pace with the parent wave until the proto-vortex has strengthened into a self-maintaining entity.

This hypothesis is obviously a "coin with two sides," combining the notion of repeated column moistening with the equally important notion that the critical layer is protected from lateral entrainment of air – air which, in the case of the AEJ, is often dry and dusty if associated with the Saharan Air Layer in the lower free troposphere (Thorncroft et al., 2003; Dunion and Velden, 2004; Wong and Dessler, 2005). Hypothesis 2 also adds the notion of rapid vertical transport by convection to what otherwise has been, in our discussion thus far, a description of moist barotropic or shallow-water disturbances superposed on an easterly off-equatorial jet. These quasi-2-D disturbances organize the flow laterally via parcel displacement and create kinematic boundaries to lateral mixing; they also organize moist convection that lofts moisture into the free troposphere. Such convection, of course, is ubiquitous in the tropics and represents the primary mechanism of vertical transport that is rapid in comparison to other vertical motions such as isentropic up-glide along frontal zones and diabatic subsidence in the Hadley

[11] Although the single developing system (Guillermo) observed during TEXMEX in the eastern Pacific was originally thought to contain a low-level anticyclone in its earliest stage, subsequent analysis revealed a cyclonic circulation all the way to the surface (Raymond et al., 1998).

circulation caused by radiative cooling. In cases where the ambient cyclonic vorticity and moisture are positively correlated above the boundary layer, gyre formation is accompanied by horizontal entrainment of moisture, shortening the time required to approach column saturation. The "quasi" closure of streamlines or trajectories in H2 conveys two important caveats that will apply in all of the discussion to follow: (i) there is always a temporal development of the closure, as local wave amplitude grows and parcels become irreversibly entrained in the gyre, and (ii) there is often a nonzero divergent component of motion across the outer edge of a "closed" gyre as defined by the bounding contour of (nondivergent) stream function. We have greater confidence in the rotational component of motion than the divergent part, quantitatively speaking, and therefore attach greater significance to the appearance of a closed gyre in *stream function*. This is not to say that the analyzed divergent wind is unreliable; its sign usually agrees with the expected inflow (outflow) of mass in the lower (upper) troposphere in the neighborhood of a developing storm. At lower levels the divergent component of motion therefore contributes to the entrainment of vorticity and moisture as does the temporal development of the rotational component.

We do not limit deep convection to the critical layer (!) but advance the notion that convection within the critical layer is likely to create a vertical profile of diabatic heating with a lower- to mid-tropospheric maximum (Tory et al., 2006a, b, 2007) instead of the more widely observed "top-heavy" heating profile of canonical mesoscale convective systems (Houze, 1989; Mapes and Houze, 1995). The canonical profile represents a combination of convective and stratiform effects in which evaporative cooling in adjacent stratiform anvil regions offsets the low-level heating in deep convective cores. These two components superpose constructively in the mid- to upper troposphere. A top-heavy profile is important to the tropical general circulation (Hartmann et al., 1984), the mature phase of MJO (Lin et al., 2004) and generation of stratospheric gravity waves (D. Ortland, personal communication) but inimical to tropical cyclogenesis. The argument favoring a convective heating profile in TC genesis rests on an inference by Tory et al. (2007) that simulated storms initialized in actual environments (real-life

examples) are accompanied by such a profile when development ensues, and vice versa. This profile also can be inferred indirectly from the observed divergent circulation response (Sect. 5.3) or "directly" from TRMM retrievals in the re-circulating gyre (Dunkerton et al., 2008a[12]). The heating profile is tightly coupled to column moistening, and vice versa. As a region of re-circulating quasi-horizontal flow, the critical layer is bounded by closed material contours – a Lagrangian concept that provides a more general definition of the TC "pouch" in cases where a critical layer is not well defined or consists of a solitary shed vortex (as illustrated in Fig. 3; for further commentary on this figure see Sect. 3). The critical layer is expected to trap, that is, to *contain* moisture or moist entropy lofted by convection. The net heating and its vertical profile depends, in turn, on the amount of moisture lofted. Lower tropospheric air close to saturation is less likely to experience evaporative cooling, and the critical layer (for purely kinematic reasons) favors maintenance of nearly saturated conditions, especially if there exists a concentrated and sustained population of shallower "congestus" type convection in such a region, as suggested by some recent observations. For low-level mass convergence and vorticity amplification, a convective type of heating profile in the LT critical layer, without significant stratiform heating/cooling – or with less stratiform component than typical elsewhere – favors bottom-up development (M06) and concentration of upward mass flux in the lower troposphere (Raymond and Sessions, 2007). This is not to say that mid-level spin-up might not also occur in such cases, but to suggest that a low-level scenario is plausible in which the mid-level spin-up is unnecessary or of secondary importance to TC genesis[13]. This theoretical notion and its implications agree with forecaster's experience and their common observation of a "surface low along the

[12]Dunkerton, T. J., Lussier III, L. L., Montgomery, M. T., Wang, Z., and Tory, K. J.: Spatial and statistical distribution of convective and stratiform clouds in the gyre-pouch of incipient tropical cyclones, J. Geophys Res., in preparation, 2008a.

[13]ERA-40 data examined here suggest, for what it is worth, that mid-level convergence resolved by the analyses occurs in developing systems but is secondary to low-level convergence chronologically as the proto-vortex develops upward.

wave" in the development of a tropical depression.

Routine inspection of satellite water vapor imagery suggests that genesis is always associated with a relatively moist free troposphere as observed in the 6.7 micron band. There are many dynamical mechanisms governing the distribution of moisture; formation of a closed gyre in a tropical wave critical layer is but one of these. Quasi-stationary tropical features and extratropical disturbances also play a role. As already noted, the developing gyre entrains whatever moisture exists in the adjacent environment. Depending on whether or not this environment is dry or wet, the gyre itself may or may not be primarily responsible for self-moistening via deep moist convection within. Once moistened, it is desirable that the gyre (or some portion of it) remain so in order to facilitate TC formation. A key property of the proto-vortex required for subsequent development is its resilience to lateral intrusions of dry air which are common throughout the Atlantic during the hurricane season and at other times and places. The proto-vortex of a nascent TC, however, lacks a strong transport barrier (cf. McIntyre, 1989, 1993; Montgomery and Kallenbach, 1997; Bassom and Gilbert, 1999; Moulin and Flor, 2005), is vulnerable to dry-air intrusion and vertical shear (e.g., Reasor et al., 2004) and therefore needs help from the parent wave. The critical latitude within the low pressure region of the wave ensures weak relative flow between the wave-spawned proto-vortices and the local mean flow. This implies a reduction of dry air intrusions from outside (Tuleya and Kurihara, 1981) and a tendency for the heat released by cumulus convection to be retained in a relative frame of reference moving with the wave (Krishnamurti et al., 1994). The latter observation by Krishnamurti et al. (1994) is incorporated in a third hypothesis (below).

According to the marsupial paradigm, the critical layer guarantees some measure of protection from intrusion. But actual flow fields are transient and contain mesoscale finestructure, making the Lagrangian kinematics rather messy. A group of smaller vortices, e.g., will entrain the surrounding air more readily than a single larger vortex[14].

[14]Relevant to this discussion are two studies outside the atmospheric literature. The effects of entrainment on the buoyancy of rotating Bénard convection were discussed by Julien et

As for how these smaller vortices are created in the first place, there are essentially two possibilities: (i) *upscale aggregation* of mesoscale convective vortices associated with MCSs and/or VHTs, and (ii) eddy shedding that works its way to smaller scales via a *forward enstrophy cascade*, such as might be associated with wave breaking at the critical layer. Tropical cyclogenesis evidently represents a kind of process in which the inverse energy and forward enstrophy cascades (originating respectively from cloud system and synoptic scales) collide at some intermediate scale to form a diabatic vortex larger in horizontal scale than the vortices associated with individual cloud systems but substantially smaller in scale than the mother pouch created by the synoptic wave. This GFD aspect is perhaps the most fascinating and daunting of TC genesis; one that has not yet been fully explored (owing to limitations of horizontal resolution in observations or models) but may be advanced as a framework for understanding the multi-scale nature of the problem. Of relevance to H2 are the following considerations: (i) A group of *cloud-system vortices* at meso-γ may delay saturation of the column by a single master VHT, by mixing drier area within the pouch with moister air lofted by the VHT. (ii) A group of *mesoscale vortices* (resulting either from dry or moist processes at meso-β) may entrain drier air from outside the pouch via chaotic advection, partially offsetting the cumulative moistening of this area by persistent deep convection. Requirements for horizontal resolution differ depending on which of these mechanisms is more relevant; they are less stringent for chaotic advection than for upscale aggregation.

A third hypothesis is motivated by the fact that a critical layer is where local sources or sinks of momentum and entropy are amplified owing to the fact that parcels spend a considerably longer time in such regions compared to those outside the critical layer. In linear theory the net effect of fixed sources and sinks is inversely proportional to intrinsic frequency. This response, as noted by Held and Ting (1990), contrasts sharply with topographic wave excitation in which the response is proportional to the mean flow speed relative to the obstacle. It exists for purely kinematic reasons and is entirely

al. (1999). Organization of deep ocean convection by mesoscale eddies was examined by Legg et al. (1998).

independent of any presumed relationship between the wave and induced sources or sinks. In fact, since the wave trough is a preferred region for diabatic heating in tropical waves, and its longitude is at the center of the cat's eye (Fig. 1) the effect of diabatic heating due to deep moist convection is doubly amplified in the critical layer. (i) The heating is stronger here (owing primarily to mesoscale processes that favor convection in the trough) and (ii) its rectified effect on the wave is also stronger owing to the kinematics of parcel motion in the critical layer. Hence we propose that

H3. The parent wave is maintained and possibly enhanced by diabatically amplified eddies within the wave (proto-vortices on the mesoscale), a process favored in regions of small intrinsic phase speed.

This hypothesis, incidentally, agrees with the common observation that a tropical wave is considerably weakened or eliminated when the diabatic vortex leaves the pouch, having acquired its own identify and propagation characteristics independent of the parent wave. A typical scenario[15] is that a westward propagating wave carries its proto-vortex for a time, and if a depression ensues, the strengthened and enlarged vortex acquires a poleward component of propagation while its zonal component begins to slow relative to the phase speed of the parent wave. The parent wave continues its westward motion at more or less the same speed it originally had, but with severely diminished amplitude. In the Atlantic sector the wave speed is typically 4–6° per day westward, while the vortex speed is ∼2° per day west-northwestward. Individual cases may resemble this scenario or differ considerably; nevertheless, the basic description is robust.

The observed combination of westward moving tropical wave and incipient vortex evokes a "marsupial" paradigm for TC genesis, as charmingly illustrated in the popular online encyclopedia[16]. In contemporary jargon the marsupial paradigm combines elements of a *diabatic Rossby wave* (Wernli and Kenzelmann, 2006) with those of a

[15] Sometimes two or more visible proto-vortices are involved, a scenario may be more common in the western Pacific monsoon trough environment (Edson and Lander 2006).

[16] http://en.wikipedia.org/wiki/Marsupial

diabatic Rossby vortex (Moore and Montgomery, 2004, 2005, 2006). We suggest that the diabatically activated easterly wave is a hybrid wave/vortex structure, particularly in cases leading to formation of a tropical depression[17].

2.3 The role of vertical shear

A final element of the marsupial paradigm is the role of mean vertical shear in TC genesis. It is widely appreciated, especially by forecasters, that strong vertical shear is inimical to genesis. This fact is thought to account for the reduction of Atlantic hurricanes in warm ENSO events, as the eastern Pacific "warm pool" forces upper-level westerlies over the Caribbean (Gray, 1984a, b; Goldenberg and Shapiro, 1996). Although reasons suggest themselves, none are entirely convincing. Vertical shear in the UT is sometimes imagined to "ventilate" deep convection, but since the water content is very small at these altitudes, thermodynamic consequences arising from the phase change of water in the UT are likely to be very small as well. Similarly, the clear-sky radiative impacts of water vapor redistribution in the UT are probably too slow to affect genesis on time scales of 1–2 days, although their effects on longer time scales (e.g., MJO) may be significant. An indirect effect of vertical shear, if westerly, is an implied wave duct for quasi-stationary waves of midlatitude origin in the tropical upper troposphere. This dynamical opening between tropics and extratropics (Webster and Holton, 1982) is responsible for the appearance of synoptic-scale troughs sometimes observed to

[17] It is noteworthy that most tropical depressions become named storms, although the reasons are unclear. The cumulative experience of forecasters is evidently important in assigning depression status and in knowing at what formative level further development is virtually assured. This property of tropical depressions suggests a finite-amplitude instability for cyclogenesis above a certain threshold amplitude (e.g., Emanuel, 1989). As to what the relevant criteria are, they likely include some measure of tangential circulation strength and persistence of deep convection near the center. Such criteria, in any case, must be invariant under a Galilean transformation, that is, Lagrangian properties of the flow. A coordinate-dependent Eulerian measure (e.g., westerlies south of center, in the resting frame) is inadequate.

penetrate the tropics in the hurricane season. If this condition persists over a substantial part of the season it may ostensibly suppress genesis in some years (e.g., as in Atlantic 2006). The extratropical disturbances themselves may enhance genesis (TT pathway: Davis and Bosart, 2001; Hendricks et al., 2004; Hidalgo, 2007) or suppress it (via dry air intrusion or cyclonic flow aloft) so their net effect is not obvious and may be sensitive to the juxtaposition between upper- and lower-level disturbances (Davis and Bosart, 2004; Bosart, 2006).

It is well-known that vertical shear can be detrimental to hurricane intensification; the strongest and most circularly symmetric storms have little environmental shear or shear tendency. It is precarious, however, to take whatever mechanisms are responsible for the effects of shear on hurricane-strength vortices and assign them to the predepression stage. Whereas in a mature system, vertical shear interacts with a single large vortex, in genesis, the shear is interacting with one or more deep convecting elements, rotating or not (Frank and Johnson, 1969; Gentry et al., 1970; Hendricks et al., 2004; M06; Hendricks and Montgomery, 2006). At this stage, the effects of shear are more likely to be felt in *convective organization* rather than via the dynamics of a single large vortex. We speculate that strong shear in the genesis stage (i) may lead to linear rather than circular organization, and that (ii) longitudinally radiating gravity waves or density currents coupled to convection are more likely to be excited when the LT shear is strong (LeMone et al., 1998). Mechanisms of convective organization in vertical shear were studied by Corbosiero and Molinari (2002) and Molinari et al. (2004, 2006); interest in this aspect of the problem extends back to Ritchie and Holland (1997) and others. In any event, it is safe to say that vertical shear has important consequences for genesis and that none of its mechanisms in this stage are well understood. Forecasters' experience notwithstanding, we cannot be certain that genesis is optimized in exactly zero vertical shear. If it were, the fact that easterly-wave amplitudes maximize near the altitude of AEJ maximum (~600 hPa) would be convenient to the marsupial paradigm because wave + mean vertical shear is zero at this altitude, by definition. We suspect that the role of vertical shear in the marsupial paradigm, if any, is more subtle.

3 Data and methodology

3.1 Datasets and filters

The time period of interest encompasses the peak hurricane seasons (August and September) of 1998–2001, the years when the two primary datasets used in our study overlap: (i) ERA-40 6-hourly re-analyses were used to derive tropical wave disturbances. The data are available from NCAR at multiple pressure levels in T106 spectral resolution (~1.125×1.125°). Properties of ERA-40 and other analyses (e.g., circulations and physical fluxes) were recently evaluated and compared by Grotjahn (2007). A 2.5–9 day band-pass filter (Doblas-Reyes and Deque, 1998) was applied to the original data to extract wave propagation signals, while a 2.5-day low-pass filtered wind field was used to define the total flow (i.e., wave + mean fields). The response functions of the filters are shown in Fig. 4. It is important to note that the *band-pass* data supply information on wave packet structure and propagation, while the *total* flow (except for its high-frequency component) defines critical *layers*, stream function or streamlines, Lagrangian boundaries, and so forth. *Low-frequency* data (periods longer than 9 days) were used casually to estimate the mean flow and its critical *latitudes* as seen by the waves, not by individual parcels, which respond instead to the total flow sans high frequency component. (Parcel displacements are relatively insensitive to high frequency oscillations because they are inversely proportional to intrinsic frequency in linear theory.) (ii) Rainfall data from TRMM 3B42[18], available every 3 h and having a spatial resolution of 0.25×0.25°, were used in the study as a proxy for indicating deep moist convection. The level 3 gridded data are convenient for this purpose but occasionally suffer gaps in coverage owing to the satellite orbit. ERA-40 re-analyses and TRMM rainfall are independent data. The time period of ERA-40 used in this study (1998–2001) derives from Stream 1 (1987–2002) which incorporates satellite data from ATOVS, SSM/I and ERS, in addition to satellite data from VTPR, TOVS and cloud motion winds used

[18] http://daac.gsfc.nasa.gov/precipitation/TRMM_README/TRMM_3B42_readme.shtml

in Stream 3 (1972–1988). ERA-15 analyses for tropical waves were validated against rawinsonde data by Dunkerton and Baldwin (1995). We consider the ECMWF product to be optimum for synoptic-scale waves, particularly for the rotational component of horizontal winds in the lower and upper troposphere and (presumably) for the associated horizontal transports of moisture in the lower troposphere as analyzed in Stream 1. The divergent component is problematic in global analyses, whether from ECMWF or elsewhere, particularly when associated with deep convection. Vertical motions are not observed directly, but are obtained from a cumulus parameterization. Regions of deep convection, moreover, tend to concentrate vertical motions at the grid scale, making the resulting maximum upward velocities resolution-dependent (in such a way as to conserve approximately the vertical *flux* of mass, which is driven by the cumulus scheme). Convective precipitation from TRMM is a derived product which we employ here, not for quantitative precipitation, but for geolocation of convecting features relative to the ECMWF product. It was shown by Julian (1984) that a deep cloud proxy (OLR) is quantitatively correlated with upper tropospheric divergence. Needless to say, the TRMM geolocation (∼25 km) is accurate enough for the purpose at hand. We therefore regard the juxtaposition of ERA-40 and TRMM data to be a useful way of relating actual convection (an indicator of TD development) to actual waves, in the discussion to follow. Forecaster's best-track data provide a third independent source for genesis location and storm track although as we will argue, their identification of genesis *time* is sometimes delayed, perhaps owing to a conservative mindset[19]. Storm geolocation based on geostationary imagery is accurate to within the nominal 4 km pixel resolution at the sub-satellite point, superior to any of the other products used in our analysis. August and September were chosen because they represent the peak of the Atlantic hurricane season (Kimball and Mulekar, 2004).

[19]The best-track (retrospective) estimate of genesis time can be earlier than the initial (real-time) estimate by as much as 2 days. Our point is that, in some cases, even the best-track estimate is late, relative to the analyzed Lagrangian criteria.

3.2 Critical latitude definition

At the critical latitude or level, the intrinsic wave frequency goes to zero, or the mean flow and wave phase speeds are equal, $c = \boldsymbol{k}^* \cdot \boldsymbol{U}$, where $\boldsymbol{U}$ is the mean vector wind, and $\boldsymbol{k}^*$ is the unit vector in the wave propagation direction. For zonally propagating waves, this equation can be simplified, and the critical latitude is defined as the location where $c = U$, where U is the zonal component of mean vector wind.

3.3 Wave tracking algorithm

For quasi-monochromic easterly waves, a semi-automated wave tracking algorithm was developed in order to track the incident waves and to calculate their zonal phase speeds. The tracking algorithm is based on a Hovmöller diagram of 2.5–9 day band-pass meridional wind along the genesis latitude as identified in the best-track data. The exact choice of latitude is relatively unimportant, as nearby grid points give similar results. What is more important is the choice of genesis *time*, as noted below. Meridional wind anomalies are first located at the genesis time within ∼16.9° (15 grid points) on both sides of the genesis longitude (x), and are traced backward in time (t) from this point for 72 h. For such an anomaly to be acceptable it was required that the local maximum and minimum wind perturbations last at least 12 h. To identify and select the wind anomalies which are presumably most directly related to genesis, the time series of maximum and minimum perturbations nearest in x surrounding the genesis point were selected, and two phase speeds, c^+ and c^-, were derived based on a linear regression (t upon x) of the areas (in the x, t plane) of southerly and northerly wind perturbations, respectively, exceeding 1 ms^{-1} in absolute value. Two additional estimates of phase speed were likewise obtained for the period from −48 h to +24 h. This procedure for quantifying wave characteristics semi-automatically is similar to that shown in Fig. 11 of Dunkerton and Baldwin (1995). The algorithm as described above was found superior to an alternative (less stable) procedure following only the local maxima and minima of v' instead of the full anomaly area. If the phase speeds as

determined by the tracking algorithm were found to represent adequately the observed wave propagation, as indicated by the slopes of the meridional wind in the Hovmöller diagrams, their average (c_m) was used to define the incident wave phase speed at this altitude. Note that we do not mix adjacent altitudes for this purpose.

Our default was to select phase speeds based on a time period 72 h before genesis. It is preferable to exclude data after genesis because the incident waves are often changed by the tropical depression, and in many cases, new waves are excited (this secondary excitation will be described elsewhere). It should be noted, however, that best-track data do not necessarily indicate the exact moment of genesis because the time chosen for the first advisory is based on a human decision. The subjective nature of the operational procedure will become evident in one of the cases highlighted below (Chris 2000) wherein a depression-strength closed gyre in a Lagrangian view ∼30 h prior to "genesis" in the Eulerian frame. We allow, therefore, and only where necessary, for an alternative definition of phase speed based on data extending from 48 h before best-track genesis to 24 h after genesis. This alternative definition was adopted if and only if one or more of the default values of phase speed were unsuitable, as determined by a visual evaluation of the goodness of fit.

3.4 Vertical structure

Prior to genesis, easterly waves are generally confined to the lower troposphere at or below ∼500 hPa, with equivalent barotropic structure or slight vertical phase tilt. In some cases the phase tilt in the lower troposphere is observed to change with time during the storm development stage. It is instructive therefore to examine their propagation at two representative levels, 850 and 600 hPa. In most cases chosen for analysis, the same wave packet could be identified at both of these levels with similar propagation characteristics. Their averaged phase speeds on each level (c_m as defined above) generally differ – usually by a small amount, but sometimes significantly – so it is preferable to use the phase speed *at a particular level* when analyzing data at that level, rather than a *blend of phase speeds from different levels* to characterize the incident wave

propagation. The vertical structure of tropical waves participating in TC genesis is an interesting part of the marsupial story, and its evolution throughout the depth of the troposphere has several typical characteristics. The transition of wave structure from a trapped LT disturbance to deep "first baroclinic mode" structure immediately before genesis, subsequent vortex shedding in the lower troposphere and radiation of new waves (if any) have been identified using multi-dimensional visualization software from Pixotec. Some aspects of vertical structure are highlighted in Sect. 5.3.

3.5 Translating coordinate system

A key element in the analysis is a depiction of the horizontal flow in a frame of reference moving westward with the incident easterly wave. It should be clear from the opening remarks of Sect. 2 that the critical layer of a traveling wave becomes stationary when viewed in a coordinate system moving horizontally at the phase speed of the wave. The simplest case is a single wave with constant phase speed that is uniform in time and space; the translation speed is then a constant, and whatever unsteadiness remains in the wave field is attributable to amplitude evolution or structural change, rather than phase propagation. An interesting extension is to have a modest spread of frequencies about a central frequency, with the possibility of horizontal dispersion, forming a *wave packet* with group propagation differing from the phase propagation (for a general discussion of waves in fluids see Lighthill, 1978; for examples of group propagation in tropical waves see Liebmann and Hendon, 1990; Dunkerton and Baldwin, 1995). As long as the packet contains multiple phases in physical space, as implied by a *modest* spread in spectral space, it is appropriate to translate the coordinate system at the dominant phase speed, resulting in a non-zero zonal group propagation as viewed in the moving frame. Cases of TC genesis involving the intersection of two or more waves with substantially different phase speeds, as sometimes observed in the western tropical and subtropical Pacific, are outside the scope of this paper and will be discussed in the remaining papers of this series.

The purpose of the coordinate translation is to render the wave phases exactly sta-

tionary, to the extent this is possible, in order to minimize the temporal evolution of the flow pattern. In steady flow, streamlines are equivalent to trajectories (Holton, 2004). If the flow pattern consists of a steady mean flow and quasi-monochromatic wave, streamlines in a coordinate system moving at the phase speed of the wave may then be used as a surrogate for parcel trajectories. Allowing for a modest dispersion or other kind of amplitude evolution, the temporally evolving streamlines still provide a useful, albeit approximate, depiction of particle paths. For example, if a wave packet in the translating frame were to slowly creep eastward, forming new phases to the east while old ones decay to the west (resembling surface waves on water), parcel motions near the longitude of interest could be anticipated simply by waiting for the packet to arrive at that longitude. Whether or not such amplitude evolution occurs, the most important aspect of flow visualization (approximate equivalence of streamlines and trajectories) has been captured by translating the coordinate system at the phase speed of the wave.

Similar reasoning applies to an isolated region of enhanced vorticity, such as might be found at the peak amplitude of a wave packet, or in a single wave phase where diabatic amplification is exceptionally strong for whatever reason. Figure 3 illustrates streamlines of a point vortex, with cyclonic circulation, translating to the west (panel a), stationary (b) or translating to the east (c) relative to the fluid. For sake of illustration we are not concerned with *why* the vortex translates, other than to assume that some external agent is responsible for the translation or lack thereof (since left to itself, the vortex would be subject to magnus and advective forces). The vortex-induced flow is a function of $x-C_pt$ – assumed steady, that is, in a frame of reference moving with the vortex at its velocity $C_p\boldsymbol{i}$, while the imposed background flow velocity is $U_b\boldsymbol{i}$. The kinematic parcel displacement field is an intrinsic fluid-dynamical property and therefore depends on the difference C_p-U_b and not on the terms individually. The vortex can be imagined to induce parcel displacements which decrease in amplitude with increasing distance from the vortex center. When the vortex translates zonally in one direction or the other, parcels experience either a temporary influence of the passing vortex (far from center) or are permanently trapped in a vortex-induced gyre (close to

center). A bounding streamline separates these outer and inner regions, and a stagnation point exists where vortex and ambient flows cancel. The stagnation point defines the dividing streamline; it is also a *saddle point* of stream function in a horizontally non-divergent flow. This flow configuration is the point-vortex analogue of the discontinuous Lagrangian mean flow associated with a steady wave critical layer described in Sect. 2.1. What is missing[20] from the point-vortex flow in Fig. 3 (panel b in particular) that was present in the critical layer of Fig. 1 is the *latitudinal shear* (for constant shear, a parabolic y-profile of ambient stream function) that suppresses the meridional component of parcel displacement at large distances from the centerline. Owing to latitudinal shear, the cat's eye has a bounding streamline, whereas the stationary vortex in a resting flow does not. (A pattern similar to the cyclonic critical layer can be obtained by stacking the upper half of panel (c) on the lower half of panel (a) and sandwiching the center part of panel (b) in between, whereupon the stagnation points migrate to the x-axis. This type of pattern is shown in Fig. 2.10.1 of Pozrikidis, 1997.) Panels (a) and (c) demonstrate that trapping of parcels nevertheless can occur close to vortex center, without shear, because the nearby influence of the vortex (a singular point) is stronger than that of the vortex-relative background flow U_b. The streamline patterns in Fig. 3 are steady in a frame of reference moving with velocity $C_r\boldsymbol{i}$ matching that of the *vortex* in the same way that the streamline pattern of a nonlinear wave critical layer is steady in a frame of reference moving with the *wave* at its phase velocity $C_p\boldsymbol{i}$. In the properly translating frame, streamlines are therefore equivalent to trajectories.

We may also interpret the panels of Fig. 3 as depicting the instantaneous view of

[20]The critical layer and point vortex flow also differ in their vorticity distributions and the horizontal flow patterns induced (via PV inversion) by the distributions of vorticity. The steady asymptotic critical layer consists of a background *vorticity gradient* plus an east-west train of cat's eyes with homogenized PV within; the point vortex consists of an isolated "PV charge" and constant background *velocity* (the constant cannot be obtained by PV inversion). When the vorticity of the point vortex is distributed monotonically over a finite circular area, a dividing streamline exists if and only if the background velocity does not exceed the maximum wind at the edge of vorticity distribution.

streamlines obtained by observers in different reference frames moving at velocity $C_r\boldsymbol{i}$ – whether "translating properly" or not. Note that proper translation requires $C_r{=}C_p$ whereupon the vortex-induced flow becomes a function of $x_r{\equiv}x{-}C_rt{=}x{-}C_pt$ and the explicit dependence on t is eliminated. For example, the viewpoint of panel (c) is that obtained in the Earth-relative frame for a vortex moving to the west in this frame. It is important to note that only one of these viewpoints is "proper" for a particular U_b in the sense that streamlines are equivalent to trajectories only in the frame moving with the vortex, because the vortex-induced flow is steady in this frame only[21]. For a westward-moving vortex, the stationary (Earth-relative) frame gives a misleading picture of flow kinematics. The frame of reference is therefore important for an optimal view of horizontal transport. Figure 3 demonstrates, among other things, that the proper choice of reference frame is essential in order to understand flow kinematics in the neighborhood of the vortex (Ide et al., 2002; K. Ide, personal communication). The number of closed contours and the sense in which the vortex "connects" to the exterior flow (i.e., at the nearest saddle point, or "separatrix") obviously depend on the choice of frame. In the context of Atlantic easterly waves we would infer, for instance, that if environmental air were moist in one direction (e.g., near the ITCZ) but dry in another (e.g., near the equator), the orientation of the connection might significantly affect diabatic processes regulating the subsequent vortex development (H2). Entrainment of absolute vorticity would be affected similarly in the presence of a mean vorticity gradient (H1). Note also that the translating views of a point vortex introduce a north-south asymmetry, reminiscent of actual easterly wave troughs, that was not present in the idealized critical layer

[21] We should therefore qualify Emanuel's (2005, p. 127) recommendation that *streamlines* – owing to their non-uniqueness – not be used to locate a storm center because, as shown in the following sections, a translation speed determined by the parent wave provides a uniquely "proper" view of translating (possibly closed) streamlines that agree with parcel trajectories over a time span of a few days and provide an optimum view of the horizontal transport of adiabatic invariants. This comment applies equally to genesis and mature stages, although in a fully developed storm the time span is considerably shorter.

of a shear flow in Fig. 1. The asymmetric structure and existence of a separatrix on one or both sides of the cat's eye proves to be a characteristic feature in many observed genesis events, including western Pacific events (Edson and Lander, 2006).

3.6 Horizontal flow potentials and the choice of "gauge"

For synoptic flows, even in the tropics, the horizontally rotational part is much larger than the horizontally divergent part, with certain exceptions, so that in most situations, streamlines can be approximated by a stream function using the Helmholtz decomposition of the horizontal velocity vector $\boldsymbol{U}$. Crucial to our analysis in Sect. 4 is that the stream function and velocity potential, like any other potential, are known only up to a "gauge", i.e., a function whose horizontal Laplacian is zero and therefore makes no contribution to relative vorticity or divergence, which are Galilean invariant; that is, invariant to a uniform horizontal translation of the coordinate system, as contemplated here. Remarkably, there are an infinite number of stream functions (velocity potentials) that are perfectly consistent with the actual vorticity (divergence). For a quasi-monochromatic wave superposed on a steady mean flow, however, only one choice of translation speed, or gauge, makes sense: viz., that corresponding to a uniform horizontal translation at the phase speed of the wave[22]. By viewing streamlines in a frame of reference moving with the wave we are able to visualize the structure of recirculation regions, their formation and subsequent modification by diabatic vortices, together with the evolution of potential vorticity, moist entropy and other adiabatic invariants in such regions.

Depending on whether the reader has a degree in physics or meteorology (or both),

[22] A more general construction of Lagrangian boundaries from an Eulerian diagnostic is possible in 2-D and 3-D flows: for some recent ideas see Haller and Yuan (2000) and Green et al. (2006) respectively. Our simpler approach is likely to succeed for general flows only in a spatio-temporally local sense: a particular gauge may be optimum in one region but not in another, depending on the local wave spectrum. It nonetheless works well for the quasi-monochromatic cases considered here.

two analogies may be offered for clarification. One is from electromagnetism: the familiar equations of Maxwell, and the introduction of potential functions to calculate the remote influence of charges that evolve in time. The simplest choice of potential, or Coulomb gauge, is not the best choice for this equation set, because it seems to imply (at first sight) instantaneous action at a distance: given a certain charge at some point in space, the entire space is seemingly affected at once by the charge, and its time variation. This inference violates the theory of special relativity, overlooking the finite speed of electromagnetic wave propagation, on which the theory is based, as implied by the equations themselves[23]. An alternative potential, or *Lorenz* gauge – which is also *Lorentz* invariant[24] – correctly accounts for the finite propagation speed by building a temporal part into the definition of the potential function – the so-called "retarded potential". This choice of gauge is not obvious from the single equation for electric field induced by a charge, but turns out to be the preferred choice for the whole set of equations; in particular, for the radiation of electromagnetic waves from time-varying distributions of charge. In our case, the proper choice of gauge – a function that converts the stream function into something appropriate for visualizing the Lagrangian flow – is not obvious from a Helmholtz decomposition of the Eulerian flow in a resting frame. Its definition is motivated by the inclusion of a quasi-monochromatic wave in the problem, if the phase speed of this wave is known a priori.

A second and hopefully more familiar analogy is the popular "storm relative velocity"

[23]The inference is actually incorrect, and with extra effort (Brill and Goodman, 1967) the Coulomb gauge can be shown to be consistent with the theory of special relativity, a result more easily obtained if the Lorenz gauge is adopted in the first place. It is remarkable though overlooked initially that Einstein's theory of special relativity is contained in Maxwell's equations, insofar as the electric and magnetic permittivities, whose inverse product defines the speed of light squared, are constants independent of the choice of coordinate system, whether moving or not. The moral of this story, and the present one, is that the laws of physics do not change with a coordinate transformation, but some pathways to enlightenment are considerably shorter than others!

[24]http://en.wikipedia.org/wiki/Lorenz_gauge_condition

used in the depiction and interpretation of Doppler radar reflectivity from precipitation cells embedded in mesoscale (convective or stratiform) systems that move horizontally with the synoptic-scale flow. By translating to a coordinate system moving with the storm system as a whole, it is often possible to visualize mesocyclones (important for tornado genesis) and other circulation features associated with the system. The ingredients in this situation are analogous to those of our translating tropical wave critical layer: a storm system that is steered at more or less constant speed by the environmental flow, evolving slowly in a frame of reference moving horizontally with the flow. Use of storm relative velocity is a simple way to minimize the translational evolution of the *pattern* of precipitation cells while retaining the evolution of the cells within the translating pattern.

4 Morphology of waves and TC genesis in representative cases

Sixty-one named storms formed over the Atlantic (including the Caribbean Sea and Gulf of Mexico) and eastern Pacific during August and September 1998–2001, almost one-half of the 136 (named or numbered) tropical depressions that formed during all four hurricane seasons within these two ocean basins and their adjacent seas. Fifty-four (88%) of the 61 named storms fell into the "monochromic easterly wave" category based on the above-mentioned criteria (Sect. 4.3). In the remaining (seven) cases, either a multiple-wave interaction was involved, or easterly waves were not well-defined, and other processes (such as tropical transition at subtropical latitudes >25° N) played a dominant role in genesis. Among the 54 monochromic easterly wave cases, most storms formed from African easterly wave disturbances, while others formed from wave disturbances originating in the ITCZ over the eastern Pacific. Although the ITCZ disturbances may have a different morphology from African easterly waves, they still support the marsupial paradigm; genesis again is found to occur within the wave critical layer. In addition to the 54 cases from the Atlantic and eastern Pacific, we include a single case from the central Pacific just east of the Dateline (178° E), bringing the total number

of named storms in the monochromatic easterly wave category to 55.

4.1 Easterly wave/TC genesis events

The time of TC genesis, lat/lon location and accompanying wave phase speeds at 850 and 600 hPa of the 55 "monochromatic easterly wave" cases are summarized in Table 1, together with the uncertainty of the phase speed estimate, and various properties of the flow in which the proto-storm develops, such as (i) the area of the surrounding closed gyre in the translating frame, (ii) orientation of the nearest separatrix associated with the dividing streamline that bounds the gyre, and (iii) two measures of recirculation time about the proto-storm center, to be discussed in Sect. 5.1. For most of these quantities the median of the distribution is shown at the bottom of the table, together with one-half the inter-quartile range, representing the difference between the 75th and 25th percentiles, divided by two. Phase speeds are similar at the two levels, though slightly larger in median at 600 hPa. About 60% of the members have larger phase speed at 600 hPa, a bias that seems somewhat more prevalent in the eastern Pacific. A physical interpretation is that some of the waves in question are not *modes* with fixed vertical structure, but rather a sheared disturbance or quasi-mode with vertical alignment that varies with time. Clearly evident is that Earth-relative waves faster than $\sim 7\,\mathrm{ms}^{-1}$ westward are found only in the Atlantic sector, although slower waves are found here, too, similar to those of the eastern Pacific. The ratio of 600 to 850 hPa phase speed is generally larger for slower waves than for faster waves.

The uncertainty of phase speed was obtained performing a least-squares fit on the Hovmöller diagram in up to four ways: fitting the positive and negative lobes of band-pass meridional velocity anomaly individually, either 3 days prior to genesis, or 2 days (prior) + 1 day (after) genesis. The latter contingency allows a reliable estimate in a few cases where a well-defined wave did not exist more that 48 h before genesis. We are naturally reluctant to use wave properties *after* genesis to estimate gyre kinematics *before* genesis because the wave morphology and propagation change significantly once a tropical depression is born. For this reason the phase speed estimates and

uncertainty thereof were based primarily on the pre-genesis behavior of the waves.

Gyre properties such as size and orientation vary widely among the 55 cases selected for study, whereas the estimates of recirculation time occupy a much narrower range, probably because these estimates (as explained in Sect. 5.1) are derived from dynamical information closer to the center of the gyre. It should be kept in mind that gyre size, as displayed here, is a metric of *area*: e.g., the value 25 is approximately equivalent to a 5×5 array of grid points, the side of each grid box equal to $\sim 1.125^{\circ}$. A *linear* metric would reveal a narrower range, to be sure, but the range of gyre areas is impressive nonetheless (varying by a factor of 200). Given that the Atlantic and eastern Pacific storms under consideration (unlike western Pacific typhoons of the tropical depression category) are usually modest in horizontal size, relative to some of the larger gyres, a reasonable preliminary conclusion might be that beyond a certain size (in these two sectors) a very large gyre area is not relevant to storm development. Regarding separatrix angle, a pronounced dearth of angles occurs near -90° (due south) – a key observation for identifying the Lagrangian flow around the proto-storm and the air mass from which environmental properties have been entrained. We emphasize this point in the examples to follow.

Despite the wide range of sizes at both levels, the 600 hPa gyres are systematically larger, but with a proportionately larger range. There are several examples of late-developing gyres (magenta). Allowing for inclusion of these cases to fill gaps left by the 36-h statistics, all but two of the storms have closed translating gyres at 600 hPa. (This number is reduced to one (Dean) for reasons explained in Sect. 4.5.) There are several storms with no apparent gyre at 850 hPa – still a small fraction of the total – which seems consistent, at least, with the tendency for gyres to be smaller at this level and therefore more vulnerable to fall below the finite horizontal resolution of the analyses. A few gyres (mostly at 850 hPa) contain only one grid point; for these cases a 3×3 grid box was substituted for the purpose of calculating gyre averages as described in Sect. 4.3.

The time and longitude of events provides an important clue regarding the possible

role of in situ instability in tropical cyclogenesis which may be expected to give birth to paired systems within a short time interval. There are 4 paired events in Table 1 (1 in the mid-Atlantic, 3 in the eastern Pacific) where both depressions were declared within 24 h, and 15 paired events where both were declared within 6 days – all such events occurring within 20° longitude of each other. Amazingly these events (whether combined or segregated by basin) can be modeled by a linear regression of longitude vs time separation with slope (phase speed) of −4.2 to −4.6 ms^{-1} and y-intercept (zonal wavelength) of 17.1 to 17.6° longitude, with extremely high R^2 values (0.88 to 0.91). But whereas this model seems to explain the paired systems of the eastern Pacific quite well, most of the Atlantic waves in the paired group have phase speeds about twice as fast as the model estimate. Pairing does not suffice to prove instability; it simply indicates that a wave packet had two adjacent gyre-troughs favorable to genesis. In theoretical terms the question is whether the ITCZ supports "absolute" instability that may occur in situ without an upstream stimulus (Pierrehumbert, 1984). We cannot answer this question here. Nevertheless, the observed pairing of genesis events strengthens the marsupial paradigm by showing that large-scale organization of rotating convection spans more than a single wavelength of incident waves.

All 55 wave/genesis events have been examined, and our conclusion is that in most cases (i) sustained deep convective activity occurs near the local critical latitude of the wave's surface low and (ii) the tropical storm eventually occurs very near the intersection of the critical latitude and the trough axis. To illustrate our basic results, five representative storms during August 2000 were selected; the evolution of easterly waves and convection (as measured by TRMM accumulated precipitation) before TC genesis are discussed in detail for these cases.

4.2 Illustrative cases from August–September 2000

Hovmöller diagrams of 2.5–9 day bandpass meridional velocity at the best-track genesis latitude for each of the five highlighted cases are shown in Fig. 5 at the 850 and 600 hPa levels. The large dot near the center of each panel indicates the longitude and

time of genesis according to the best-track data, while filled squares trace the storm's longitude subsequent to genesis, at 6-h intervals. (The latitude of the storm is not shown here; it is listed in Table 1 and shown in the maps to follow.) Each storm originated between a negative and positive meridional velocity anomaly to the west and east, respectively, a region of anomalous cyclonic vorticity. In the first four examples, easterly waves at the two levels were aligned almost perfectly in the vertical, while in the remaining case (Shanshan) a slight eastward phase tilt with height can be detected. The tilt diminishes approaching genesis time as the 600 hPa wave (with approximately twice the phase speed: Table 1) catches up with the 850 hPa wave. In such cases an improving vertical alignment of the wave is part of the pre-genesis sequence. Characteristic of these examples and almost all of the events in Table 1 is that easterly wave anomalies (i) are present prior to genesis time, (ii) are reasonably monochromatic for at least the two preceding days, and (iii) become well aligned vertically in the lower troposphere below 500 hPa before genesis occurs. The fact that wave anomalies appear vertically aligned does not imply, however, that the flow kinematics are identical at 850 and 650 hPa, as will be evident in some of the cases highlighted.

Of the ten panels shown in Fig. 5, only the first two display what might be described as a reasonably uniform pattern of wave amplitude and zonal phase propagation across the entire longitude range and time period spanned by the figure. It turns out that pictures like Fig. 5a and b are the exception and not the rule. Most often we find one or more of the following in the Hovmöller plots of meridional velocity anomaly: (i) a group of wave phases originating to the west (east) of the genesis location, followed by eastward (westward) apparent group propagation across the diagram (the eastward scenario is preferred and nicely illustrated in Fabio and Shanshan); (ii) seemingly abrupt amplification of the wave packet prior to or surrounding the genesis point (as in Beryl); (iii) diminution of wave amplitude towards the end of the storm track (in all panels except Shanshan 850 hPa) and (iv) a pronounced wave packet in the upper right quadrant of the Hovmöller diagram (in all cases highlighted) indicating either that the incident wave is maintained for a time by diabatic processes operating within the proto-vortex (note

that the vortex remains in the trough of the wave for a few days in each of the examples shown) or that new waves are excited by the vortex as it develops into a full-fledged tropical storm, and these waves subsequently propagate as a group to the east. In order to understand the last feature it proves necessary to examine the wave/vortex structure in four dimensions. Most aspects of the subsequent "wave radiation" – if this is the correct way to think of it – are not relevant to genesis and will be discussed elsewhere. On the other hand, the transition of wave structure from equivalent barotropic in the LT to a deep quadrupole[25] or "first baroclinic mode" pattern occupying the entire troposphere in the longitude-height plane (along the genesis latitude) represents a key signature of genesis process insofar as this structural transition indicates deep convective mass transport coupled to the incident wave and generally precedes the best-track genesis time by a day or more. This transition will be discussed further in Sect. 5.3. A first baroclinic mode structure was found to be dominant in the western Pacific during boreal summer (Dunkerton, 1993) and probably characterizes the tropical depression disturbances that populate this region. It is noteworthy that a similar structure appears in marginal basins (e.g., Atlantic and eastern Pacific) just prior to TC genesis. The coherent response in the upper troposphere associated with the quadrupole pattern is apparently responsible for the subsequent radiation which, to our knowledge, has not been discussed previously in the literature but may have important consequences for the UT/LS.

A perfectly monochromatic wave, with a discrete ground-based frequency and zonal wavenumber, would necessarily look like Fig. 5a and b... from which it is obvious that most incident waves are *not* perfectly monochromatic and therefore contain a modest spread of wavenumbers and frequencies in spectral space. The zonal-wavenumber bandwidth (Δk) of incident waves can be estimated from Heisenberg's Uncertainty Principle $\Delta k \Delta x \sim 2\pi$ or equivalently $\Delta k/k \sim 1/N$ where N is the number of full cycles

[25] A quadrupole structure describes the appearance of meridional velocity anomalies in a longitude-height plane intersecting the vertical axis above the developing storm, with cyclonic (anticyclonic) flow at lower (upper) levels.

observed in the wave packet in the x-direction. A similar estimate applies to frequency bandwidth using the number of full cycles in the t-direction. Judging from Fig. 5 one might assume a typical value range $N \sim 1$–3. Easterly waves, like most tropical waves, are local and episodic in physical space (Dunkerton, 1991). The term *intermittency* (Mandelbrot, 1974) has been used in recent years to describe (i) waves that come and go, having peak quadratic fluxes (of momentum, heat or constituents) much larger than their time-averaged value (Alexander and Dunkerton, 1999); or (ii) turbulence that is inhomogeneous in space or time, containing coherent structures that disrupt the self-similar character of the inertial subrange (Frisch, 1996). As noted in the Introduction, we believe it is necessary to invoke wave *and* turbulence concepts in order to understand tropical cyclogenesis. In the real world, nonetheless, there is usually a natural order to genesis such that *waves precede turbulence* in a logical and chronological sense. Since we are considering many wave/vortex events as individual events, not as part of a time-averaged spectrum of geophysical turbulence, it would be better to say that "waves precede vortices." One could then regard the proto-vortex and resulting storm as a coherent structure arising from the wave and interacting with it for a time before acquiring a separate life of its own. The typical sequence of events will become evident from the examples highlighted next.

4.2.1 Central Atlantic: Hurricane Debby

The sloping lines in Fig. 5 represent the mean phase speed derived from the linear regressions of the southerly (solid lines) and northerly (dashed lines) meridional wind anomalies. The Hovmöller diagrams for Debby, shown in Fig. 5a and b, suggest that the wave has an equivalent barotropic structure in the lower troposphere as noted in the preceding discussion; the difference of the phase speeds at 850 hPa and 600 hPa is less than 1 ms^{-1}. The similarity of phase speeds is consistent with the fact that the barotropic structure is evident over the entire diagram.

Figures 6 and 7 show the relative vorticity (representing time scales longer than ~2.5 days) at the 850 and 600 hPa levels at 6 h intervals, before the genesis of Debby, from

1200 Z 18 August to 1800 Z 19 August 2000. As discussed in Sect. 2, the Lagrangian mean flow in the critical layer is zero in a frame of reference moving at the phase speed of the wave (Fig. 1). Alternatively, the streamlines of a steady vortex are advected by the basic flow (Fig. 3). To illustrate this concept, the streamlines of 2.5-day low pass flow in a "wave-centric" frame of reference are also shown in Figs. 6 and 7. (In unsteady flow, streamlines are different from particle trajectories, but serve as a reasonable first approximation.) The low-pass filter is intended to represent the total (wave + mean) flow in order to include both the nonlinear interaction between the wave and mean flow, and low-frequency variations with time scales longer than 9 days (including the MJO) which have been previously suggested to have an impact on tropical cyclogenesis in the deep tropics (Maloney and Hartmann, 2000; Maloney and Dickinson, 2003).

At 850 hPa, the best-track genesis location for Debby coincides almost perfectly with the center of a closed gyre in the translating frame. The thick curve passing through the center of the gyre denotes the isopleth of zero zonal velocity in the translating frame. Along this curve the translating streamlines are oriented meridionally by definition. The thick curve is bracketed by two adjacent curves representing the uncertainty in our phase speed estimate. Adjacent to the center of the gyre, approximately 800 km to the ENE, is a saddle point or "separatrix" of the translating streamlines. A dividing streamline intersecting the separatrix can be imagined to surround the genesis point, spanning a distance of about 700 km north to south. Streamlines passing near the separatrix are shown in red. Owing to a small but nonzero divergent component of horizontal motion, the dividing streamline is not exactly closed, but converges towards the center of the gyre in the latter part of the sequence. Significant cyclonic vorticity exists not only within the closed gyre but in a wider area to the south. This additional region of vorticity is less associated with the gyre (as curvature vorticity) than with the jet itself (as shear vorticity). We return to this point in the next example when discussing an alternative measure of vortical flow, the so-called Okubo-Weiss parameter.

At 600 hPa, the best-track genesis location likewise coincides with the center of a closed gyre which is much larger in horizontal extent than the gyre at 850 hPa. Once

again the principal separatrix is located about 800 km to the east. A secondary saddle point is seen at both levels about 1400 km to the NW. Three gyres arrayed along an approximately zonal axis from WNW to ESE can be imagined to comprise a series of "cat's eyes" along the critical latitude for this wave. Strictly speaking, the thick curve in both figures denotes the effective center of the critical *layer*, not the critical latitude of the wave itself. Supposing that a mean flow *as seen by the wave* should be represented by a modified low-pass filter (periods >9 days) excluding the period of the wave itself (3–4 days), we find that a critical *latitude* – defined as the locus of points where this *low-frequency* zonal wind matches the zonal phase speed of the wave – again intersects each of the gyres arrayed zonally in Figs. 6 and 7 (last panel of each). In other words, the critical layer has formed more or less at the critical latitude of the incident wave, as expected from linear theory. This is useful knowledge for wave dynamics but we caution that what actually matters for mesoscale developments is the extent of a finite-amplitude critical layer and its subsequent role in TC genesis.

The importance of the choice of "gauge" for flow potentials becomes clear when comparing the translating streamlines to those of a resting frame. Figure 8a and b illustrates the latter at genesis time only. At 850 hPa there is a closed gyre with principal separatrix misplaced to the SW of the genesis point by about 700 km. This pattern seems to have little relation to the distribution of vorticity, even though the choice of gauge in this instance (zero everywhere) is – like any other choice – completely consistent with the vorticity itself. For example, streamlines in the resting frame cross the southern boundary of the cyclonic vorticity region quite happily even though the actual vorticity evolution in the translating frame shows no evidence of vorticity advection in this manner. This intersection did not appear in the translating frame because streamlines and isopleths of vorticity were approximately parallel while curving around the southern boundary of the gyre (not unlike the ideal nonlinear critical layer of Fig. 1). At 600 hPa in the resting frame there is no closed gyre at all. Although we do not claim that the choice of translation speed and resulting streamlines in Figs. 6 and 7 provide a *perfect* picture of the flow kinematics in this case, the translating frame is

clearly superior to the resting frame from a vorticity advection point of view[26]. The near perfect coincidence of a closed gyre in the translating frame with the actual location of TC genesis is also striking. In the resting frame they are far apart. Debby is by no means unique in this respect. Although this event provides one of the cleanest and simplest examples of incident wave propagation, we find an actual or probable closed gyre in the translating frame surrounding the genesis point in almost all of the cases in Table 1 (see Sect. 4.5). Note that an optimum overlap of streamlines and vorticity isopleths maximizes Kelvin's circulation around the translating gyre as calculated along the bounding streamline.

Streamlines in the translating frame also provide a plausible explanation for the distribution of moisture in the free troposphere above the boundary layer (as represented by the saturation fraction[27] averaged from the surface to 500 hPa, shown in Fig. 9) and of deep moist convection (as represented by the TRMM 3-hourly accumulated precipitation, shown in Fig. 10). Their role is "plausible" in the sense that moisture and persistent deep moist convection are located within the translating gyre; a specific role for entrainment of moisture into the developing gyre is less certain (in this case, at least). It is clear from the evolution of saturation fraction that horizontal advection alone cannot explain its distribution. While advection might account, in part, for the wrapping of moist

[26] For nondivergent barotropic flow the advection of vorticity is described by the horizontal Jacobian of horizontal stream function with its horizontal Laplacian; translation of the coordinate system with the wave minimizes this quantity by eliminating unsteadiness due to wave propagation. There is nothing dynamically inconsistent with vorticity advection as viewed in the resting frame, insofar as it causes the pattern to propagate in the direction of the wave. Nonetheless, it is desirable to eliminate (via translation) this dominant contribution to the tendency in order to expose more clearly the evolution of the synoptic flow pattern and mesoscale features embedded therein.

[27] Saturation fraction represents how much water vapor is in the column relative to the maximum that the column might hold, given the observed temperature as a function of pressure (Raymond et al., 2006). A similar quantity was defined by Bretherton et al. (2004). It is akin to a vertical integral of relative humidity weighted by saturation mixing ratio.

air around the northern side of the gyre, and its transport eastward out of the domain, the entire moistened area in the southern half of the gyre creeps steadily westward against the prevailing flow (with the wave) as if to suggest that the precipitation cells in this region (Fig. 10) are supplying moisture to the gyre. A symbiotic relation between convective moistening and closed gyre circulation evidently exists in this sequence. Convection moistens the free troposphere, the moisture is subsequently contained by the gyre, which favors further deep convection in the gyre. Seeing how some of this moisture is able to escape to the east, we regard the closed circulation as critically important to depression development to the same extent that moist thermodynamic processes are also important in the gyre. Progressive saturation of the column (in a single-column point of view) is arguably important to genesis (Raymond and Sessions, 2007; Emanuel, 2007). Our description of the approximately two-dimensional, equivalent barotropic flow kinematics and dynamics in a translating frame of reference adds a critical (no pun intended) dimension to the single-column model (SCM) viewpoint while preserving the essential element of deep convective moistening and its consequences. Without the quasi-2-D kinematics and dynamics, the SCM viewpoint has no context within which to explain tropical cyclogenesis.

4.2.2 West Atlantic: Tropical Storm Chris

A similar story may be told regarding the birth of Chris, but with an odd twist: closed gyres are evident at both levels 12–30 h prior to the best-track genesis time, as shown in Figs. 11 and 12, but by the time the first advisory was issued, the streamlines (and stream function contours) have opened up. The genesis location is consistent with that expected from westward translation of the closed gyres from the time of their disappearance. A principal separatrix existed 12–30 h before genesis (just to the north of the closed gyre at either level) but is either gone or displaced northward out of the picture by the time genesis was officially declared. A secondary saddle point far to the WSW is present throughout the sequence at either level. It seems odd that a closed gyre does not appear around the best-track genesis point, even though it was

present a short time before. A possible explanation is that ERA-40 data do not fully resolve the horizontal structure of the tropical depression. Note, however, that the critical latitude seen by the waves (red curve in final panel; this quantity is based on 9-day low-frequency data and changes little in 30 h) together with the analyzed trough axis pinpoints the best-track genesis location to within ∼100 km – as observed at one or both levels in each of the five storms highlighted here. The silver lining in this event may be that we are able to detect a depression-strength closed gyre more than a day in advance of the official time, simply by translating the frame of reference at the speed of the incident wave, which was also present several days before. A key consideration for operational purposes is that for this technique to be useful in real time, the easterly wave must be identifiable sufficiently in advance: identifiable, that is, not only before the *official* genesis time (since the depression at this time would be identified anyway without knowledge of the translating streamlines), but before an *earlier* point in time when we wish to issue a forecast in advance of the first. Little would be gained by issuing a forecast at the genesis time based on wave information accumulated up to *that* point; such knowledge is needed well in advance of the official time. With this caveat, an earlier identification of tropical depressions seems entirely possible in cases like Chris.

Streamlines in the resting frame once again are almost useless for this system, as there are no closed streamlines anywhere (Fig. 13). The best indication of possible development might have been inferred from a trough extending from SW to NE, a tilted version of the "right-side-up" omega pattern of an isolated vortex in the resting frame (Fig. 3). As in Debby the translating, but not resting, streamlines provide a reasonably consistent picture of the containment of cyclonic vorticity by a closed gyre (except for its disappearance in the analyses just prior to genesis time). An alternative measure

of vortical flow is provided by the Okubo-Weiss parameter[28]

$$OW = \varsigma^2 - S_1^2 - S_2^2 = (V_x - U_y)^2 - (U_x - V_y)^2 - (V_x + U_y)^2 \quad (1)$$

as shown in Fig. 12 at the 600 hPa level for the genesis sequence. This quantity highlights regions of strong rotational flow (curvature vorticity), while suppressing the display of shear vorticity in regions of strong shearing deformation (third term of Eq. 1) flanking the jet axis[29]. At both levels the center of the cyclonic OW anomaly coincides almost perfectly with the best-track genesis location. A disadvantage of this quantity is that anticyclonic regions are highlighted equally. In general, we expect that OW will be useful for pinpointing genesis in situations where an elongated vortex strip rolls up into one or more closed vortices, by isolating the curved regions of flow at the expense of the elongated features (viz., the basic state vorticity that caused roll-up in the first place). Perhaps the most important conclusion to draw from the OW parameter inside the translating gyre is that the flow within is relatively free of strain and shear (McWilliams, 1984), favoring nominally the formation of smaller proto-vortical structures within.

With regard to saturation fraction (Fig. 14) and precipitation (Fig. 15) similar conclusions may be inferred as in the previous case: convective precipitation moistens the column along an axis extending SW-ward from the gyre center while advection carries this moisture to the NE, allowing some to escape the domain while containing the remainder in the northern half of the gyre. It is difficult to evaluate the importance of the containment effect since precipitation is rather constant near the genesis location

[28] In geosciences the Okubo-Weiss parameter has been most frequently used in physical oceanography and two-dimen-sional turbulence studies; a few atmospheric applications have been reported (Lukovich and Shepherd, 2005; Rozoff et al., 2006). An improved definition of the parameter for transient flow was developed by Patrice Klein and co-workers (Lapeyre, 2000).

[29] Curvature vorticity is useful for this purpose if calculated in the translating frame, not the resting one.

throughout the sequence. The distribution of precipitation in relation to vorticity is interesting: an apparent spatial correlation with shear vorticity (but not OW) early in the sequence, oriented to the SW of center (following the trough axis: black curve) followed by precipitation at the center only (correlated with OW, but not shear vorticity). There may have been some initial tendency for frontogenesis in the distended flow along the axis to the SW, possibly triggering the deep convection, but as the genesis time approached this convective line was replaced by rotating convection, or convection tied to the rotating flow near the genesis location.

4.2.3 Gulf of Mexico: Tropical Storm Beryl

Tropical storm Beryl demonstrates that westward propagating anomalies of meridional velocity may influence TC genesis as far north as the Gulf of Mexico. In this case, however, the incident wave was relatively weak compared to that of the previous examples, while propagating into a more complex flow pattern in such a way as to enhance the prevailing vortical flow, resulting in genesis. The full sequence of events in the translating frame is shown in Figs. 16 and 17 at the 850 and 600 hPa levels, respectively. The viewpoint in the resting frame at genesis time only is shown at these two levels in Fig. 18. Since the translation speed is relatively small in this case, compared to the previous examples, either reference frame (translating or resting) is able to capture the closed gyre and correctly anticipate the genesis location and time. Close inspection of Fig. 18, however, once again reveals a slightly misaligned streamline pattern, implying vorticity advection that does not exist in the sequence. In the translating frame the principal separatrix exists to the NE of the closed gyre and a secondary saddle is located to the SW. A second and fairly significant gyre exists in the SW corner of the figures, making the entire pattern look like a critical layer aligned from SW to NE, tilted $\sim 45^{\circ}$ relative to a latitude circle. The incident wave alone cannot explain this pattern. Without further analysis (outside the scope of this paper) it is difficult to say how much of the flow kinematics should be attributed to the prevailing flow and to what extent this flow was altered by the incident wave, other than to amplify the "pocket" of cyclonic vorticity

that eventually became a closed circulation thanks to the incident wave. Although the orientation differs from the other cases highlighted, the transition from a linear vorticity pattern to a more circular one at the end of the sequence suggests that the incident wave was instrumental not only in enhancing the local vorticity maximum but also in altering the flow topology around this maximum in such a way as to produce a much larger region of closed recirculating flow than was present initially. This contribution is apparent at both levels. The prevailing distributions of saturation fraction (Fig. 19) and precipitation (Fig. 20) display a persistent ribbon, or in Newell's terminology (Zhu and Newell, 1999) a "river" of moisture along the same SW-NE axis as the prevailing critical layer. As with vorticity, the shape of the moist convecting region is altered from an extensive linear pattern (aligned from SW to NE) to a more confined circular patch during the sequence – all of this *before* best-track genesis. We are evidently dealing with a more complex situation than that imagined in our simple scenario outlined in Sect. 2 and as illustrated by the preceding examples in the central Atlantic. Nonetheless, the gyre circulation in this event displays a tantalizing relationship to the prevailing moisture and convection that was also seen in the simpler cases highlighted above: *the closed gyre evidently forms at, or close to, a boundary between relatively wet and dry air*. By the end of the sequence (genesis time), the moisture and its associated convection have engulfed most of the enclosed circulation. Is there something about the initial moisture gradient that is instrumental either in the formation of a closed circulation pattern or in the genesis to follow? The next example, from the eastern Pacific, provides another illustration of this intriguing relationship and piques our curiosity further.

4.2.4 East Pacific: Tropical Storm Fabio

The evolution of vorticity and translating streamlines in the development of Fabio is shown in Fig. 21 at 850 hPa, while Fig. 22 shows the corresponding pattern (substituting OW for vorticity) at 600 hPa. Patterns of saturation fraction, precipitation and vertical shear in the lower and upper troposphere for this event are shown in Figs. 23–26, respectively. At both levels, closed streamlines formed near the intersection of the

critical latitude and the trough axis, delineating a critical layer of finite width. Strong cyclonic/rotational vorticity, high saturation fraction and weak vertical shear simultaneously coincide within the critical layer and provide a favorable sub-synoptic scale environment for tropical storm formation. TRMM data suggests that convective activity is present near the critical latitude 30 h before genesis was declared by the forecasters. Near the critical latitude the convective activity becomes sustained, and more focused, while the convective activity away from the local critical latitude dies out. It is striking that genesis eventually occurs very close to the intersection of the trough axis and the critical latitude (as true for the other cases highlighted). Also striking is that the eventual location of TC genesis lies just within a wet zone delineated by a strong north-south gradient of moisture. This configuration is expected in cases where genesis occurs poleward of, but close to, the ITCZ. Expansion of the closed gyre during the pre-genesis sequence exaggerates the weak undulation of moisture ribbon that was present at the start. With fully developed hurricanes nearby, the amplified pattern may result in a severe deformation or demise of the original ITCZ (Dunkerton, 2006) although this is not yet apparent in the final panel of Fig. 23. By this time, however, deep convection has become notably absent in the diffluent region (lower right corner) in the final panel of Fig. 24. Farther east, deep convection has become invigorated in a second closed gyre.

The genesis of Fabio, over the eastern Pacific, may be more closely related to the ITCZ than the other storms highlighted thus far in the sense that cyclonic vorticity, convection and high humidity all have a zonally elongated pattern. The actual storm, however, is located well to the north of the ITCZ, and is associated with a break in the zonally elongated pattern. As noted by Dunkerton (2006), it is common for tropical storms to displace poleward or to obliterate the ambient ITCZ. The role of the ITCZ in such cases is not obvious. Although the hydrodynamic instability pathway yields a similar outcome, as instabilities become nonlinear and detached from their source (viz., an unstable strip of PV along the original ITCZ: see, e.g., Fig. 5 of Wang and Magnusdottir, 2005) it is plausible that neutral easterly waves propagating parallel to

the ITCZ have a similar effect in cases where genesis ensues. In Fabio, the easterly wave exists ahead of time (as shown by the Hovmöller plots) and the original critical latitude and isopleth of zero PV gradient (blue curve) were nearly coincident. It appears that the wave prior to genesis was nearly neutral (according to the Rayleigh criterion) or at most, marginally unstable[30].

A final point regarding Fabio is that the best-track genesis location does not coincide with the minimum vertical shear as measured by either of our two metrics (lower to mid- or upper troposphere). It is clear from this case and others, and also from our modeling study, that the horizontal distribution of vertical shear is not the deciding factor in where a storm will form. As will be shown later, shears of this magnitude do not prevent development, so it is not surprising that Fabio's origin does not coincide with the location of minimum shear. Of more importance is that vertical shears in the neighborhood of the genesis point are not extremely large (much greater than 10 ms^{-1}).

4.2.5 Central Pacific: Super Typhoon Shanshan

The sequence of events prior to the birth of Shanshan illustrates vortex roll-up similar to that of Fabio, but more clearly. The 850 hPa flow, shown in Fig. 27, consists of a band of vorticity that acquires a more circular symmetry as time proceeds. It appears from Fig. 5i and j that a weak wave propagating at 850 hPa from the east intersected a stronger wave (or instability?) to the west of the genesis location, also with westward phase propagation, but apparent eastward group propagation at 600 hPa. The proper choice of translation speed is more difficult to determine in this case compared to the preceding examples. As expected from a relatively fast westward translation, the pattern of 600 hPa streamlines in the translating frame, shown in Fig. 28, looks markedly different than either the corresponding pattern at 850 hPa (with slower translation speed) or those at either level in the resting frame (as shown in Fig. 29 for the

[30] The marsupial paradigm embraces the instability pathway insofar as the critical layer (relevant to TC formation) is an essential part of the synoptic-scale instability itself, as noted above.

genesis time only). The translating and resting patterns at 850 hPa are similar because the translation speed is slow – the slowest of any of the examples thus far. Either choice, translating or resting, yields a closed gyre (although the gyre at 600 hPa is much larger in the translating frame) and the relationship of streamlines and vorticity contours is plausible either way. The deciding factor at 600 hPa is the existence of a second gyre near 165° E that is absent in the resting frame. In the left half of Fig. 28f we see the familiar critical layer pattern aligned in the zonal direction, as in the ideal case (Fig. 1). The ERA-40 analyses in this case do not seem able to capture much of the structure in saturation fraction, other than a general moistening along the southern half of the zonally elongated closed gyre at 850 hPa (not shown). The distribution and evolution of TRMM precipitation in this case is similar, nonetheless, to that of Fabio as shown in Fig. 30, with ITCZ convection gradually replaced by convection predominantly in the closed gyre as visualized in the translating streamlines at 600 hPa. The excellent correspondence of convection and closed circulation in the translating frame (absent in the resting frame) further supports our preference for the translating frame in this instance. It is not uncommon for easterly waves and/or ITCZ to extend into the central Pacific from the east, so it is plausible that genesis occurred in a manner similar to the easterly wave cases highlighted above. Whether characterized primarily as "incident waves from upstream" or as "in situ instability of the ITCZ" their westward phase propagation plays a key role in the genesis sequence.

4.3 Relation of wave and vortex subsequent to genesis

The Hovmöller diagrams in Fig. 5 indicate that the five storms propagate at approximately the same zonal speed as their parent waves and stay near the wave trough (midway between meridional velocity minimum and maximum) in the first 2–3 days after formation. In Debby, Beryl and Fabio the vortex propagation is nearly parallel to the trough propagation, whereas in Chris and Shanshan, some motion of the vortex relative to the wave can be seen. If we adopt a convention that ground-based frequency ω is always positive, while the horizontal component of wavevector $\boldsymbol{k}$ points in any az-

imuth, for easterly waves the wavevector points to the west, implying that wave phase increases downward and to the left in the Hovmöller diagrams. If the vortex does not keep up with the wave it may said to be moving towards a lower wave phase. Closer inspection of Fig. 5 reveals that the vortex in each of the five storms drifts by either a small or large distance towards lower phase. We note also that the two Pacific storms (Fabio and Shanshan) originated slightly west of the zero phase (trough) line. What can not be shown in the time-longitude diagrams is the meridional movement of the storms. While Fabio kept a nearly zonal track, Beryl and Debby moved poleward at a speed 1.5∼2° per day. Given the typical meridional wavelength ∼20°, this meridional speed suggests that the storms were still within the wave trough region in the time period shown in the Hovmöller diagrams.

Some storms propagate at a much slower speed than the parent wave, and become detached from the parent wave shortly after formation. These cases represent a more extreme migration of the vortex to lower values of wave phase. Table 2 summarizes the median phase change (vortex relative to wave trough) and its inter-quartile range from the genesis time to 3 days later (or duration of event, if less than 3 days) for the 55 events altogether and segregated according to basin. These statistics are also segregated according to whether or not the storms drift eastward in the resting frame at any time during the first 3 days after genesis ("eastward-also"). In the majority of cases storms in both basins move exclusively westward with their parent wave ("westward-only") in the resting frame during the time period shown in the Hovmöllers and, regardless of whether this is true, a vast majority of cases also display an eastward drift of the vortex with respect to the wave trough in the translating frame (toward lower phase). Remarkably, though, much of the relative drift in the median value is accounted for by eastward-also storms. When these storms are eliminated from the statistics, the median drift that remains is either small (at 600 hPa, middle group of rows) or nearly absent (at 850 hPa). Most impressive in the latter case is that the median storm center nearly coincides with the wave trough (zero phase) and stays there. Storms in the eastern Pacific, however, tend to originate a little west of the trough (positive phase)

and migrate towards the trough during the first 3 days, unless the eastward-moving storms are eliminated, in which case the storm-trough relationship remains constant at 850 hPa. Since the best-track "vortex" location is independent of height by definition, the differences in evolving phase relationship only can be explained by a change of wave phase tilt with height between the two levels, from initially vertical alignment to a modest westward tilt after 3 days. For waves in the eastern Pacific we infer a final tilt of about 27° (82°) for westward-only (eastward-also) storms. For westward-only storms the final wave tilt brings the vortex and trough into approximate alignment (−7°) at 600 hPa while the vortex remains west of the trough at 850 hPa (positive phase). For eastward-also storms the vortex passes through the trough and ends on the eastern side at 600 hPa (negative phase). No evidence of significant phase tilt can be inferred in the median of Atlantic cases.

The marsupial paradigm is supported by the observed wave-vortex relationship in the first few days after genesis, that is, after a tropical depression is recognized by forecasters. The vortex remains in the same phase of the parent wave in most cases or drifts slowly to lower wave phase. The resulting TD is evidently a continuation of the "surface low along the wave" existing before the first advisory, but with amplification of features required to define a depression. That vortex propagation immediately after genesis no longer matches exactly the wave propagation is consistent with the increasing autonomy of the vortex as it gains strength (recall that most depressions become named storms, and the exceptions have been excluded from our survey). This is in contrast to the critical layer itself, which may be regarded as an intrinsic feature of the wave prior to genesis. A transition from "tropical wave critical layer" to "tropical depression" plausibly describes the marsupial paradigm from a synoptic point of view.

4.4 Amplitude of waves subsequent to genesis

It cannot be determined from these statistics alone why the "eastward-also" storms make an earlier than normal departure from the parent wave; e.g., whether the wave is unusually weak to begin with (implying less influence on vortex motion, consistent

with H1/H2) or weakens due to the early departure of the vortex (H3). In the eastern Pacific the waves are evidently becoming tilted over towards the west (consistent with the prevailing vertical shear in this region) which would reduce wave amplitude via the Orr mechanism without having to appeal to changes in diabatic forcing brought about by the departure of the vortex. This explanation does not apply to the Atlantic cases. A simpler reason for wave decay, consistent with forecasters' experience, is that the departing vortex carries away a substantial part of the original wave's vorticity anomaly and its associated diabatic forcing and mesoscale convective organization (H3). In regard to the highlighted cases, it is interesting to note that the waves appear to become invigorated after the formation of Fabio and Beryl while retaining their intensity after the formation of Debby. Although these diagrams alone cannot prove H3, they are consistent with the hypothesis that convective processes within the wave trough help maintain the wave as it traverses westward. A sequence of (i) wave growth in the short term, followed by (ii) wave decay along the original propagation path after TD formation, with (iii) secondary excitation of waves beginning at this time, forms a canonical picture of the easterly wave lifecycle in its latter stages, with considerable variation from one event to another.

Looking at statistics for the entire sample (Table 2), wave amplitude shows a small decline from day 0 to day +3 when averaged over all cases, although the standard deviation is 2–6 times a large as the observed change. The results are similar in both basins. An interesting result is that "eastward-also" storms occur in waves with smaller amplitude, although the wave shows little, if any, decline in such cases. If the smaller initial amplitude in such cases proves significant in a wider sample, it is consistent with the notion that waves with larger amplitude provide a more compelling reason for the vortex to remain with the wave, than do smaller waves. The initial wave amplitude at day 0 in westward-only cases is markedly larger, by about 50% relative to eastward-also cases, but experiences a rather significant decline (10–20%) which is more noticeable at 850 hPa. It is possible that immediately prior to genesis, there is something about the proto-vortex, in westward-only cases, that enhances the wave

amplitude near genesis time. This interpretation agrees with notion of a wave-vortex hybrid advanced in Sect. 2.2, lending some support to H3, but with the qualification that a persistent zonal, as opposed to meridional, propagation of the proto-vortex is needed in order for the synergy between wave and vortex to work optimally. We return to this point in Sect. 5.3. The fact that wave amplitude is less variable in "eastward-also" cases suggests that the wave-vortex interaction is indeed weaker in such cases.

This analysis does not discriminate between waves that exist a priori and act as parent waves from those that might be excited a posteriori by the developing tropical cyclone. In order to ascertain from the same data (i) the decay of incident waves responsible *for* the depression and (ii) the excitation of secondary waves *by* the depression, it is necessary to unravel the structure and propagation characteristics of these two wave groups. We believe that a separation of waves is possible but requires a more sophisticated analysis. Further discussion of post-genesis wave evolution is beyond the scope of this paper (beyond the range of time shown in the Hovmöller diagrams) and a detailed 4-D analysis of the waves will be reported elsewhere.

4.5 Survey of events 1998–2001

Our diagnoses of the 55 named storms in Table 1 and represented by the five cases highlighted in the preceding subsections support the hypotheses (H1–H2) that the critical layer containing the surface low of the parent wave is a preferred sweet spot region for TC genesis. The intersection of (east-west) critical latitude and (north-south) wave trough corresponds to the center of the "cat's eye" of nonlinear critical layer theory (Fig. 1). Such features correspond to regions of closed Lagrangian circulation which, on the southern side of the AEJ axis, have cyclonic vorticity and abundant moisture.

An obvious closed gyre in ERA-40 data is found at 600 hPa in the translating frame within 30 h prior to genesis in 53 of the 55 cases, in one of the remaining cases (Joyce) the gyre is probable and in another (Dean) possible[31]. At 850 hPa the statistics are

[31] In Joyce, the estimate of zonal translation speed in Table 1 is exaggerated owing to a northward component of wave propagation that is not accounted for by this analysis; a closed gyre at 850 hPa is found in a slightly slower gauge (-4 to $-5\,\mathrm{ms}^{-1}$; not shown). In Dean, storm formation occurred at the separatrix of a cutoff anticyclone on the SW side of the Bermuda High, a narrow trough whose kinematic features are partially attenuated by the ERA-40 reanalysis and possibly also by our 2.5-day low-pass filter. A northward component of propagation is evident in this event also. All of these challenges (and others not mentioned) make the identification of Lagrangian boundaries more difficult in such cases.

almost as good: 50 of 55 are obvious, 1 probable, 3 possible, and 1 unlikely. The westward-only and eastward-also cases do not differ in this respect, although it happens that the unlikely case (Dean) belongs to the eastward-also class, for which (as noted above) wave amplitudes are generally smaller.

A closed gyre implies one or more separatrix in the vicinity. Inspection of the 55 selected cases reveals a remarkable result that, whereas this point is usually located to the south of the gyre center in the resting frame, it is almost never located to the south in the translating frame (Table 1). Meteorological charts displaying Earth-relative streamlines are a standard tool in the forecasting industry, but generally provide a misleading picture of actual flow kinematics, or Lagrangian displacement of air, in propagating tropical waves. These maps typically display an upright omega pattern in the lower troposphere straddling the wave's trough axis. In fact the omega pattern is often upside-down in the translating frame, with separatrix to the north. In other cases, the separatrix is to the east or west (or both). To the extent that horizontal advection explains the topology of streamlines, and therefore indicates where air in the closed gyre has detached from, it is firmly established in our 55 cases that air at 600 hPa is not derived from or being exchanged (by resolvable motions) with air closer to the equator. For the most part, this is also true at 850 hPa. Rather, it is coming from (or previously associated with) air to the east, north or west of the gyre center. This result is probably the most important take-home message of our paper for operational purposes and weather briefings.

Using the concept of "translating closed gyre" it is straightforward to calculate statistical properties of dynamical fields (e.g., vorticity, Okubo-Weiss parameter and vertical

shears) and thermodynamical fields (e.g., saturation fraction, deep convective precipitation) relevant to TC genesis within the observed gyres – fields that were illustrated for representative cases in the preceding figures. Rather than display these statistics in obscure tabular form, we summarize the results pictorially in Figs. 31–32 for the 850 and 600 hPa levels, respectively. We focus here on the simplest of all statistics: the mean. Various spatio-temporal averages were constructed by selecting from two choices of spatial average (horizontal expanse of the translating gyre versus a 3×3 matrix of ERA-40 grid points surrounding the genesis point – more precisely, a linear east-to-west trajectory ending at this point) and two choices of temporal average (genesis time versus a 36-h average preceding and slightly overlapping genesis time). To put these average values in context, they are compared to "climatological" values defined simply as the August–September 1998–2001 average at the location of each gyre or local array. The climatological values are independent of time by definition, but depend on spatial position; the variety of observed gyres effectively samples the climatology in many different ways, depending on gyre location and extent, and optimum translation speed C_p. It is important to note that what distinguishes this analysis from all previously published studies of the genesis environment is that we include in our menu of averaging operators a *zonal translation* of the array of selected points; that is, the spatial array is a function of *time*, owing to wave propagation.

Space precludes a detailed discussion of each storm. Apart from a small number of oddballs, the message is clear: the observed storms formed in relatively moist, precipitating environments with large values of vorticity and Okubo-Weiss parameter. This is true for gyre and local averages alike, but the local average contains some exceptionally large values of precipitation and Okubo-Weiss parameter, suggesting that (i) the TRMM satellite has observed enhanced precipitation associated with the developing storm, concentrated at the best-track location rather than distributed throughout the gyre, and (ii) ECMWF analyses have correctly pinpointed the location of the developing vortex within the gyre and identified its vorticity as predominantly rotational rather than deformational, i.e., not deformed by strain or shear. The *persistence* of TRMM precip-

itation in the 30+ h preceding genesis is clearly evident – the translation of coordinate system is crucial for proper alignment – and the same can be said for relative vorticity and Okubo-Weiss.

Although vertical shear is not necessarily small in the pre-genesis environment, the values of shear observed in developing environments are either comparable to (at 850–500 hPa) or somewhat less than (at 850–200 hPa) the climatological shears[32]. The local shear is often smaller than the gyre-wide shear, especially for 600 hPa gyres which can be quite expansive. This suggests that the center of the gyre (or proto-storm location) is already a favorable spot for genesis, relative to the gyre as whole. Note that the average shear as defined here represents the average of a positive definite quantity (modulus of the shear vector at each point within the gyre) and therefore disallows any cancellation of opposing shears in different parts of the gyre. The average indicates, rather, a typical vertical shear that might be seen by convective elements in each grid-box column, regardless of shear vector orientation. Storms are evidently able to form in environments containing a wide range of shear values from 3–12 ms^{-1}. These values admittedly are not huge, and as forecasters are aware, local shears in hostile environments can be much larger, exceeding 20 ms^{-1}. For developing storms, as displayed in Figs. 31–32, vertical shears *in the Eulerian frame* are comparable to the differences in optimum phase speed C_p between the lower and upper troposphere (Sect. 5.3). Neither of these quantities exceed 10 ms^{-1}, except on rare occasions, so it is likely that the *Lagrangian shear* seen by the developing vortex is small as well.

[32] Climatological shears were obtained by first calculating the modulus of the shear vector, then averaging together to form the climatology. Throughout most of our storm development regions, vertical shear of the climatological wind velocity is small (~3 ms^{-1}, not shown). Developing systems generally form in shear that exceeds the "shear of the climatology" but is comparable to or less than the "climatology of the shear". The climatology of Okubo-Weiss parameter was obtained in a similar way, by first calculating the quadratic products and then averaging. Developing systems generally form in environments with Okubo-Weiss parameter well above its climatological range.

Once formed, the storm may help to maintain small shear, to the extent that it can. Divergent outflow originating above the storm center ensures that modest vertical shear will continue to exist off-center (even when the environmental shear is negligible) while remaining small on-center. Hendricks and Montgomery (2006) suggested that deep convection associated with vortical hot towers can erode vertical shear. This mechanism is important in tropical transition, where vertical shear owing to the UT cyclone upstream (to the NW of the developing low-level center) is unfavorable for further development and must be kept at bay (Davis and Bosart, 2004). Further study of this aspect of the problem using idealized cloud resolving numerical simulations will be presented in a following paper of this series. In the next section the vertical structure and evolution of waves and their associated critical layer is described in more detail for Hurricane Debby (2000).

5 Three-dimensional structure and evolution of a tropical wave critical layer

Two observations are evident from the historical record of TC genesis and early intensification over the Atlantic and eastern Pacific for events having a clear signature of tropical waves prior to genesis. (i) A "surface low along the wave" is a necessary, but not sufficient, condition for genesis of a tropical depression. (ii) In the vast majority of cases, genesis of a tropical depression is a sufficient condition for further intensification to named storm (tropical storm and possibly hurricane). Our definition of "genesis" in Sect. 1 is equivalent to the development of a depression-strength vortex, not to any subsequent intensification. From the results reported above, the development of a critical layer in the lower troposphere is evidently a *necessary* condition for genesis (and early intensification to named storm) by statistical association (Table 1) and by physical reasoning as outlined in the three hypotheses of Sect. 2.2. It is obviously desirable to find conditions, in addition to the existence of a critical layer, that would be *sufficient* for a tropical depression. By "sufficient" one could mean either that (i) in an ensemble of realizations, a tropical depression forms in most cases, or (ii) in a single realization, such

development is guaranteed. The latter definition is more strict and arguably impractical for the chaotic dynamics of geophysical turbulence as it would require observations on all relevant scales accurate and fine enough to overcome (with predictive capability, too) the uncertainties of vortex aggregation and triggering of deep moist convection (M06; Van Sang et al., 2008; Schecter and Dunkerton, 2007). The former definition opts instead for a statistical measure, e.g. of variances or co-variances of mesoscale fields, when considering possible conditions for up-scale development and formation of a tropical depression.

Unfortunately even a statistical measure is difficult to obtain, as it is impossible to calculate mesoscale (co-)variances either from analysis data, which are too coarse in horizontal resolution, or from field campaigns, which are too brief to provide good statistics. It seems that modeling studies are needed for this purpose (Montgomery et al., 2007). We can, however, dig a little deeper here into the available observations to refine and augment the marsupial paradigm and to define conditions that come closer to sufficiency for tropical depression formation. In this section we provide additional details that may be relevant for this purpose as well as for quantitative evaluation of the three hypotheses outlined in Sect. 2.2. We provide a partial but incomplete evaluation, for the fundamental reason mentioned above. Our analysis will focus on the kinematics of parcel motions, the vertical structure of the incipient hurricane embryo, and the vertical structure of waves that create that embryonic environment. For this purpose our discussion will highlight aspects of Debby (Atlantic 2000) that are broadly typical of the cases selected (Table 1).

5.1 Comparison of streamlines and trajectories, 1000–600 hPa

In Sect. 4, streamlines in a translating frame of reference were used as an approximation for parcel trajectories to delineate the critical layer. Although trajectories and streamlines generally differ for unsteady flow, we demonstrate in this section that the translating streamlines so constructed serve as a reasonable first approximation within a few days of genesis. Only the horizontal (isobaric) component of motion is consid-

ered here. For a circular vortex moving at a constant speed C, the relationship between the local curvature of the streamlines (r_s) and the local curvature of the trajectories (r_t) satisfies (e.g., Holton, 2004)

$$r_t = r_s(1 - \frac{C\cos\gamma}{V}) \tag{2}$$

where V is the horizontal wind speed, and γ is the angle between the streamlines and the direction of the vortex translation. For a cyclonic vortex moving westward (eastward), the curvature of the trajectories is stronger (weaker) than that of the streamlines south of the center of the vortex and weaker (stronger) north of the center. For a vortex embedded in and advected by a constant ambient flow, the trajectories are corkscrew in shape due to rotation and translation of the vortex. In a frame of reference moving at the horizontal speed u_c, $X_L=(x_L, y_L)^T=X-X_c$ represent the cardinal coordinates moving with the vortex, and $x_c=u_c(t-t_0)$ is the center of the vortex. Particle trajectories in this frame of reference satisfy the following equations

$$\begin{cases} \frac{dx_L}{dt} = \frac{dx}{dt} - \frac{dx_c}{dt} = u - u_c \\ \frac{dy_L}{dt} = \frac{dy}{dt} = v \end{cases} \tag{3}$$

As illustrated in Fig. 3, if $u_c=C$, the streamlines are stationary and coincide exactly with the horizontal trajectories. If the westward phase speed is underestimated (overestimated), the curvature of the trajectories is stronger (weaker) than that of the streamlines south of the center of the vortex and weaker (stronger) north of the center. Here we will use Hurricane Debby as an example to examine the three-dimensional structure and evolution of the critical layer.

Figure 33 shows in the left column streamlines at 600, 850 and 1000 hPa in a moving frame of reference averaged over the 36-h period leading up the genesis time of Hurricane Debby. Also shown in the figures is the stream function obtained from the horizontal velocity components by a Helmholtz decomposition. Streamlines and stream function contours are nearly parallel at 850 hPa, indicating a non-divergent flow, except

near South America where air flows into the gyre from the west. The 600 hPa flow is almost non-divergent as well. The Helmholtz decomposition is linear, so that transient divergent flows are eliminated by time averaging or, if they are small to begin with (as true at these two levels for the individual analyses used in the time average), the divergence remains small when averaged in time. The exact location of flow separatrix is evidently sensitive to the small divergent component, because the horizontal wind speed vanishes at this location (by definition). Note that, despite this error, the separatrix inferred from stream function is within 100–300 km of the separatrix inferred from streamlines. Unlike the first two levels, the 1000 hPa level displays significant convergence into the gyre from the north and west, and into a zonally elongated ITCZ in the eastern half of the figure, from north and south. This feature is described in Sect. 5.3. The flow entering the gyre from the north makes little effort, as it were, to avoid the center of the gyre by turning to the west, as at the other two levels. Although the genesis location (black dot) is ~100 km south of the gyre center at all three levels, the exact latitude of center is sensitive to our choice of C_p, moving ~80 km southward for each 1 ms^{-1} increase of C_p towards zero (Generally this depends on vorticity or circulation. A weaker circulation implies a stronger sensitivity to C_p). Values of $C_p=-8$ to -9 ms^{-1} place the 1000 hPa closed gyre precisely over the genesis location. These values are outside the range of uncertainty based on the Hovmöller method, but are optimum for steadiness of flow in the translating frame, as described in Sect. 5.2. Steadiness in the translating frame implies that streamlines and trajectories should be similar in this frame. To settle the question of which gauge is best, streamlines and trajectories can be compared.

Figure 33 shows in the right column 2-D parcel trajectories superimposed on the stream function averaged over the same time interval. The trajectories are calculated in the moving frame of reference, as shown in Eq. (2). The red curves are one-day forward trajectories from day 0 to day +1, and the blue curves are four-day backward trajectories from day 0 to day −4. (Trajectories are not shown outside of the domain.) The gyre or critical layer at 600 hPa, as indicated by the closed stream function con-

tours, is quite expansive. Six particles are picked, five of them (A–E) inside the gyre at the genesis time, the other one (F) just outside of the gyre. The particles moved counterclockwise around the gyre center, and their trajectories are nearly parallel to the stream function contours from day −2 to day +1. Since the flow is non-stationary, the trajectories are different from the stream function contours or streamlines from day −4 to day −2, but it nevertheless confirms our hypothesis that *particles inside the critical layer tend to stay inside.* Compared to 600 hPa, the gyre at 850 hPa is less expansive. The evolution of the streamlines (not shown) showed that the wave at 850 hPa propagated on the northern flank of the AEJ over West Africa. It turned southward and merged with the wave on the southern flank (maximum at 600 hPa) off the west coast, and meanwhile the closed circulation extended to the surface. A tropical depression formed within the wave about two days later. Six particles are picked at 850 hPa: particles A–C are inside the gyre and D–F outside the gyre. Particles D–F moved from west to east in the translating frame of reference, and stayed outside of the gyre. Particles A–C also came from the west. They took a small loop, and entered the gyre around day −2. This is consistent with the formation of the gyre at 850 hPa around day −2, as shown by the evolution of the streamlines. The trajectories of all the six particles are nearly parallel to the stream function contours from day −2 to day +1. At 1000 hPa, the gyre is much more confined. Particle A is picked near the genesis location, B close to the gyre center, and C–F outside of the gyre. Particles A–E came from the north, and particle F, which is far from the gyre center, moved from the west, which suggests that the closed circulation near the surface is directly related to the northern wave.

To test the robustness of this result, we increased the sample size by examining the trajectories of 40 particles inside or just outside of the gyre at each of the three vertical levels (not shown). Similar to what is shown in Fig. 33, the particles inside of the gyre tend to stay inside from day −2 to day +1, and all the trajectories are nearly parallel to the stream function contours during this time interval. This suggests that the stream function in the frame of reference moving with the wave serve as a reasonable first approximation within about 2 days of genesis. From the trajectories, we can also estimate

the recirculation time of a parcel inside the CL or the eddy turnaround time, which is about 2–3 days and close to the tropical storm development time scale. This is also the length of time that streamlines, stream function and trajectories are roughly equivalent near the gyre center. Table 1 includes two estimates of gyre recirculation time, one derived from the maximum vorticity in the gyre, the other from the average Okubo-Weiss parameter in the cyclonic vorticity region only. The maximum vorticity estimate (typically 2–5 days) is shorter than the O–W estimate (typically 3–8 days) because the latter pertains to a broader region of the pouch, and subtracts the contributions from straining and shearing deformation. Actual recirculation times probably fall between these two extremes. Note, however, that horizontal convergence in the boundary layer shortens the recirculation time as the effective radius of trajectory curvature contracts while parcels begin their ascent near the proto-storm center.

5.2 Vertical structure and evolution of the mother pouch

The need to translate the coordinate system zonally for an optimum view of Lagrangian flow kinematics has been stressed throughout the paper. Towards this end, a method for determining the optimum translation speed was devised using bandpass meridional velocity anomalies in time-longitude Hovmöller diagrams just prior to genesis. The purpose of the translation is to render flow streamlines approximately equivalent to trajectories, as demonstrated in the preceding subsection. If one were to instead measure explicitly the temporal variance of the flow in a variety of gauges, in a coordinate system moving at the speed of the selected gauge, it would be found that synoptic variance in the vicinity of the developing storm is indeed minimized at a phase speed close to that selected by the Hovmöller method. The reason is that when one chooses an incorrect phase speed for translation, the wave's phase propagation contributes significantly to the temporal variance in the incorrectly translating frame. When the proper translation speed is selected, this temporal variance is mostly eliminated. We have applied the alternative method to stream *function* (as opposed to stream*line*) which represents a field, that is, function of space and time (unlike *particles* whose location is simply a

function of time). Because the flow is dominated by the rotational[33] component, stream function in the correctly translating frame nicely illustrates the structure and evolution of the parent wave's "pouch". Representative examples of stream function for the mother pouch of Debby were shown in Fig. 33. The definition of Lagrangian boundary in steady flow can be made precise by locating the separatrix nearest the gyre center and equating the gyre boundary with the value of stream function intersecting that point.

In regard to the vertical structure of Debby's pouch, two salient features emerge with other interesting details. (i) A closed gyre is found at all levels from 1000–500 hPa for at least 30 h prior to genesis, for translation speeds in the range 8 to 10 ms^{-1} westward. The signature of this disturbance decreases abruptly in amplitude above 500 hPa. (ii) Above the mid-troposphere is a second closed *anticyclonic* gyre having somewhat larger spatial extent and located slightly to the east of center, but having a significantly slower range of possible translation speeds in the range 3 to 7 ms^{-1} westward. Close inspection of gyre properties, such as the steadiness of pattern, stationary center location and minimum temporal variance near the center (all evaluated in the translating frame) establishes a pair of optimum translation speeds: 9 ms^{-1} westward in the lower troposphere and 5 ms^{-1} westward in the upper troposphere. Streamlines and stream function at 200 hPa in the $-5\,ms^{-1}$ gauge at genesis time are shown in Fig. 34. The two signals (-5 and $-9\,ms^{-1}$) are found to have a common origin in the convective flare-up at 36–38° W at 30 h before genesis (Fig. 10a) explaining why the upper tropospheric signal is located to the east of the storm center at genesis time. The LT wave continues its westward propagation near 9 ms^{-1}, reaching the genesis location 30 h later, while the UT anticyclone drifts westward about half as fast, reaching 40–42° W as shown in Fig. 34. Stream function is a reasonably good proxy for streamlines over the left and upper halves of the figure, but misses completely the strongly

[33]The rotational component is larger in most places except, e.g., the upper branch of the local Hadley circulation, where the divergent component is comparable in a relatively shallow layer near 200 hPa (Dunkerton, 1995) and in the lower branch of local Hadley circulation, or boundary layer.

divergent outflow above the proto-storm center as well as the local Hadley circulation outflow (along the ITCZ to the east) directed back to the Equator.

Mean vertical shear over the whole troposphere is relatively light in this case. The flow speed in the upper troposphere near 300 hPa is about 4 ms^{-1} westward, so that when the coordinate system is translated westward near this speed, most of the jet structure disappears, leaving an anticyclonic gyre slightly to the east of the genesis location, with other meridional meanderings elsewhere. As a result, weak southerly flow (3 ms^{-1}) occurs over the depression at genesis time, in the translating frame as shown in Fig. 34. (The meridional component, of course, does not depend on the choice of gauge when the translation is zonal. It is the vanishing of zonal component in the translating frame that makes the flow appear southerly in this frame, rather than west-southwesterly as in the resting frame.) The UT gyre may be significant for development by providing favorably light winds above the proto-storm. Further investigation is needed to uncover the source of this upper tropospheric disturbance. The developing storm itself may have had a role to play in carving out the UT anticyclone as a result of a convective event at 36–38° W (next subsection). Averaged over the 36 h (6 consecutive analyses) prior to genesis, the structure of relative wind speed (modulus of vector $\boldsymbol{U}$ minus $C_p\boldsymbol{i}$) in the two appropriate gauges (9 and 5 ms^{-1} westward for LT and UT, respectively) is shown in Fig. 35a and b. The temporal standard deviation of wind speed over the same time interval is also shown in each gauge (c, d). Contours indicate a zonal-temporal average over a 30° longitude interval eventually centered at the genesis point and translating zonally prior to this time for 30 h at speed C_p. (The time span represents 6 consecutive analyses, or 36 h.) These wave-centric views illustrate in approximate fashion the structure of the mother pouch in a latitude-height cross section. Superposed as shaded pixels are wind speed and its temporal standard deviation *within the boundaries of the translating closed gyres* in each frame, as defined by their maximum extent in this longitude/time interval. As already noted, the purpose of the translation is to minimize the temporal variation of streamlines in the translating frame, rendering streamlines approximately equivalent to trajectories. Comparison of Fig. 35c

and d indicates that the temporal variation of wind speed *within the gyre* over 36 h is considerably smaller in the $-9\,\mathrm{ms}^{-1}$ gauge (0.3–0.7 ms^{-1} in the LT) than in the $-5\,\mathrm{ms}^{-1}$ gauge (0.7–1.6 ms^{-1}) whereas the $-5\,\mathrm{ms}^{-1}$ gauge is superior for the UT anticyclone (a closed a/c gyre at these altitudes does not appear at all in the $-9\,\mathrm{ms}^{-1}$ gauge). In the $-9\,\mathrm{ms}^{-1}$ gauge, relative wind speeds in the LT are *smaller* inside the gyre (1.4–3.4 ms^{-1}) than over all longitudes (4–6 ms^{-1}), whereas in the $-5\,\mathrm{ms}^{-1}$ gauge, these values (4–6 ms^{-1}) are *comparable*. The moral of the story: the slower translation speed is inappropriate in the lower troposphere, and its effect in reducing the relative flow or variation thereof inside the LT gyre is inconsequential. It is easy to understand why the *temporal variation* is minimized in the $-9\,\mathrm{ms}^{-1}$ gauge, because the wave's phase propagation has been accounted for. This translation speed closely approximates that of the LT wave, while the slower speed does not. The reason why the gyre's *relative flow* is reduced in this gauge is more subtle. Like the separatrix, the gyre extremum is a *stagnation point* where the relative flow is weak, albeit rotating cyclonically in such a way as to make a complete revolution about gyre center in a few days or less. Both gauges exhibit a closed translating gyre, implying a stagnation point either way, so why is the faster gauge ostensibly superior in the metrics of Fig. 35? The "secret of success" in the $-9\,\mathrm{ms}^{-1}$ gauge – for rendering the relative flow and its temporal variation small within the translating gyre (Fig. 35a) – is that the gyre keeps perfect step with the wave *and* is not too large in horizontal extent. In the $-5\,\mathrm{ms}^{-1}$ gauge the gyre is much larger and includes a peripheral region of stronger relative flow. This peripheral flow is so strong, in fact, that the gyre-average relative flow (shaded pixels in Fig. 35c) is stronger than that of all longitudes (contours)! We emphasize, however, that small relative flow per se is not necessarily significant. It will be noted (Fig. 35b) that a small relative flow (1–2 ms^{-1}) is also observed at 400 hPa in the $-5\,\mathrm{ms}^{-1}$ gauge near the genesis latitude. There is no closed gyre at this level; rather, the selected translation speed is similar to the zonal flow speed here. Translation eliminates the zonal component of relative flow at 400 hPa, leaving weak meridional meanderings at this level which have little, if any, importance dynamically – other than to ensure weak relative

flow above the proto-storm.

In regard to temporal evolution, a closed LT gyre in the properly translating frame can be found all the way back to 54 h before genesis time. The traveling gyre emerges from a quasi-stationary gyre near the west coast of Africa, presumably a monsoonal feature. The exact time of gyre closure is a function of altitude and translation speed C_p. A closed surface circulation exists at least 60 h prior to genesis in the $-5\,\mathrm{ms}^{-1}$ gauge, but as already noted, this speed is inappropriate for the LT wave[34]. In the properly translating frame ($-9\,\mathrm{ms}^{-1}$) the surface circulation closes at 1800 Z on 17 August, 48 h prior to best-track genesis. There is an implied delay (albeit short) between the formation of a closed circulation in the lower free troposphere relative to the surface. It is too early to say whether downward burrowing of a closed gyre to the surface from above is a universal behavior in all 55 cases; the largest and/or earliest translating gyres can be found at *any* of the analyzed LT levels (1000–600 hPa) depending on the storm. A closed surface circulation, nonetheless, is present in most cases together with a modest vertical shear extending to the UT and other environmental stimulants as identified in Figs. 31–32. These observations confirm H1, establishing that the locus of gyre formation and organization of deep convection is in the lower half of the troposphere, while leaving some important details (e.g., communication between the lower free troposphere and boundary layer) for future study. On balance, conditions throughout the depth of the troposphere in this event seem very favorable for tropical cyclogenesis via the tropical wave pathway. But as already noted, Debby was not unique in this respect. Similar conditions are found in most of the cases selected for the "quasi-monochromatic easterly wave" category.

[34]Monsoon circulations (although tied to stationary land surfaces) fluctuate slowly in time, implying a non-zero band-width in frequency; closed monsoon gyres are therefore expected in a modest spread of gauges about zero translation speed, as observed in this case. Monsoons do not give birth to tropical depressions, but tropical waves and monsoon depressions do. For genesis it is not the translation speed of monsoon circulations that is important, but that of waves.

5.3 Vertical signature of waves and diabatic vortex prior to genesis

A distinct *signature* of the parent wave and diabatic proto-vortex just prior to genesis can be seen in Debby and in other cases examined to date, that is, a set of defining characteristics that help to discriminate these two entities. Recognition of how these characteristics evolve in the day or two immediately preceding genesis may prove useful for diagnosis and prediction of incipient storm development. The vertical structure of wave and vortex seem especially important in this regard. As noted in the preceding subsection, the parent wave of Debby translates westward at about 8–10 ms^{-1}, with little vertical phase tilt up to the mid-troposphere and abrupt decrease of amplitude above. Meanwhile, an extensive anticyclonic gyre develops in the upper troposphere and propagates west, but with slower phase speed than the wave, about 5–6 ms^{-1}. It is thought that the UT anticyclone may have originated from diabatic forcing by deep moist convection at 36–38° W about 30 h prior to genesis time. Figure 10 indicated that persistent convection was seen by TRMM during this sequence, aligned well with the translating gyre, especially at the beginning. Remarkably, the ERA-40 stream function and velocity potential, when examined together, seem to confirm these two signatures – noting the important caveat that the analyzed divergence is driven in part by the model's cumulus parameterization and therefore subject to uncertainty. Velocity potential in the upper troposphere indicates a strong divergence anomaly in the upper troposphere propagating westward during the 30-h sequence from 36–38° W to the exact location of genesis at genesis time, accompanied by a convergence anomaly in the lower troposphere propagating westward in parallel, 1 or 2° south of this track as shown in Fig. 36a–d . The vertical alignment of these anomalies of opposite sign is similar to the "first baroclinic mode" structure of tropical depression disturbances in the western Pacific (Dunkerton, 1993) but very different from the vertically trapped, ∼ equivalent barotropic structure typical of Atlantic easterly waves that are not diabatically activated. We conjecture that a vertical dipole structure indicates activation by one or more diabatic vortices and their associated deep moist convection within the

mother pouch of the wave. In Debby and in other cases examined, excitation of a UT anticyclone above the LT disturbance provides a spectacular early warning signal in the dynamical fields that seems to corroborate well with convective precipitation retrieved from TRMM measurements.

Forecasters consider in advance many signatures of possible TD genesis; for some of these the upper tropospheric flow plays a role, as in vertical shear, upper-level diffluence or divergence, and of course, deep convective cloud-top temperature. For such indicators it is often impossible to distinguish cause and effect, since one could just as well interpret their presence as indicating that a tropical depression already exists, but has not yet been officially recognized. The main hurdle in identifying a TD-stage disturbance is the inability to see a closed rotational flow the lower troposphere in visible or infrared imagery when obscured by clouds aloft. In this respect it is worthwhile to recognize the often crucial role played by the upper tropospheric flow in identifying conditions which either are favorable to development or indicate that development is already in progress. Owing to tremendous strides in the assimilation of cloud and water-vapor winds in operational analyses over the last two decades (e.g., Velden, 1997, 2005) the free troposphere flow is well-represented on the synoptic scale (a compliment that excludes the TTL and lower stratosphere, due to insufficient cloud coverage or water vapor content, and lower troposphere in regions where thick clouds obscure). To the extent that both lower *and* upper troposphere horizontal winds are captured faithfully by the analyses on the synoptic scale, it is possible to identify TD-like conditions in the parent wave from the vertical structure of wind anomalies: specifically, a "first baroclinic mode" structure or stacked arrangement of LT cyclone and UT anticyclone.

Such features – as one might expect us to say, by now – are best revealed in a frame of reference translating with the parent wave. But in the case of Debby and more generally, *there is no need for the optimum translation speeds to be identical throughout the depth of the troposphere*. Indeed, it is likely that a trapped LT disturbance propagates at a slightly different speed than a diabatically activated LT-UT dipole. There are multiple reasons, the simplest being that gross moist stability is reduced by the la-

tent heating associated with deep moist convective precipitation, causing wave phase speed of moister waves to be slower than that of drier waves. In the language of tidal theory it could be said that the equivalent depth of the proto-vortex and its induced flow is smaller than that of the original parent wave, which sees a larger area and more dilute distribution of precipitation than the proto-vortex itself and its upper tropospheric signature. We therefore expect a diabatic Rossby wave and diabatic Rossby vortex to propagate at slightly different speeds, the speed of the wave depending, among other things, on the degree of convective heating seen by the wave, via the gross moist stability. An isolated vortex is expected to propagate at the speed of the local mean flow (excluding the effects of unbalanced motions, if any) which, as noted in Sect. 2, matches the phase speed of the wave at the critical latitude. There are kinematic reasons for the parent wave and proto-vortex to remain together, at least within some maximum distance as determined by the dimensions of the translating gyre. But they do not necessarily walk in lock step. The marsupial paradigm evidently allows some "slop" in the exact position of the vortex relative to the wave trough, i.e., slightly different propagation speeds which (as in Debby and other cases) are *measurably* different. Key to the success of the marsupial mechanism is that the respective horizontal velocities not differ too much either in speed or azimuthal direction.

Broadly speaking, for diagnostic purposes and short-term prognosis, we conclude that (i) stream function in the lower to mid-troposphere provides a good representation of the incident wave structure, along with velocity potential in the lower free troposphere above the boundary layer, while (ii) velocity potential in the boundary layer and upper troposphere, along with stream function in the upper troposphere, provide a good representation of diabatic vortex and/or modification of wave structure once diabatic activation has occurred.

6 Conclusions, new visions and directions

The genesis of tropical cyclones was described by Emanuel (2005) as one of the remaining "great mysteries of the tropical atmosphere." The persistence of the mystery over many decades underscores the difficulty of the problem: like the conquest of Mount Everest, a formidable "ascent" from observational, numerical *and* theoretical directions. Some of the processes involved in genesis occur at horizontal scales which are very small and unresolved by analyses such as ERA-40 on a $\sim 1^{\circ}$ grid. Numerical models need much finer resolution than this in order to capture the mesoscale construction of the incipient PV monolith in a realistic manner (e.g., M06). But the mystery also exists because of an imperfect theoretical understanding of fluid dynamics and thermodynamics that comes from working in an Eulerian framework. We have produced and advocated in this paper a pseudo-Lagrangian framework for the study of tropical cyclogenesis and have chosen the simplest of all scenarios to present the fundamental concepts involved in a Lagrangian description. These genesis events were associated with quasi-monochromatic easterly wave disturbances which account for the majority of tropical cyclones in the Atlantic and eastern Pacific sectors (if we allow in some cases for hydrodynamic instability to account for the waves themselves). To the extent that the phase speed of waves is reasonably constant over their life cycle, the coordinate system may be translated westward to match the phase speed of the incident wave. By examining streamlines in the translating frame a pseudo-Lagrangian picture of the flow is obtained in which trajectories and streamlines are nearly equivalent over a time span of a few days. Because the divergent component of horizontal flow is small relative to the rotating component, with certain exceptions, streamlines in the translating frame are closely approximated by a stream function with the appropriate "gauge" added corresponding to the speed of translation. This device enables us to identify approximate Lagrangian boundaries in the flow without actually performing trajectory calculations. To confirm inferences from the pseudo-Lagrangian diagnostics we calculated back-trajectories from within the closed gyre (Sect. 5.1).

The evolution to a tropical depression evidently requires the formation of closed streamlines in the translating frame, comprising a westward-moving cyclonic gyre at meso-α. In ERA-40 analyses, closed streamlines are observed prior to TD formation as declared officially, sometimes by 30 h or more. In the quasi-monochromatic cases examined here, we have identified the tropical wave critical layer with these closed streamlines, known in nonlinear critical layer theory as "cat's eyes". One or more cat's eyes aligned zonally are present prior to genesis in virtually all cases. Formation of closed streamlines is also common in quasi-2-D turbulence and involves, as it were, the creation of new vortex coordinate system when a separatrix appears in the flow. It is at this point that the Jacobian of the mapping from isentropic PV (or isobaric vorticity) to physical coordinates becomes singular as material contours connecting the vortex to its parent flow are distended into a thin, wispy filament. For practical purposes (as accomplished, e.g., by contour surgery) we end up with a detached vortex with its own identity and closed isopleths of PV (vorticity). In the translating frame the good agreement between vorticity isopleths and streamlines or stream function contours, and the near-coincidence of gyre center with eventual TC development in most cases, confirms our choice of translation speed or "gauge" and strongly suggests that the flow kinematics within the critical layer influence mesoscale developments subsequent to gyre formation. Our first hypothesis (H1) is confirmed by these observations.

In a nonlinear critical layer the Lagrangian mean zonal flow is asymptotically discontinuous at the edge of the cat's eyes (Fig. 1; Andrews and McIntyre, 1978) indicating the creation of three separate air masses. In cyclonic latitudinal shear the cat's eyes themselves are cyclonic and their isolation effectively separates the air within from the exterior flow. Thus, even though an *easterly* jet (e.g., AEJ) does not afford the same barrier to meridional transport[35] as typical of *westerly* jets in rotating planetary atmo-

[35]Among the reasons cited by Dunkerton and Scott for the apparent transport barrier is the fact that a westerly jet core on a stable gradient of PV cannot be the locus of a free Rossby wave critical level/latitude; therefore, isopleths of PV tend to remain elastic at this location (McIntyre, 2003) and irreversible displacements, if any, are limited in meridional extent (e.g.,

spheres (Dunkerton and Scott, 2008), the critical layer south of the jet axis may itself provide some degree of protection from dry air to the north, air often associated with the Saharan Air Layer (SAL). Such protection is available only if persistent waves exist on the jet with amplitude that is neither too small (as to be insignificant) nor too large (as to draw air from the SAL north of the jet axis)[36].

In real life the ideal critical layer sometimes appears, but more often takes the form of an isolated or asymmetric vortex. The flow kinematics of an isolated vortex are very different when viewed in translating and resting frames. The location of principal separatrix in the translating frame, connecting the proto-vortex to the exterior flow to the east, north or west, but not south[37] of the gyre center, has two implications:

(i) The critical latitude of stable incident waves lies equatorward of the inflection point where cyclonic vorticity is maximum, therefore the developing gyre is able to tap the relatively high vorticity that exists near the inflection point closer to the axis of the jet[38].

(ii) Air entering the gyre, for the most part, is not coming from distant points to the

Panetta, 1993). This situation contrasts with an easterly jet core, which can serve as the locus of instability with critical level/latitude near the core (Lindzen et al., 1983) or (if stable) the locus of critical-layer development owing to the weakness of shearing deformation along the jet axis (Brunet and Warn, 1990; Brunet and Haynes, 1995). Whatever barriers to meridional transport that may exist on an easterly jet will depend on the *inhomogeneity* of stirring that comes about owing to the finite extent of the critical layer itself.

[36]Large-amplitude easterly waves, that is, with large meridional extent, may be ineffective for TC genesis owing to the latter reason. These waves are often observed to precede a new SAL air mass as it sweeps across the tropical Atlantic.

[37]The resting frame is misleading in this respect: an upright omega pattern with separatrix south of center is usually implied, consistent with Fig. 3c.

[38]A disturbance growing on an unstable meridional gradient of PV would tap mean vorticity at the inflection point *equatorward* of its critical level. The observed distribution of separatrix location does not preclude instability altogether, but seems to argue against this simplest of instability configurations in the context of TC genesis. A more accurate portrayal of "instability" in this context depicts either (i) eddy shedding *to the west* of a moist vortex strip (as in the African/Atlantic sector) or (ii) unstable interaction between a monsoon gyre and waves incident

south, whether wet (as from an ITCZ far away) or dry (as from the equator). Instead – consistent with our comparison of the analyzed saturation fraction and observed precipitation – moisture is provided to the gyre by moist convection directly.

Moisture injected into the free troposphere above the boundary layer by deep convection is then transported horizontally, some of it into the center of the gyre and some to the east, escaping the region of interest. When *ambient* moisture is also available, it is entrained passively into the cat's eye along with cyclonic vorticity, from adjacent environments (convergence zone or monsoon gyre to the east or west) in which these two variables are positively correlated above the boundary layer. Whether or not entrainment of pre-existing moisture is significant, the Lagrangian boundaries of the developing gyre serve to protect this region from lateral intrusions of dry air. Thus, the same convection that aids the development and concentration of cyclonic vorticity also provides moisture to the column, maintaining the preference for convective over stratiform precipitation – a preference, as we have argued above, favors low-level development. Our second hypothesis (H2) is confirmed, in part, by the juxtaposition of analyzed moisture (ERA-40) and observed deep convective precipitation (TRMM) within the gyre. The morphology of deep convective and stratiform cloud, and inferred profile of diabatic heating in the gyre, also support H2.

The marsupial paradigm provides a convenient and self-consistent framework for the coupled dynamical/thermodynamical processes that are essential to tropical cyclogenesis. Our analysis has highlighted the role of tropical wave critical layers as preferred loci for the formation and aggregation of diabatic vortices which represent moist coherent structures on the mesoscale. The critical layer is where the mean flow in the direction of wave propagation, and wave phase speed, are similar, implying that cutoff vortices will be able to travel with the wave (in this case, westward) for a time. The coherent relationship that exists between the wave and vortex serves to preserve both. It preserves the vortex because the Lagrangian boundaries formed by the wave at its critical layer remain in the same phase of the wave as it propagates. These boundaries

from the east (as in the western Pacific).

appear stationary or slowly varying in the translating coordinate system. Also, diabatic heating associated with the spawned vortices acts coherently to maintain the wave to the extent that these vortices are able or inclined to keep step with the wave, as implied by the preceding argument. This phase locking, however, does not persist indefinitely, and when a vortex becomes sufficiently strong[39] it may acquire its own propagation characteristics which usually involves some degree of meridional propagation that the wave did not have originally as well as a slower horizontal speed. The vortex is then no longer propagating with its parent wave. This sequence of events we have described as the marsupial paradigm because the wave is providing a pouch or sweet spot for cyclonic vortex development, up-scale aggregation, convective moistening and diabatic amplification. This process has a finite gestation period. Once the vortex leaves, the wave is often observed to weaken or die when viewed in NHC/TPC surface analyses. Multi-dimensional visualization of ERA-40 data suggests also a subsequent radiation of waves, either from the genesis region itself or from the new translating vortex, that introduces new variance in the upper troposphere that would otherwise be absent if the parent wave simply died.

Our third hypothesis (H3) is consistent with these observations; further quantitative proof is outside the scope of this paper. Phase-locking of wave and proto-vortex for ±3 days about the best-track genesis time is more prominent in stronger waves than in weaker waves, the latter seeming to exert less influence on the direction of vortex propagation. As for the effect of vortex on wave, there are numerous instances in which the speed of zonal phase propagation is reduced after genesis, although this behavior is not universal. Model results (to be reported separately) confirm that a diabatically activated easterly wave is slowed, by about 20%, relative to its initial speed

[39] Our modeling study establishes that vortex merger and convective amplification play equally critical roles in the selection of a dominant vortex in the "pouch" (Montgomery, M. T., Wang, Z., and Dunkerton, T. J.: Intermediate and high-resolution simulations of the transition of a tropical wave critical layer to a tropical depression, Atmos. Chem. Phys. Discuss., in preparation, 2008.).

prior to vortex development. Observations from ERA-40 indicate a prominent signature of diabatic activation in the upper troposphere above the developing storm, as seen by a quadrupole structure of meridional velocity anomaly in the longitude-height plane. Similar structure comprised the leading mode of meridional velocity variance in the western Pacific during boreal summer (Dunkerton, 1993). Its occasional presence in Atlantic and eastern Pacific sectors, uniquely associated with TC genesis in these regions, may prove important in diagnosis and short-term prediction. Forecasters show keen interest in anticyclonic outflow in the UT when it exists prior to intensification. Divergence and anticyclonic rotation above the proto-storm adds a piece of information to the marsupial paradigm and supports the notion that the mother gyre and child vortex have different personalities, i.e., contrasting vertical structures and slightly different horizontal propagation speed and/or direction.

In freely evolving 2-D turbulence or in nonlinear waves on a shear flow, closed recirculation regions occur as a result of horizontal advection induced by the PV itself. Such features are relatively long-lived and robust in their inner core ("coherent structures") while contributing to deformation (or instability) on their flanks and in the neighboring flow. In some sense, coherent structures can be said "to contribute to the forward enstrophy cascade while remaining immune from its immediate effects." Our analysis of pre-genesis environments has demonstrated (i) the robustness of the tropical wave critical layer as well as (ii) its contribution to vorticity/moisture entrainment/containment and (iii) protection of the proto-vortex from the exterior flow. These properties suggest a role for the forward enstrophy cascade in TC genesis extending beyond the formation of a tropical wave critical layer in the first place. In the real world, however, simple analogies with waves and 2-D turbulence are inadequate, owing to moist diabatic processes associated with deep convection, an essential ingredient in proto-vortex development. Horizontal advection by synoptic and meso-α motions alone cannot account for TC formation, even though they are expected to create variance at meso-β via the forward enstrophy cascade. In discussing vorticity evolution and the topology of streamlines it is essential to distinguish the tropical cyclone from the sub-synoptic gyre in which it

forms:

(i) In tropical cyclones, isolated vortices are significantly amplified by diabatic processes associated with deep moist convection. It is impossible to obtain the values of vorticity observed in these systems by advective rearrangement alone; cloud system processes enhance vorticity by tilting and stretching of vortex tubes (on the order of 100 times ambient values: M06). It is thought by nearly everyone (by top-down and bottom-up schools, in diabatic Ekman turbulence and VHT pathways) that vortices created on the cloud-system scale undergo horizontal upscale aggregation subsequently to form the tropical cyclone; this aggregation further organizes deep convection and vortex-scale convergence due to the radial overturning circulation.

(ii) In the marsupial paradigm, the creation of an isolated vortical air mass by advection in the horizontal plane pertains not to the tropical cyclone itself, but to the gyre in which TC formation may subsequently occur. (The role of upscale aggregation in the critical layer will be discussed in our modeling study.) We believe that whereas upscale aggregation of vorticity and its amplification by deep convection are essential to TC formation, they are not entirely responsible for the formation of a closed tropical depression in the first place. This formation is at least partly due to the dynamics of moist waves and involves a direct enstrophy cascade from larger synoptic-scale disturbances to mesoscale vorticity anomalies. This argument rests on the coherent relationship observed between the critical layers of tropical waves and tropical cyclogenesis events occurring such regions. Storm formation at or near the center of the translating gyre in many cases seems almost uncanny and suggests to our minds an invisible "guiding hand" from synoptic and meso-α scales.

Firmly established in our observations of gyres in the translating frame is that the advective rearrangement of vorticity draws air with cyclonic vorticity into the cat's eye from an inflection point north of the critical latitude (in hydrodynamically stable cases) supporting H1. Such a transport pathway, visible in the translating frame but oblivious to observers in the resting frame, does not immediately suggest moistening of the gyre by horizontal advection from an ITCZ to the south, nor drying from latitudes closer to

the equator. Moreover, it was suggested in Sect. 2.2 that chaotic advection associated with mesoscale circulation anomalies may dilute or delay moistening of the critical layer by deep moist convection. What we neglected to say at that point, by way of speculation, is that the same anomalies may create *low-level vorticity boundaries* within the critical layer that stimulate deep convection via Ekman pumping, providing in situ moistening of the column, an essential ingredient in H2. This is one of a limited number of mesoscale mechanisms that may link chronologically the formation of a closed gyre at meso-α with TC genesis at meso-β. Another mechanism relies on lateral confinement of small-scale waves excited by convection in the proto-vortex (Ritchie et al., 2003). A third mechanism assists development by lateral confinement of outflow boundaries (M06). All three mechanisms involve some degree of "imbalance" due to boundary-layer drag, inertia-gravity waves or density currents in the lower troposphere. The first mechanism (Ekman triggering) is likely to dominate in a rotating environment approaching column saturation, while the latter mechanisms (involving waves or density currents) typify convective clouds in a sub-saturated environment, with their downdrafts and cold-pool outflow. Outflow boundaries in SAR imagery are distinctly absent in the inner core of developing storms but commonly seen in the outer bands (Katsaros et al., 2000; Black et al., 2005; Dunkerton et al., 2008b[40]). From these precious observations we infer that successful development entails a transition from (i) a canonical MCS mixture of updrafts and downdrafts (with unbalanced motions in all azimuthal directions having a negative net impact on boundary-layer moist entropy) to (ii) a smoother and more axially symmetric in-up-out meridional overturning circulation organized and maintained by a combination of interior heating and Ekman convergence. The radial inflow and resulting tangential circulation assist further development by wind-induced surface evaporation.

These ideas provide a road map for exploration of synoptic-mesoscale linkages essential to tropical cyclogenesis, an exciting area of research in the years ahead. For

[40]Dunkerton, T. J., Walter, B. A., Perrie, W., Long, D. G., Nie, C., Zhang, J., Rogers, R., and Black, P.: Images of Katrina (2005) below the cloud, Science, in preparation, 2008b.

tropical cyclogenesis in tropical waves, our analysis begins to close the gap between observationally resolvable scales (synoptic, meso-α) and cloud scales (meso-γ) that require numerical models. To recap: processes accounting for the formation of cyclonic anomalies in a tropical wave critical layer are preferentially associated with tropical cyclogenesis (H1). The formation of closed streamlines implies that the air within the materially closed space is protected, to some degree, from lateral entrainment of dry air (H2). Therefore the closure serves not only to concentrate vorticity via the direct cascade but may also account for the accumulation of moist entropy and saturation of the tropospheric column by persistent deep moist convection that occurs within. This containment has a very important effect in allowing a convective type of heating profile to dominate the closed region with a relatively lesser contribution from stratiform precipitation that is otherwise common in mesoscale convective systems (Tory and Montgomery, 2006). The maximum heating occurs at a lower altitude than normal for organized tropical convection, favoring surface convergence and rapid spin-up of one or more low-level vortices. We conjecture that this process, representing a "non-advective" transport of PV (Haynes and McIntyre, 1987) by hot towers in an environment of large saturation fraction (exceeding ~80%) provides a direct "bottom-up" pathway to tropical cyclogenesis (Halverson et al., 2007) more or less independent of the mid-level PV transport associated with typical mesoscale convective systems in the tropics.

Persistent deep convection in the gyre and its signature in the upper troposphere observed prior to official TD declaration suggests that anomalous diabatic processes are already operating in this region: anomalous with respect to temporal duration, vertical profile of heating and the resulting profiles of vorticity and divergence. How these anomalies translate into TC formation remains something of a mystery because the mesoscale processes most relevant to storm development are uncertain, while available observations lack sufficient resolution to settle the matter. For this reason, we cannot establish that gyre formation in the translating frame is completely sufficient for tropical depression formation. Nonetheless, a critical role for a closed surface gyre

is supported by these observations. Further insight into mesoscale processes that link gyre formation to ensuing developments will help to establish how far the forward enstrophy cascade penetrates the mesoscale before cloud-system processes trigger the inverse cascade and ultimately dominate the intensification phase via upscale aggregation. With a Lagrangian framework for flow kinematics (relevant to the forward cascade) and a cloud-system resolving model (needed for the inverse cascade) a direct assault on mesoscale processes leading to tropical cyclogenesis at meso-β is now feasible. The summit of the mountain is within reach, so to speak.

The multi-scale problem just described would be complicated enough if confined to a horizontal plane, but nature provides a vertical dimension, or degree of freedom, absent from the 2-D model. We have attempted to draw some preliminary conclusions from the vertical structure of waves, proto-vortex and mean flow (Sect. 5) but most of the work on this aspect of the problem remains to be done. Identification of a gyre boundary in the translating frame enables a quantitative estimate of vertical shear seen by the developing storm, in addition to its intrinsic properties (vorticity, moisture, deep convection and recirculation time; Table 1, Figs. 31–32). It seems that genesis is favored in regions of weak vertical shear. The shear need not be identically zero, nor as small as the "shear of the climatology", but the typical 850–200 hPa shear at the genesis point observed in our survey of events is modest ($<12\,\mathrm{ms}^{-1}$) in agreement with previous studies. Zero shear would imply that the flow kinematics at any two levels are the same. Of course this is never exactly so. Horizontal transports of cyclonic vorticity and moisture are therefore likely to be somewhat different in all cases, but they are seldom radically different. Nor would it be correct to regard TC genesis in these basins as resulting from little more than "stratified turbulence" in which horizontal flows at different levels overlap randomly. Incident waves are usually observed at both levels with similar amplitude and phase. In regard to the vertical structure of horizontal transport (of vorticity and moisture) the *marsupial paradigm*, with its approximately equivalent barotropic structure of lower-tropospheric waves, provides a much more realistic picture of tropical cyclogenesis than the *stratified turbulence paradigm*. The latter may

describe better the relation of upper tropospheric flow to that of lower levels, the upper levels often influenced by intrusion of extratropical anomalies uncorrelated with the lower tropical troposphere.

Vertical alignment of the marsupial pouch as a favorable condition for TC genesis helps to mitigate the deleterious effect of vertical shear on the nascent storm:

"A major inhibitor of genesis is the presence of vertical wind shear, defined as the change in direction and/or speed of the wind with altitude... If there is no wind shear, a nascent tropical system just moves along with the wind (which, in the absence of shear, has the same speed and direction at all altitudes). No air flows through the storm. But if wind shear is present, the storm tries to move along at an average wind speed, and at some altitudes wind must blow through the storm. This storm-relative flow can import dry air from outside the cloud cluster, destroying the humid column of air that is needed for genesis. For this reason, wind shear is inimical to genesis." (From *Divine Wind: The History and Science of Hurricanes* by K. Emanuel, 2005, p. 97.)

Although additional reasons were noted in Sect. 2, having to do with the effects of vertical shear on convective organization, two aspects of the marsupial paradigm were anticipated in Emanuel's reasoning: the need for weak storm-relative flow and some protection from dry-air intrusion. The role of the critical layer in helping to provide these conditions was formulated in our second hypothesis (H2). Later in the same chapter, the author describes the transition from a subtle surface signature of easterly-wave passage, to a more robust closed surface circulation:

"We observe that occasionally, especially in late summer and early fall, the amount of convection associated with a particular wave increases, and winds near the surface evolve from a typical wavy pattern of an easterly wave into a closed circulation. A tropical depression is born." (Ibid., p. 99.)

We would go, of course, a step further and identify a closed cyclonic circulation *in the translating frame* as the critical ingredient for depression formation (see Appendix A). The author, nonetheless, recognizes the apparent need for a closed gyre at or close to the surface, a feature which by no means is present in all waves, but clearly exists

in the developing cases considered in this paper. As to why the surface gyre forms, and why it is important to genesis, we are left to speculate that (i) diabatic activation[41] of the wave by deep moist convection is needed to amplify the effect of an otherwise "dry" critical layer[42] (H3) while (ii) Ekman pumping from the tropical boundary layer is needed (or desirable, at least) to organize convection in a ring-like pattern about the proto-vortex (Eliassen and Lystad, 1977; Van Sang et al., 2008). In a rotating environment such pumping is sensitive to the radial gradient of absolute vorticity (Ooyama, 1969; Hack and Schubert, 1986). The role of boundary-layer forcing in a translating frame was studied in the classic paper by Shapiro (1983) for mature hurricanes. Wind speeds in the proto-vortex are considerably less, but (as in a mature system) surface drag varies quadratically with wind speed for speeds greater than a few ms^{-1} but less than 25 knots. Therefore, azimuthal asymmetries of BL forcing are relevant to tropical depression formation.

A curious observation especially over the eastern Pacific is that the location of TC genesis often lies on or very near a boundary between moist and dry air in the environmental flow. Without further study it is unclear what impact this moisture boundary has either on the dynamics of the incident wave (instability) or the development of coherent structures on the mesoscale. It seems possible that the ambient moisture and its horizontal transport in such situations have a greater role to play than implied in the preceding discussion. A closed gyre with ∼50% overlap of an initially moist region inevitably will entrain the existing moisture in addition to any further moistening by deep

[41] It is clear from Berry and Thorncroft (2005) that the amplitude of waves emerging from West Africa into the Atlantic sector is generally not a good indicator of future development, except near the coast.

[42] Tropical waves display moist propagation speed even when not coupled to convection if background convection is present (Dunkerton and Baldwin, 1995) so we may regard the incident easterly waves as linearly moist waves prior to their diabatic activation by a proto-vortex in the critical layer. Subsequent to activation, organization of convection by the wave-vortex hybrid implies a "conditional" or phase-dependent diabatic heating.

convection triggered by the development of the gyre. Such entrainment, as already noted, shortens the time required to saturate the column. This argument does not account, however, for the overlap of gyre and moisture gradient in the first place. Perhaps the moisture gradient is helping to define the effective moist PV gradient (Sobel et al., 2001) seen by the incident wave (instability) and the resulting selection of phase speed, hence, critical latitude. More investigation of this observation is warranted.

An over-arching conclusion emerging from this study regarding easterly waves – whether neutral waves, quasi-modes, or hydrodynamic instabilities – is that the juxtaposition of wave critical latitude, inflection point, and moisture gradient (if any) is centrally important to genesis. The first and most easily appreciated conclusion is that the critical latitude south (not north) of the easterly jet axis is the locus of cyclonic vorticity and its subsequent amplification. The second and less obvious conclusion, which becomes obvious in the translating but not resting frame, is that a neutral or slowly-decaying quasi-mode having its dominant phase speed *outside* the range of mean flow speeds within the region of reversed potential vorticity gradient is able to tap the mean cyclonic vorticity near the inflection point of the jet. This situation contrasts with that of an unstable disturbance with critical latitude *inside* this range, closer to the jet axis. A possibly significant role for hydrodynamically *stable* waves in this context is counter-intuitive: one might be tempted to think that large-scale instability implies a more vigorous sequence of events that would invariably lead to genesis more readily than what might be triggered by a neutral or slowly decaying wave. But we must be willing to entertain less intuitive ideas in order to understand the possible preference for neutral or slowly decaying modes in TC genesis. (i) These modes are maintained by diabatic heating, in addition to their "dry" maintenance (compact spectral content). (ii) Genesis is an interactive multi-scale process and not simply a consequence of moist hydrodynamic instability. If the quasi-mode configuration as described above favors mesoscale development, then it may actually be more favorable for genesis than a more vigorous unstable wave. Oddly enough, the fact that the instability paradigm in reality applies only to a minority of cases seems to support such counter-intuitive thinking.

Perhaps the most impressive and humbling aspect of these observations is the great variety of flow configurations seen in the 55 cases selected for study. Although generally similar and tending to support the marsupial paradigm, no two events are exactly alike. Their similarities prevent us from labeling TC genesis as an entirely turbulent process, thanks to the underlying synoptic wave structure and its implications for flow kinematics when superposed on the adjacent easterly jet. In the translating frame, the region of closed circulation displays a preferred, non-random orientation with respect to the jet axis and its associated gradients of vorticity and moisture. The basic state represents a "coherent structure" in the lingo of contemporary GFD, just as the tropical depressions that form on it, and grow for a time within their parent waves. So the real world of TC genesis is not a story about quasi-2-D turbulence nor a moist generalization thereof – not exclusively, at least. Nonetheless, differences from one event to the next compel us to recognize the disordered and variable nature of the sub-synoptic dynamics, a characteristic partly attributable to quasi-2-D turbulence on the mesoscale but easily magnified by rotating 3-D-convective turbulence, as contained in the ubiquitous "vortical hot towers" (Frank and Johnson, 1969; M06). One can hardly imagine a more fascinating interactive, multi-scale system in nature than this.

Appendix A

Translation of non-sequential imagery

Our method for translation of analyses and imagery into a frame of reference moving with the parent wave is easily applied to non-sequential images (e.g., sparse or irregular temporal sampling from polar-orbiting satellites) if the wave's propagation speed and direction are known from other data sources. For historical cases a retrospective estimate of C_p is straightforward (see text) whereas in real-time applications a one-sided estimate should suffice. In either event, analyses from meteorological centers and global forecast models will provide the requisite information about waves. The

existence of a closed gyre is insensitive to small ($\sim$1 ms^{-1}) errors in the estimate of C_p while its exact location and orientation of flow separatrix are more sensitive to this choice. Larger errors are fatal: as demonstrated in Sect. 4, major differences generally exist between streamline and stream function patterns in a resting frame (C_p=0) and a frame of reference moving westward at a speed typical of Atlantic easterly waves ($C_p\sim-5$ to -10 ms^{-1}). We suggest a rule of thumb that a priori information of waves be good enough (sufficiently large and/or persistent waves, plus reliable analysis) to specify C_p to within 1–2 ms^{-1}. If this criterion is met, a simple correction to the resting view of non-sequential imagery can be made if the speed of incident waves is reasonably constant. (If wave properties vary too much, but the temporal evolution of flow pattern is known reliably, a more elaborate correction to determine Lagrangian boundaries and gyre flow can be devised.) We illustrate the effect of translation on the surface wind field obtained from a QuikSCAT image of Hurricane Felix (2007) in the western Atlantic/eastern Caribbean Sea (Fig. 37). Felix was born within an easterly wave with phase speed typical of central Atlantic waves ($C_p=-6.7\pm0.5$ ms^{-1}). By the time of best-track genesis on 31 August (panels c and d) there was considerable rain contamination of retrieved winds (cyan shading). Similar to what was observed in Chris 2000, a closed gyre is seen in the translating frame of reference (b) 48 h prior to "genesis" whereas the resting frame (a) on 29 August gives the appearance of an open wave. Once again the resting frame is misleading and misses a key element in the genesis sequence: the closure of near-surface circulation. Although our analysis of Felix is retrospective, no temporal filter was needed either in Fig. 37 or in the derivation of phase speed C_p on which the zonal translation is based. Rain contamination was not an issue at this time, except in the NE quadrant of the gyre. QuikSCAT imagery evidently can play an important role in identifying a closed surface circulation in the Lagrangian sense (translating frame) particularly in the earliest stages of genesis when deep convective precipitation is less prevalent or intense than in later stages. It was noted previously by Sharp et al. (2002) that vorticity anomalies in QuikSCAT often can identify storms prior to their best-track genesis time. Vorticity is Galilean invariant but a

noisy quantity; translating streamlines provide an alternative measure that is less subject to retrieval errors, unresolved finestructure and rain contamination, provided that the speed of translation is known from other data sources.

Acknowledgements. Our work was motivated, in part, by the continuous and tireless efforts of operational forecasters at the National Hurricane Center/Tropical Prediction Center of NOAA, whose skill at teasing rotational signals out of remotely sensed imagery is unsurpassed. We appreciate the enthusiastic reception of our colleagues attending the recent NASA AMMA/TCSP workshop in Baltimore (May 2007) where an overview of this work was first presented by MTM. This research was supported in part by the National Aeronautics and Space Administration, MIPR NNG07HU171 and Contract NNH04CC63C, the National Science Foundation Grants ATM-0715426, ATM-0649944, ATM-0649946 and ATM-0227632, and by the US Naval Postgraduate School in Monterey, California.

References

Alexander, M. J. and Dunkerton, T. J.: A spectral parameterization of mean-flow forcing due to breaking gravity waves, J. Atmos. Sci., 56, 4167–4182, 1999.

Andrews, D. G. and McIntyre, M. E.: An exact theory of nonlinear waves on a Lagrangian mean flow, J. Fluid Mech., 89, 609–646, 1978.

Andrews, D. G., Holton, J. R., and Leovy, C. B.: Middle Atmosphere Dynamics, Academic Press, 504 pp., 1987.

Bassom, A. P. and Gilbert, A. D.: The spiral wind-up and dissipation of vorticity and a passive scalar in a strained planar vortex, J. Fluid Mech., 398, 245–270 ,1999.

Bengtsson, L., Hodges, K. I., Esch, M., Keenlyside, N., Kornblueh, L., Luo, J.-J., and Yamagata, T.: How may tropical cyclones change in a warmer climate?, Tellus, 59A, 539–561, 2007.

Berry, G. J. and Thorncroft, C.: Case study of an intense African easterly wave, Mon. Weather Rev., 133, 752–766, 2005.

Bessafi, M. and Wheeler, M. C.: Modulation of South Indian Ocean tropical cyclones by the Madden-Julian oscillation and convectively coupled equatorial waves, Mon. Weather Rev., 134, 638–656, 2006.

Bister, M. and Emanuel, K. A.: The genesis of Hurricane Guillermo: TEXMEX analyses and a modeling study, Mon. Weather Rev., 125, 2662–2682, 1997.

Black, P. G., Katsaros, K. B., Drennan, W. M., Lehner, S., and Vachon, P. W.: Interpretation of SAR-observed boundary layer flow structures in hurricanes, NASA Final Report, Work Order No. W-19-835, 58 pp., 2005.

Borth, H.: Fundamental circulation modes in moist rotating atmospheres, Talk presented at a workshop on tropical dynamics, University of Mainz, Mainz, Germany, 2007.

Bosart, L.: The tropical transition of hurricane Alex (2004): An observational perspective, 27th Conference on Hurricanes and Tropical Meteorology, American Meteorological Society, Monterey CA, 2006.

Bracken, W. E. and Bosart, L. F.: The role of synoptic-scale flow during tropical cyclogenesis over the North Atlantic Ocean, Mon. Weather Rev., 128, 353–376, 2000.

Bretherton, C. S., Peters, M. E., and Back, L. E.: Relationships between water vapor path and precipitation over the tropical oceans, J. Climate, 17, 1517–1528, 2004.

Brill, O. L. and Goodman, B.: Causality in the Coulomb gauge, Am. J. Phys., 35, 832–837, 1967.

Brunet, G. and Warn, T.: Rossby wave critical layers on a jet, J. Atmos. Sci., 47, 1173–1178, 1990.

Brunet, G. and Haynes, P.: The nonlinear evolution of disturbances to a parabolic jet, J. Atmos. Sci., 52, 464–477, 1995.

Burpee, B.: Characteristics of North African easterly waves during the summers of 1968 and 1969, J. Atmos. Sci., 31, 1556–1570, 1974.

Carlson, T. N.: Synoptic histories of three African disturbances that developed into Atlantic hurricanes, Mon. Weather Rev., 97, 256–276, 1969.

Chang, C. P., Morris, V. F., and Wallace, J. M.: A statistical study of easterly waves in the western Pacific: July–December 1964, J. Atmos. Sci., 27, 195–201, 1970.

Chang, C.-P., Liu, C.-H., and Kuo, H.-C.: Typhoon Vamei: an equatorial tropical cyclone formation, Geophys. Res. Lett., 30(3), 50–53, 2003.

Davis, C. A. and Bosart, L. F.: Numerical simulations of the genesis of Hurricane Diana (1984). Part I: control simulation, Mon. Weather Rev., 129, 1859–1881, 2001.

Davis, C. A. and Bosart, L. F.: The TT problem: forecasting the tropical transition of cyclones, Bull. Amer. Meteor. Soc., 85, 1657–1662, 2004.

DeMaria, M., Mainelli, M., Shay, L. K., Knaff, J. A., and Kaplan, J.: Further improvements to the Statistical Hurricane Intensity Prediction Scheme (SHIPS), Weather Forecast., 20, 531–543, 2005.

Doblas-Reyes, F. J. and Déqué, M.: A flexible bandpass filter design procedure applied to midlatitude intraseasonal variability, Mon. Weather Rev., 126, 3326–3335, 1998.
Dunion, J. P. and Velden, C. S.: The impact of the Saharan Air Layer on Atlantic tropical cyclone activity, Bull. Amer. Meteor. Soc., 85, 353–365, 2004.
Dunkerton, T. J.: Intensity variation and coherence of 3-6 day equatorial waves, Geophys. Res. Lett., 18(8), 1469–1472, 1991.
Dunkerton, T. J.: Observation of 3–6-day meridional wind oscillations over the tropical Pacific, 1973–1992: vertical structure and interannual variability, J. Atmos. Sci., 50, 3292–3307, 1993.
Dunkerton, T. J.: Evidence of meridional motion in the summer lower stratosphere adjacent to monsoon regions, J. Geophys. Res., 100(D8), 16 675–16 688, 1995.
Dunkerton, T. J.: A tale of two ITCZs – the Jim Holton perspective, Bull. Amer. Meteor. Soc., 87, 1492–1495, 2006.
Dunkerton, T. J. and Baldwin, M. P.: Observation of 3–6-day meridional wind oscillations over the tropical Pacific, 1973–1992: horizontal structure and propagation, J. Atmos. Sci., 52, 1585–1601, 1995.
Dunkerton, T. J. and Crum, F. X.: Eastward propagating ∼2- to 15-day equatorial convection and its relation to the tropical intraseasonal oscillation, J. Geophys. Res., 100(D12), 25 781–25 790, 1995.
Dunkerton, T. J. and Scott, R. K.: A barotropic model of the angular-momentum conserving potential vorticity staircase in spherical geometry, J. Atmos. Sci., 65, 1105–1136, 2008.
Edson, R. T. and Lander, M.: Characteristics of the early stages of tropical cyclones as viewed with microwave data, AMS 27th Conference on Hurricanes and Tropical Meteorology, Monterey CA, 2006.
Emanuel, K. A.: The finite-amplitude nature of tropical cyclogenesis, J. Atmos. Sci., 46, 3431–3456, 1989.
Emanuel, K. A.: The physics of tropical cyclogenesis over the eastern Pacific, in: Tropical Cyclone Disasters: Proceedings of ICSU/WMO International Symposium, edited by: Lighthill, J., Zhemin, Z., Holland, G. J., and Emanuel, K., Peking University Press, 136–142, 1993.
Emanuel, K. A.: Some aspects of hurricane inner-core dynamics and energetics, J. Atmos. Sci., 54, 1014–1026, 1997.
Emanuel, K. A. and Nolan, D. S.: Tropical cyclone activity and the global climate system, Talk presented at the AMS 26th Conference on Hurricanes and Tropical Meteorology, Miami, FL,

2004.
Emanuel, K. A.: Divine Wind: The History and Science of Hurricanes, Oxford University Press, New York, 285 pp., 2005.
Emanuel, K. A.: The hurricane embryo, Talk presented at short program workshop entitled "Small scales and extreme events: The Hurricane", NSF Institute for Pure and Applied Mathematics (IPAM), UCLA, 2007.
Eliassen, A.: Slow thermally or frictionally controlled meridional circulation in a circular vortex, Astrophys. Norv., 5, 19–60, 1951.
Eliassen, A.: On the Ekman layer in a circular vortex, J. Meteorol. Soc. Japan, 49, 784–789, 1971.
Eliassen, A. and Lystad, M.: The Ekman layer of a circular vortex: A numerical and theoretical study, Geophys. Norv., 31, 1–16, 1977.
Frank, N. L. and Johnson, H. M.: Vortical cloud systems over the tropical Atlantic during the 1967 hurricane season, Mon. Weather Rev., 97, 124–129, 1969.
Frank, W. M. and Roundy, P. E.: The role of tropical waves in tropical cyclogenesis, Mon. Weather Rev., 134, 2397–2417, 2006.
Frank, W. M. and Young, G. S.: The interannual variability of tropical cyclones, Mon. Weather Rev., 135, 3587–3598, 2007.
Gentry, R. C., Fujita, T. T., and Sheets, R. C.: Aircraft, spacecraft, satellite and radar observations of Hurricane Gladys, 1968, J. Appl. Meteor., 9, 837–850, 1970.
Goldenberg, S. B. and Shapiro, L. J.: Physical mechanisms for the association of El Niño and West African rainfall with Atlantic major hurricane activity, J. Climate, 9, 1169–1187, 1996.
Gore, A.: An Inconvenient Truth, Paramount Classics, US gross revenue to date: $49,047,567, 2006.
Gray, W. M.: Atlantic seasonal hurricane frequency. Part I: El Niño and 30 mb Quasi-Biennial Oscillation influences, Mon. Weather Rev., 112, 1649–1668, 1984a.
Gray, W. M.: Atlantic seasonal hurricane frequency. Part II: forecasting its variability, Mon. Weather Rev., 112, 1669–1683, 1984b.
Green, M. A., Rowley, C. W., and Haller, G.: Detection of Lagrangian coherent structures in 3D turbulence, J. Fluid Mech., 572, 111–120, 2007.
Grotjahn, R.: Different data, different general circulations? A comparison of selected fields in NCEP/DOE AMIP-II and ECMWF ERA-40 Reanalyses, Dyn. Atmos. Oceans, 44, 108–142, 2008.

Hack, J. J. and Schubert, W. H.: Nonlinear response of atmospheric vortices to heating by organized cumulus convection, J. Atmos. Sci., 43, 1559–1573, 1986.
Hack, J. J., Schubert, W. H., Stevens, D. E., and Kuo, H.-C.: Response of the Hadley circulation to convective forcing in the ITCZ, J. Atmos. Sci., 46, 2957–2973, 1989.
Hall, N. M. J., Kiladis, G. N., and Thorncroft, C. D.: Three-dimensional structure and dynamics of African easterly waves. Part II: dynamical modes, J. Atmos. Sci., 63, 2231–2245, 2006.
Haller, G. and Yuan, G.: Lagrangian coherent structures and mixing in two-dimensional turbulence, Physica D, 147, 352–370, 2000.
Halverson, J., Black, M., Braun, S., et al.: NASA's Tropical Cloud Systems and Processes Experiment, Bull. Amer. Meteor. Soc., 88, 867–882, 2007.
Harr, P. A. and Elsberry, R.: Structure of a mesoscale convective system embedded in typhoon Robyn during TCM-93, Mon. Weather Rev., 124, 634–652, 1996.
Hartmann, D. L., Hendon, H. H., and Houze, R. A.: Some implications of the mesoscale circulations in tropical cloud clusters for large-scale dynamics and climate, J. Atmos. Sci., 41, 113–121, 1984.
Hayashi, Y.: A theory of large-scale equatorial waves generated by condensation heat and accelerating the zonal wind, J. Meteorol. Soc. Japan, 48(2), 140–160, 1970.
Heifetz, E., Bishop, C. H., and Alpert, P.: Counter-propagating Rossby waves in the barotropic Rayleigh model of shear instability, Quart. J. Royal Meteorol. Soc., 125, 2835–2853, 1999.
Held, I. M.: Rotating radiative-convective equilibria at low resolution in large domains, Talk presented at short program workshop entitled "Small scales and extreme events: The Hurricane", NSF Institute for Pure and Applied Mathematics (IPAM), UCLA, 2007.
Held, I. M. and Ting, M.: Orographic versus thermal forcing of stationary waves: the importance of the mean low-level wind, J. Atmos. Sci., 47, 495–500, 1990.
Hendon, H. H. and Liebmann, B.: The structure and annual variation of antisymmetric fluctuations of tropical convection and their association with Rossby-gravity waves, J. Atmos. Sci., 48, 2127–2140, 1991.
Hendricks, E. A., Montgomery, M. T., and Davis, C. A.: On the role of "vortical" hot towers in the formation of tropical cyclone Diana, J. Atmos. Sci., 61, 1209–1232, 2004.
Hendricks, E. A. and Montgomery, M. T.: Rapid scan views of convectively generated mesovortices in sheared tropical cyclone Gustav (2002), Weather Forecast., 21, 1041–1050, 2006.
Herring, J. R. and McWilliams, J. C.: Lecture notes on turbulence from the NCAR-GTP summer school, June 1987, Lecture notes by Lilly, D., 171–218, World Scientific, ISBN 9971-50-805-

2, 1989.
Hidalgo, J. M.: Vortical hot towers, their aggregate effects and their resolution dependence in the formation of Hurricane Diana (1984), PhD dissertation, Colorado State University, 184 pp., 2007.
Holton, J. R.: An Introduction to Dynamic Meteorology, Elsevier Academic Press, 4th ed., 535 pp., 2004.
Hoskins, B. J., McIntyre, M. E., and Robertson, A. W.: On the use and significance of isentropic potential vorticity maps, Quart. J. Royal Meteorol. Soc., 111, 877–946, 1985.
Houze Jr., R. A.: Observed structure of mesoscale convective systems and implications for large-scale heating, Q. J. Roy. Meteor. Soc., 115, 425–461, 1989.
Ide, K., Kuznetsov, L., and Jones, C. K. R. T.: Lagrangian data assimilation for point-vortex systems, J. Turbulence, 3(53), 1–7, 2002.
IPCC: Climate Change 2007, Fourth Assessment Report (AR4) of the United Nations Intergovernmental Panel on Climate Change, 2007.
Julian, P. R.: Objective analysis in the tropics: a proposed scheme, Mon. Weather Rev., 112, 1752–1767, 1984.
Katsaros, K. B., Vachon, P. W., Black, P. G., Dodge, P. P., and Uhlhorn, E. W.: Wind fields from SAR: could they improve our understanding of storm dynamics?, Johns Hopkins APL Tech. Digest, 21(1), 86–93, 2000.
Kiladis, G. N., Thorncroft, C. D., and Hall, N. M. J.: Three-dimensional structure and dynamics of African easterly waves. Part I: observations, J. Atmos. Sci., 63, 2212–2230, 2006.
Kimball, S. K. and Mulekar, M. S.: A 15-year climatology of North Atlantic tropical cyclones. Part I: size parameters, J. Climate, 17, 3555–3575, 2004.
Knutson, T. R.: High resolution modeling of hurricanes in a climate context, presentation at AGU Fall Meeting, San Francisco, 2007.
Knutson, T. R., Sirutis, J. J., Garner, S. T., Held, I. M., and Tuleya, R. E.: Simulation of the recent multidecadal increase of Atlantic hurricane activity using an 18-km-grid regional model, Bull. Amer. Meteor. Soc., 88, 1549–1565, 2007.
Knutson, T. R., Sirutis, J. J., Garner, S. T., Vecchi, G. A., and Held, I. M.: Simulated reduction in Atlantic hurricane frequency under twenty-first-century warming conditions, Nature Geoscience, 1, 359–364, doi:10.1038/ngeo202, 2008.
Krishnamurti, T. N., Bedi, H. S., Oosterhof, D., and Hardiker, V.: The formation of Hurricane Frederic (1979), Mon. Weather Rev., 122, 1050–1074, 1994.

Kurgansky, M. V.: Helicity production and maintenance in a baroclinic atmosphere, Meteorol. Z., 15, 409–416, 2006.
Lapeyre, G.: Topologie du mélange dans un fluide turbulent géophysique, Doctoral Thesis, Univ. of Paris, 204 pp., 2000.
Lau, K.-H. and Lau, N.-C.: Observed structure and propagation characteristics of tropical summertime synoptic scale disturbances, Mon. Weather Rev., 118, 1888–1913, 1990.
LeMone, M. A., Zipser, E. J., and Trier, S. B.: The role of environmental shear and thermodynamic conditions in determining the structure and evolution of mesoscale convective systems during TOGA COARE, J. Atmos. Sci., 55, 3493–3518, 1998.
Liebmann, B. and Hendon, H. H.: Synoptic-scale disturbances near the equator, J. Atmos. Sci., 47, 1463–1479, 1990.
Lighthill, M. J.: Waves in Fluids, Cambridge University Press, 504 pp., 1978.
Lilly, D. K.: Stratified turbulence and the mesoscale variability of the atmosphere, J. Atmos. Sci., 40, 749–761, 1983.
Lilly, D. K.: The structure and propagation of rotating convective storms. Part I: energy exchange with the mean flow, J. Atmos. Sci., 43, 113–125, 1986a.
Lilly, D. K.: The structure and propagation of rotating convective storms. Part II: helicity and storm stabilization, J. Atmos. Sci., 43, 126–140, 1986b.
Lin, J., Mapes, B., Zhang, M., and Newman, M.: Stratiform precipitation, vertical heating profiles, and the Madden-Julian Oscillation, J. Atmos. Sci., 61, 296–309, 2004.
Lindzen, R. S.: Wave-CISK in the tropics, J. Atmos. Sci., 31, 156–179, 1974.
Lindzen, R. S. and Tung, K. K.: Wave overreflection and shear instability, J. Atmos. Sci., 35, 1626–1632, 1978.
Lindzen, R. S., Farrell, B. F., and Rosenthal, A.: Absolute barotropic instability and monsoon depressions, J. Atmos. Sci., 40, 1178–1184, 1983.
Lukovich, J. V. and Shepherd, T. G.: Stirring and mixing in two-dimensional divergent flow, J. Atmos. Sci., 62, 3933–3954, 2005.
Magnusdottir, G.: The modeled response of the mean winter circulation to zonally averaged SST trends, J. Climate, 14, 4166–4190, 2001.
Maloney, E. D. and Dickinson, M. J.: The intraseasonal oscillation and the energetics of summertime tropical western North Pacific synoptic-scale disturbances, J. Atmos. Sci., 60, 2153–2168, 2003.
Maloney, E. D. and Hartmann, D. L.: Modulation of eastern North Pacific hurricanes by the

Madden-Julian oscillation, J. Climate, 13, 1451–1460, 2000.
Mandelbrot, B. B.: Intermittent turbulence in self-similar cascades: divergence of high moments and dimension of the carrier, J. Fluid Mech., 62, 331–358, 1974.
Mapes, B. E. and Houze, R. A.: Diabatic divergence profiles in western Pacific mesoscale convective systems, J. Atmos. Sci., 52, 1807–1828, 1995.
Matsuno, T.: Kelvin waves, internal gravity waves and their behaviors in numerical models, Talk presented at the 86th AMS Annual Meeting, Atlanta GA, 2006.
Matsuno, T.: Modeling tropical convective cloud systems by a very high resolution atmosphere model NICAM, Talk presented at ESSL, National Center for Atmospheric Research, Boulder CO, 2007.
McBride, J. L. and Zehr, R.: Observational analysis of tropical cyclone formation. Part II: comparison of non-developing versus developing systems, J. Atmos. Sci., 38, 1132–1151, 1981.
McIntyre, M. E.: On the Antarctic ozone hole, J. Atmos. Terr. Phys., 51, 2973–2994, 1989.
McIntyre, M. E.: Isentropic distributions of potential vorticity and their relevance to tropical cyclone dynamics, in: Tropical Cyclone Disasters: Proceedings of ISCU/WMO International Symposium, edited by: Lighthill, J., Zhemin, Z., Holland, G. J., and Emanuel, K., Peking University Press, 143–156, 1993.
McIntyre, M. E.: On global-scale atmospheric circulations, in: Perspectives in Fluid Dynamics: A Collective Introduction to Current Research, edited by: Batchelor, G. K., Moffatt, H. K., and Worster, M. G., Cambridge, University Press, paperback edition, 557–624, 2003.
McWilliams, J. C.: The emergence of isolated coherent vortices in turbulent flow, J. Fluid Mech., 140, 21–43, 1984.
McWilliams, J. C. and Flierl, G. R.: On the evolution of isolated, nonlinear vortices, J. Phys. Oceanogr., 9, 1155–1182, 1979.
Moffat, H. K.: The degree of knottendness of tangled vortex lines, J. Fluid Mech., 35, 117–129, 1969.
Molinari, J.: Paradigms of tropical cyclogenesis, Bull. Amer. Meteor. Soc., 85, 662–663, 2004.
Molinari, J., Vollaro, D., and Corbosiero, K. L.: Tropical cyclone formation in a sheared environment: a case study, J. Atmos. Sci., 61, 2493–2509, 2004.
Molinari, J., Dodge, P., Vollaro, D., Corbosiero, K. L., and Marks, F.: Mesoscale aspects of the downshear reformation of a tropical cyclone, J. Atmos. Sci., 63, 341–354, 2006.
Molinari, J., Lombardo, K., and Vollaro, D.: Tropical cyclogenesis within an equatorial Rossby wave packet, J. Atmos. Sci., 64, 1301–1317, 2007.

Montgomery, M. T. and Farrell, B. F.: Tropical cyclone formation, J. Atmos. Sci., 50, 285–310, 1993.
Montgomery, M. T. and Kallenbach, R. J.: A theory for vortex Rossby waves and its application to spiral bands and intensity changes in hurricanes, Q. J. Roy. Meteor. Soc., 123, 435–465, 1997.
Montgomery, M. T., Moller, J. D., and Nicklas, C. T.: Linear and nonlinear vortex motion in an asymmetric balance shallow water model, J. Atmos. Sci., 56, 749–768, 1999.
Montgomery, M. T., Bell, M. M., Aberson, S. D., and Black, M. L.: Hurricane Isabel (2003): new insights into the physics of intense storms. Part I: mean vortex structure and maximum intensity estimates, Bull. Amer. Meteor. Soc., 87, 1335–1347, 2006a.
Montgomery, M. T., Nicholls, M. E., Cram, T. A., and Saunders, A. B.: A vortical hot tower route to tropical cyclogenesis, J. Atmos. Sci., 63, 355–386, 2006b.
Montgomery, M. T.: Interactions of tropical waves and diabatic vortices in tropical cyclone formation, NASA-TCSP/NAMMA workshop, invited plenary presentation, Baltimore, Maryland, May, 2007.
Moore, R. W. and Montgomery, M. T.: Re-examining the dynamics of short-scale, diabatic Rossby waves and their role in midlatitude moist cyclogenesis, J. Atmos. Sci., 61, 754–768, 2004.
Moore, R. W. and Montgomery, M. T.: An idealized three-dimensional analysis of the diabatic Rossby vortex: A coherent structure of the moist baroclinic atmosphere, J. Atmos. Sci.,62, 2703–2725, 2005.
Moore, R. W. and Montgomery, M. T.: Dynamics of the 24–25 February 2005 cyclone, 13th Cyclone Workshop, Pacific Grove CA, 2006.
Moulin, F. Y. and Flor, J. B.: Experimental study on wave breaking and mixing properties in the periphery of an intense vortex, Dyn. Atmos. Oceans, 40, 115–130, 2005.
Nolan, D. S., Rappin, E. D., and Emanuel, K. A.: Could hurricanes form from random convection in a warmer world?, AMS 27th Conference on Hurricanes and Tropical Meteorology, 2006.
Ooyama, K.: Numerical simulation of the life cycle of tropical cyclones, J. Atmos. Sci., 26, 3–40, 1969.
Panetta, R. L.: Zonal jets in wide baroclinically unstable regions: persistence and scale selection, J. Atmos. Sci., 50, 2073–2106, 1993.
Pierrehumbert, R.: Local and global baroclinic instability of zonally varying flow, J. Atmos. Sci., 41, 2141–2162, 1984.

Pozrikidis, C.: Introduction to Theoretical and Computational Fluid Dynamics, Oxford University Press, 1997.
Randel, W. J.: Upper tropospheric equatorial waves in ECMWF analyses, Q. J. Roy. Meteor. Soc., 118, 365–394, 1992.
Raymond, D. J., López-Carrillo, C., and López Cavazos, L.: Case-studies of developing east Pacific easterly waves, Q. J. Roy. Meteor. Soc., 124, 2005–2034, 1998.
Raymond, D. J., Bretherton, C. S., and Molinari, J.: Dynamics of the Intertropical Convergence Zone of the East Pacific, J. Atmos. Sci., 63, 582–597, 2006.
Raymond, D. J. and Sessions, S. L.: Evolution of convection during tropical cyclogenesis, Geophys. Res. Lett., 34, L06811, doi:10.1029/2006GL028607, 2007.
Reasor, P. D. and Montgomery, M. T.: Three dimensional alignment and corotation of weak, TC-like vortices via linear vortex Rossby waves, J. Atmos. Sci., 58, 2306–2330, 2001.
Reasor, P. D., Montgomery, M. T., and Grasso, L. D.: A new look at the problem of tropical cyclones in vertical shear flow: vortex resiliency, J. Atmos. Sci., 61, 3–22, 2004.
Reed, R. J., Norquist, D. C., and Recker, E. E.: The structure and properties of African wave disturbances as observed during phase III of GATE, Mon. Weather Rev., 105, 317–333, 1977.
Ritchie, E. A. and Holland, G. J.: Scale interactions during the formation of Typhoon Irving, Mon. Weather Rev., 125, 1377–1396, 1997.
Ritchie, E. A. and Holland, G. J.: Large-scale patterns associated with tropical cyclogenesis in the western Pacific, Mon. Weather Rev., 127, 2027–2043, 1999.
Ritchie, E. A., Simpson, J., Liu, W. T., Halverson, J., Velden, C., Brueske, K. F., and Pierce, H.: Present day satellite technology for hurricane research: a closer look at formation and intensification, Hurricane! Coping with disaster: progress and challenges since Galveston, 1900, AGU monograph, 359 pp., 2003.
Rotunno, R. and Emanuel, K. A.: An air-sea interaction theory for tropical cyclones. Part II: Evolutionary study using a nonhydrostatic axisymmetric numerical model, J. Atmos. Sci., 44, 542–561, 1987.
Rozoff, C. M., Schubert, W. H., McNoldy, B. D., and Kossin, J. P.: Rapid filamentation zones in intense tropical cyclones, J. Atmos. Sci., 63, 325–340, 2006.
Schecter, D. A., Montgomery, M. T., and Reasor, P. D.: A theory for the vertical alignment of a quasi-geostrophic vortex, J. Atmos. Sci., 59, 150–168, 2002.
Schecter, D. A. and Dunkerton, T. J.: Hurricane formation in diabatic Ekman turbulence, pre-

sentation at AGU Fall Meeting, San Francisco, 2007.
Schubert, W. H. and Hack, J. J.: Transformed Eliassen balanced vortex model, J. Atmos. Sci., 40, 1571–1583, 1983.
Schubert, W. H., Ciesielski, P. E., Stevens, D. E., and Kuo, H.-C.: Potential vorticity modeling of the ITCZ and the Hadley circulation, J. Atmos. Sci., 48, 1493–1509, 1991.
Shapiro, L. J.: The asymmetric boundary layer flow under a translating hurricane, J. Atmos. Sci., 40, 1984–1998, 1983.
Shapiro, L. J. and Willoughby, H. E.: The response of balanced hurricanes to local sources of heat and momentum, J. Atmos. Sci., 39, 378–394, 1982.
Sharp, R. J., Bourassa, M. A., and O'Brien, J. J.: Early detection of tropical cyclones using Seawinds-derived vorticity, Bull. Amer. Meteor. Soc., 83, 879–889, 2002.
Simpson, R. H., Frank, N., Shideler, D., and Johnson, H. M.: Atlantic tropical disturbances, 1967, Mon. Weather Rev., 96, 251–259, 1968.
Simpson, J., Ritchie, E., Holland, G. J., Halverson, J., and Stewart, S.: Mesoscale interactions in tropical cyclone genesis, Mon. Weather Rev., 125, 2643–2661, 1997.
Smith, R. K.: The surface boundary layer of a hurricane, Tellus, 20, 473–484, 1968.
Smith, R. K., Montgomery, M. T., and Vogl, S.: A critique of Emanuel's hurricane model and potential intensity theory, Q. J. Roy. Meteor. Soc., 134, 551–561, 2008.
Sobel, A. H. and Bretherton, C. S.: Development of synoptic-scale disturbances over the summertime tropical northwest Pacific, J. Atmos. Sci., 56, 3106–3127, 1999.
Sobel, A. H., Nilsson, J., and Polvani, L. M.: The weak temperature gradient approximation and balanced tropical moisture waves, J. Atmos. Sci., 58, 3650–3665, 2001.
Takayabu, Y. N. and Nitta, T.: 3–5 day-period disturbances coupled with convection over the tropical Pacific Ocean, J. Meteorol. Soc. Japan, 71(2), 221–246, 1993.
Thorncroft, C. D. and Hoskins, B. J.: An idealized study of African easterly waves. I: a linear view, Q. J. Roy. Meteor. Soc., 120, 953–982, 1994a.
Thorncroft, C. D. and Hodges, K.: African easterly wave variability and its relationship to Atlantic tropical cyclone activity, J. Climate, 14, 1166–1179, 2001.
Thorncroft, C. D., Parker, D. J., Burton, R. R., et al.: The JET2000 project: aircraft observations of the African easterly jet and African easterly waves, Bull. Amer. Meteor. Soc., 84, 337–351, 2003.
Tory, K. J. and Montgomery, M. T.: Internal influences on tropical cyclone formation, Topic 2.2 in "Sixth International Workshop on Tropical Cyclones", San Jose, Costa Rica, World

Meteorological Organization, 22 pp., 2006.
Tory, K. J., Montgomery, M. T., and Davidson, N. E.: Prediction and diagnosis of tropical cyclone formation in an NWP system. Part I: the critical role of vortex enhancement in deep convection, J. Atmos. Sci., 63, 3077–3090, 2006a.
Tory, K. J., Montgomery, M. T., Davidson, N. E., and Kepert, J. E.: Prediction and diagnosis of tropical cyclone formation in a NWP system. Part II: a diagnosis of tropical cyclone Chris formation, J. Atmos. Sci., 63, 3091–3113, 2006b.
Tory, K. J., Davidson, N. E., and Montgomery, M. T.: Prediction and diagnosis of tropical cyclone formation in an NWP system. Part III: diagnosis of developing and non-developing storms, J. Atmos. Sci., 64, 3195–3213, 2007.
Tuleya, R. E. and Kurihara, Y.: A numerical study on the effects of environmental flow on tropical storm genesis, Mon. Weather Rev., 109, 2487–2506, 1981.
Van Sang, N., Smith, R., and Montgomery, M. T.: Tropical cyclone intensification and predictability in three dimensions, Quart. J. Roy. Meteorol. Soc., 134, 563–582, 2008.
Vecchi, G. A. and Soden, B. J.: Increased tropical Atlantic wind shear in model projections of global warming, Geophys. Res. Lett., 34, L08702, doi:10.1029/2006GL028905, 2007.
Velden, C. S., Hayden, C. M., Nieman, S. J., Menzel, W. P., Wanzong, S., and Goerss, J. S.: Upper-tropospheric winds derived from geostationary satellite water vapor observations, Bull. Amer. Meteor. Soc., 78, 173–195, 1997.
Velden, C., Daniels, J., Stettner, D., et al.: Recent innovations in deriving tropospheric winds from meteorological satellites, Bull. Amer. Meteor. Soc., 86, 205–223, 2005.
Ventham, J. D. and Wang, B.: Large-scale flow patterns and their influence on the intensification rates of Western North Pacific tropical storms, Mon. Weather Rev., 135, 1110–1127, 2007.
Vimont, D. J. and Kossin, J. P.: The Atlantic Meridional Mode and hurricane activity, Geophys. Res. Lett., 34, L07709, doi:10.1029/2007GL029683, 2007.
Wang, C.-C. and Magnusdottir, G.: ITCZ breakdown in three-dimensional flows, J. Atmos. Sci., 62, 1497–1512, 2005.
Wang, C.-C. and Magnusdottir, G.: The ITCZ in the central and eastern Pacific on synoptic time scales, Mon. Weather Rev., 134, 1405–1421, 2006.
Webster, P. J. and Holton, J. R.: Cross-equatorial response to middle-latitude forcing in a zonally varying basic state, J. Atmos. Sci., 39, 722–733, 1982.
Weisman, M. L. and Rotunno, R.: The use of vertical wind shear versus helicity in interpreting supercell dynamics, J. Atmos. Sci., 57, 1452–1472, 2000.

Wernli, H. and Kenzelmann, P.: Diabatic Rossby waves: Aspects of their dynamics, climatology and predictability, 13th Cyclone Workshop, Pacific Grove CA, 2006.
Wheeler, M. and Kiladis, G. N.: Convectively coupled equatorial waves: analysis of clouds and temperature in the wavenumber-frequency domain, J. Atmos. Sci., 56, 374–399, 1999.
Wheeler, M., Kiladis, G. N., and Webster, P. J.: Large-scale dynamical fields associated with convectively coupled equatorial waves, J. Atmos. Sci., 57, 613–640, 2000.
Wilson, J. D. and Mak, M.: Tropical response to lateral forcing with a latitudinally and zonally nonuniform basic state, J. Atmos. Sci., 41, 1187–1201, 1984.
Wing, A. A., Sobel, A. H., and Camargo, S. J.: Relationship between the potential and actual intensities of tropical cyclones on interannual time scales, Geophys. Res. Lett., 34, L08810, doi:10.1029/2006GL028581, 2007.
Wirth, V. and Dunkerton, T. J.: A unified perspective on the dynamics of axisymmetric hurricanes and monsoons, J. Atmos. Sci., 63, 2529–2547, 2006.
Wong, S. and Dessler, A. E.: Suppression of deep convection over the tropical North Atlantic by the Saharan Air Layer, Geophys. Res. Lett., 32, L09808, doi:10.1029/2004GL022295, 2005.
Zehnder, J. A., Powell, D. M., and Ropp, D. L.: The interaction of easterly waves, orography, and the Intertropical Convergence Zone in the genesis of eastern Pacific tropical cyclones, Mon. Weather Rev., 127, 1566–1585, 1999.
Zhang, C. and Webster, P. J.: Laterally forced equatorial perturbations in a linear model. Part I: stationary transient forcing, J. Atmos. Sci., 49, 585–607, 1992.
Zhu, Y. and Newell, R. E.: A proposed algorithm for moisture fluxes from atmospheric rivers, Mon. Weather Rev., 126, 725–735, 1998.

Table 1. Statistics of the 55 storms during August–September 1998–2001. The left four columns show the storm names (highlighted cases in red), genesis time (UTC-day-month-year), genesis latitude (Lat) and longitude (Lon). Other columns list the phase speed (C_p) of the easterly waves, its standard deviation (δC_p) based on 2–4 estimates, the gyre size (in terms of grid points in T106 ECMWF data), the angle of the separatrix, and recirculation time τ_1 and τ_2 (units: days) at 850 hPa and 600 hPa. (–) indicates an undefined value. The phase speed and its standard deviation are derived from the Hovmöller diagrams (see Sect. 4.2 for details). The angle of the separatrix is defined as the angle between the line from the gyre center to the separatrix and the east direction (90 indicates that the separatrix is due north of the gyre center, 180 indicates the separatrix is due west of the gyre center, and so on). The recirculation time τ_ζ is defined as

$$\tau_\zeta = \frac{4\pi}{\zeta_{\max}}$$

where $\zeta_{\max}$ is the maximum vorticity within the gyre. The recirculation time τ_{ow} is defined as

$$\tau_{ow} = \frac{4\pi}{\sqrt{\overline{\mathrm{OW}}}}$$

where $\overline{\mathrm{OW}}$ is the average of positive Okubo-Weiss in the regions with cyclonic vorticity within the gyre. If a gyre does not exist, $\zeta_{\max}$ and $\overline{\mathrm{OW}}$ are defined as vorticity and Okubo-Weiss at the genesis location, respectively. For negative $\zeta_{\max}$ or $\overline{\mathrm{OW}}$, the recirculation is undefined. The gyre is based on the 36-h pre-genesis average of stream function in the translating frame of reference (see Sect. 5.1 for details). Values at genesis time are substituted where the 36-h gyre does not exist (magenta). The median and one-half inter-quartile range of phase speed, gyre size and recirculation time are shown in the bottom two rows.

Table 1. Continued.

name	genesis time	Lat	Lon	850 hPa						600 hPa					
				Cp (m/s)	dCp (m/s)	gyre size	s'trix angle	t_z (day)	t_{ow} (day)	Cp (m/s)	dCp (m/s)	gyre size	s'trix angle	t_z (day)	t_{ow} (day)
Jeanne	06 Z 21 Sep 1998	9.6	−17.4	−4.1	1.7	33	8	1.4	2.3	−3.5	–	63	−2	2.1	4.0
Alberto	18 Z 03 Aug 2000	10.8	−18.0	−8.4	1.1	23	6	6.4	9.4	−11.1	1.0	23	18	4.7	8.5
Cindy	00 Z 19 Aug 1999	13.5	−18.9	−7.8	1.4	14	−70	5.4	8.9	−6.5	0.6	185	165	2.0	7.3
Isaac	12 Z 21 Sep 2000	11.5	−23.0	−8.7	0.9	9	54	2.4	4.4	−6.3	0.4	109	7	2.9	5.3
Gert	12 Z 11 Sep 1999	12.6	−24.2	−8.5	0.6	87	56	2.4	4.4	−8.6	0.5	78	170	3.0	5.4
Georges	12 Z 15 Sep 1998	9.7	−25.1	−6.2	0.2	25	55	4.3	6.8	−6.3	1.4	39	−55	5.2	8.9
Ivan	00 Z 19 Sep 1998	13.4	−26.6	−4.4	2.1	21	57	2.1	3.4	−4.6	0.7	38	−3	3.0	6.3
Felix	18 Z 07 Sep 2001	13.9	−28.4	−5.5	0.8	22	170	1.5	3.0	−6.6	1.3	75	158	2.9	5.4
Joyce	12 Z 25 Sep 2000	11.2	−29.6	−6.6	0.9	–	–	10.1	–	−6.6	0.7	–	–	13.1	13.7
Danielle	06 Z 24 Aug 1998	13.4	−34.3	−8.3	1.0	9	56	5.2	7.6	−8.5	0.4	115	98	3.8	8.2
Erin	18 Z 01 Sep 2001	12.5	−34.3	−10.7	0.9	–	–	5.4	6.4	−11.1	0.5	15	134	4.4	6.9
Chantal	18 Z 14 Aug 2001	12.8	−37.0	−7.5	4.1	1	−5	2.6	3.0	−10.2	0.6	5	−7	4.5	8.2
Debby	18 Z 19 Aug 2000	12.0	−44.5	−10.0	0.6	33	36	3.8	6.6	−9.1	0.3	120	56	4.0	7.4
Ernesto	12 Z 01 Sep 2000	14.8	−45.2	−8.3	0.1	4	29	5.4	8.0	−6.1	–	35	14	7.2	11.9
Floyd	18 Z 07 Sep 1999	14.6	−45.6	−7.3	0.4	65	70	3.3	5.3	−6.9	0.1	60	−4	3.1	5.7
Bonnie	12 Z 19 Aug 1998	14.7	−48.1	−8.0	0.7	114	9	2.9	5.2	−8.3	0.2	79	124	3.6	6.3
Chris	12 Z 17 Aug 2000	14.2	−51.9	−9.1	1.1	–	–	5.9	7.8	−8.5	0.5	3	73	4.8	7.5
Helene	12 Z 15 Sep 2000	14.9	−52.2	−10.2	0.2	–	–	9.0	12.1	−8.7	0.1	1	−63	12.2	15.6
Emily	06 Z 24 Aug 1999	11.5	−53.6	−4.3	0.1	9	37	3.2	6.7	−4.1	0.5	9	33	3.4	6.8
Humberto	12 Z 21 Sep 2001	25.1	−64.2	−4.5	1.0	12	125	4.2	6.6	−3.3	0.2	3	81	5.3	7.2
Dean	12 Z 22 Aug 2001	17.9	−64.3	−5.0	0.2	–	–	25.6	–	−8.4	1.6	–	–	–	–
Dennis	00 Z 24 Aug 1999	21.5	−67.7	−3.7	0.9	9	−119	3.2	4.9	−4.5	1.4	15	−132	3.1	4.7
Florence	18 Z 10 Sep 2000	30.9	−70.9	−1.9	0.6	43	−134	2.7	4.8	−3.0	0.0	6	45	2.4	4.0
Barry	12 Z 02 Aug 2001	25.7	−84.8	−2.4	0.2	5	−96	3.1	3.1	−7.7	4.4	19	94	4.0	3.8
Gordon	12 Z 14 Sep 2000	19.8	−87.3	−2.5	1.2	7	−171	4.8	7.8	−3.8	0.0	16	−174	7.0	7.3
Hermine	12 Z 17 Sep 1998	26.9	−90.3	−2.8	0.6	14	180	3.0	4.2	−3.9	0.1	71	147	2.9	5.4
Juliette	06 Z 21 Sep 2001	12.6	−91.1	−7.0	1.0	76	98	4.5	10.6	−7.9	0.8	78	−173	3.3	6.7
Charley	06 Z 21 Aug 1998	25.3	−92.3	−4.1	0.5	66	−39	4.1	6.3	−6.5	1.0	103	68	4.5	7.7
Beryl	18 Z 13 Aug 2000	22.5	−93.5	−3.8	2.8	10	50	3.7	4.6	−3.1	0.8	25	62	4.2	5.1
Earl	12 Z 31 Aug 1998	21.6	−93.5	−2.5	0.9	68	−177	1.9	3.1	−5.6	1.0	42	155	2.7	4.3
Bret	18 Z 18 Aug 1999	19.5	−94.4	–	–	1	58	14.0	–	−3.3	1.0	17	−137	4.3	7.4
Frances	18 Z 08 Sep 1998	25.5	−94.5	−5.5	–	47	151	2.9	4.6	−3.2	1.0	211	119	2.2	5.3
Ivo	12 Z 10 Sep 2001	14.8	−98.9	−6.6	0.5	–	–	8.6	–	−6.9	2.2	7	162	3.5	7.8
Dora	00 Z 06 Aug 1999	12.1	−100.9	−2.9	0.3	22	5	1.9	3.0	−4.5	1.0	63	160	3.7	8.1

Table 1. Continued.

name	genesis time	Lat	Lon	850 hPa						600 hPa					
				Cp (m/s)	dCp (m/s)	gyre size	s'trix angle	t_z (day)	t_{ow} (day)	Cp (m/s)	dCp (m/s)	gyre size	s'trix angle	t_z (day)	t_{ow} (day)
Lane	00 Z 05 Sep 2000	15.4	−102.2	−4.0	1.1	24	138	1.2	1.8	−3.3	0.5	24	155	1.6	2.6
Ileana	18 Z 13 Aug 2000	17.1	−104.0	−4.9	0.5	11	105	3.2	4.7	−4.7	0.1	25	−174	1.9	3.6
Greg	12 Z 05 Sep 1999	18.6	−105.1	−2.8	0.2	35	90	1.5	2.7	−3.3	0.6	142	153	1.9	4.4
Gilma	00 Z 05 Aug 2000	15.0	−105.2	−3.7	0.8	18	157	1.9	3.1	−4.1	0.7	38	153	1.9	3.3
Hector	18 Z 10 Aug 2000	17.8	−106.6	−5.1	0.3	15	105	6.5	6.8	−6.1	0.9	216	156	3.4	7.7
Javier	12 Z 06 Sep 1998	17.8	−106.8	−3.0	0.3	47	102	2.5	4.5	−5.0	0.4	37	172	2.2	4.6
Hilary	06 Z 17 Sep 1999	15.2	−107.1	−2.6	0.4	23	171	1.0	1.8	−2.8	0.3	54	−11	1.8	3.3
Miriam	18 Z 15 Sep 2000	19.2	−107.4	−3.2	0.0	36	85	5.0	8.0	−3.9	0.7	99	31	3.8	6.7
Flossie	06 Z 26 Aug 2001	19.1	−108.5	–	–	1	157	–	14.8	−5.3	0.6	223	66	3.0	5.4
Henriette	12 Z 04 Sep 2001	16.9	−108.8	−2.8	0.5	88	136	1.1	2.1	−4.3	1.3	20	−176	1.9	3.0
Georgette	00 Z 11 Aug 1998	11.0	−108.9	−5.8	1.4	36	125	1.9	3.6	−7.1	0.2	6	23	3.9	6.2
Isis	00 Z 01 Sep 1998	18.3	−109.2	−3.2	1.1	79	91	1.6	2.5	−3.9	1.6	88	−172	1.8	3.4
Frank	12 Z 06 Aug 1998	16.7	−111.5	−4.2	0.3	89	82	3.3	7.3	−5.8	1.6	120	164	3.1	5.8
Fernanda	06 Z 17 Aug 1999	12.4	−113.1	−5.1	0.7	47	154	3.1	4.5	−5.3	0.2	76	−103	2.9	5.1
Fabio	12 Z 03 Aug 2000	16.4	−113.6	−3.7	0.5	78	65	1.5	2.8	−3.8	0.6	64	−8	1.4	2.9
Kiko	18 Z 21 Sep 2001	15.6	−116.1	−5.8	0.7	80	139	1.5	3.1	−5.3	0.6	85	−20	2.1	4.0
Eugene	06 Z 06 Aug 1999	12.2	−119.9	−3.5	0.4	18	97	3.0	5.4	−5.8	1.2	63	92	3.3	6.6
Gil	06 Z 04 Sep 2001	15.4	−122.6	−3.1	0.9	41	176	2.6	5.6	−2.4	0.8	5	4	3.2	3.7
Kristy	00 Z 31 Aug 2000	13.0	−131.4	−3.2	1.0	25	−9	2.1	3.8	−2.1	0.9	11	6	2.6	4.4
John	06 Z 28 Aug 2000	14.9	−137.4	−3.1	0.3	27	−167	1.7	3.8	−2.7	0.3	26	178	2.4	4.3
Shanshan	18 Z 15 Sep 2000	15.1	−182.0	−2.8	0.3	70	−171	2.6	4.9	−5.7	2.8	16	152	3.0	4.9
median				−4.4		25		3.1	4.7	−5.3		39		3.1	5.6
IQR/2				1.9		18		1.4	1.8	1.5		32		0.8	1.5

Table 2. Peak-to-peak wave amplitude (band-pass meridional velocity anomaly, ms^{-1}) from genesis time to the end of the Hovmöller sequence (+3 days) and variation of vortex phase relative to wave trough (degrees) over this time interval. Negative relative phase is located to the east of the trough. The normalized distance from trough to ridge is 180° by definition. For wave amplitude (vortex phase) the average (median) and standard deviation (one-half interquartile range) of initial and final values are displayed in the first and second rows of each pair, respectively.

	850 hPa wave amplitude			600 hPa wave amplitude			850 hPa vortex phase			600 hPa vortex phase		
	initial	final	change	initial	final	change	initial	final	change	initial	final	change
all events [55]	4.3	3.8	**−0.5**	3.9	3.5	**−0.4**	8	−8	**−16**	21	−21	**−42**
	2.0	2.0	–	1.7	1.5	–	25	37	–	26	39	–
all events, Atlantic [31]	4.3	3.8	**−0.5**	3.8	3.4	**−0.5**	3	−30	**−33**	8	−26	**−35**
	1.8	1.8	–	1.5	1.5	–	20	27	–	21	27	–
all events, E Pacific [23]	4.5	3.8	**−0.7**	4.0	3.7	**−0.4**	35	21	**−14**	30	−15	**−45**
	2.2	2.3	–	1.9	1.6	–	29	38	–	29	62	–
wwd only [40]	4.7	4.1	**−0.7**	4.1	3.8	**−0.3**	0	0	**0**	0	−15	**−15**
	2.1	1.9	–	1.8	1.5	–	26	33	–	23	39	–
wwd only, Atlantic [22]	4.8	4.0	**−0.7**	4.0	3.6	**−0.4**	0	−10	**−10**	−4	−18	**−14**
	1.8	2.0	–	1.6	1.5	–	21	26	–	19	28	–
wwd only, E Pacific [17]	4.8	3.9	**−0.9**	4.2	3.9	**−0.3**	23	21	**−2**	23	−7	**−29**
	2.4	1.9	–	2.0	1.7	–	27	25	–	31	53	–
ewd also [15]	3.3	3.3	**−0.1**	3.4	2.7	**−0.7**	25	−45	**−70**	36	−50	**−86**
	1.2	2.2	–	1.4	1.3	–	29	26	–	20	41	–
ewd also, Atlantic [9]	3.2	3.1	**−0.1**	3.3	2.7	**−0.7**	18	−51	**−69**	36	−50	**−86**
	1.4	1.2	–	1.3	1.4	–	20	16	–	17	41	–
ewd also, E Pacific [6]	3.5	3.5	**0.0**	3.5	2.8	**−0.7**	45	15	**−30**	47	−65	**−112**
	0.8	3.3	–	1.5	1.2	–	35	43	–	34	59	–

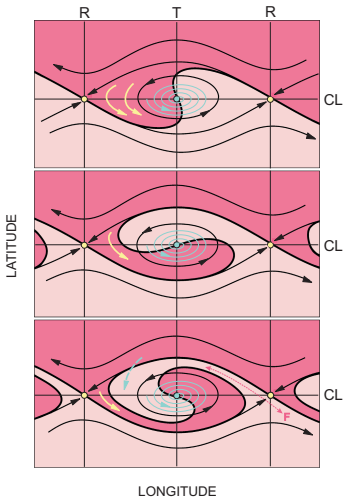

Fig. 1. Critical layer for waves in latitudinal shear, showing streamlines (solid), material contour initially east-west on center (thick solid) **C**ritical **L**atitude and **T**rough/**R**idge axes (thin solid). The sense of cyclonic vorticity transport within recirculation regions ("cat's eyes"), if deep pink indicates *higher* vorticity, corresponds to that of a wave acting on a *stable* meridional gradient of zonal mean PV with initial vorticity maximum poleward of the critical latitude. In an unstable configuration the first overturning of vorticity isopleths within the cat's eye may be imagined to originate from below, rather than from above, the CL axis, in which case higher vorticity is represented by *faded pink*. The latitudinal shear is negative in either case. When flow within the cat's eye is horizontally convergent, air parcels spiral inward to an attracting node (turquoise). Transient entrainment into the gyre, by rotational flow, is shown adjacent to the separatrix (light yellow). Divergent flow crossing isopleths of stream function may also contribute to entrainment (dashed arrow). In the neighborhood of the separatrix the flow is primarily deformational, producing a thin filamentary tail behind the entraining air mass (F). Adapted from the paperback cover of Andrews et al. (1987).

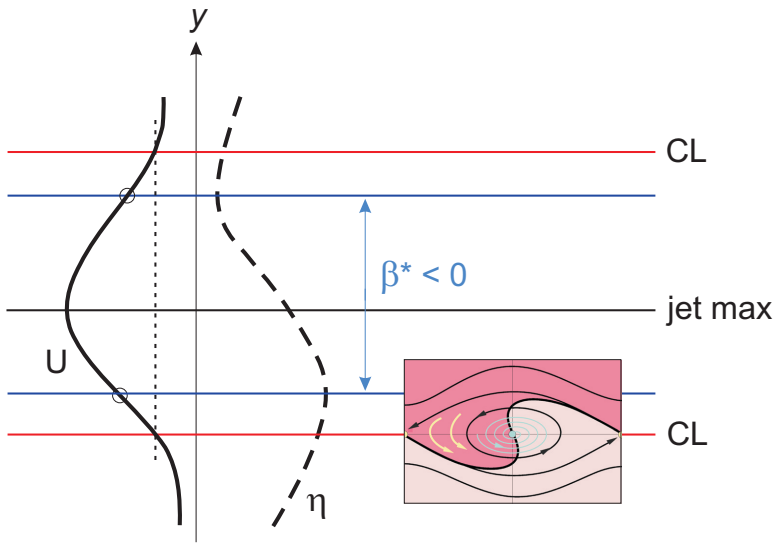

Fig. 2. Idealized profile of an easterly jet U north of the equator, on which stable easterly waves propagate westward having their critical latitudes (red lines) just outside the jet's inflection points (blue lines) where the gradient of absolute vorticity η or "effective β" is zero. Unstable waves may be imagined to have their critical latitudes just inside the latitude of inflection points. Cyclonic roll-up along the critical latitude south of the jet axis is indicated as in Fig. 1 (insert).

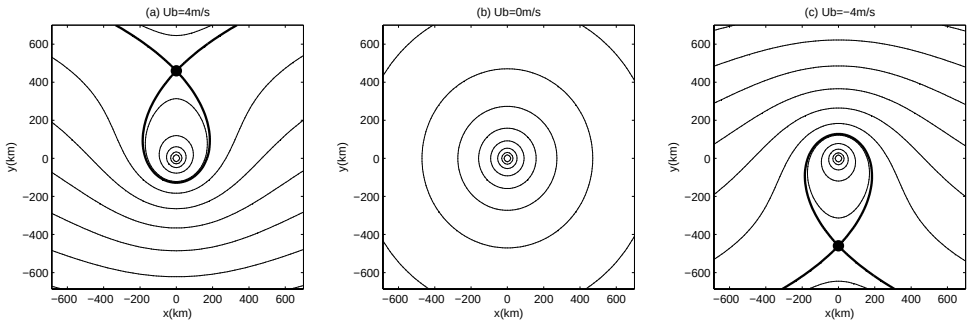

Fig. 3. Total streamline structure of a point vortex with cyclonic circulation Γ immersed in a constant mean zonal flow U_b. In the frame of reference displayed here (with zonal translation speed equal to zero) the vortex is spatially and temporally fixed at the origin. The total flow is given by the superposition of a constant background zonal wind and a circularly symmetric flow induced by the point vortex. This flow is an exact steady solution of the 2-D Euler equations. As noted in the text, identical streamline patterns are obtained in a *resting* basic state when the vortex translates zonally at speed $C_p = -U_b$. The numerical value of Γ is based on the gyre circulation analyzed for pre-Debby in August 2000. Three cases are sketched: **(a)** $U_b = 4\ \mathrm{ms}^{-1}$ (moderate westerly flow over the vortex), **(b)** $U_b = 0$ (zero background flow) and **(c)** $U_b = -4\ \mathrm{ms}^{-1}$ (moderate easterly flow). Light solid curves denote streamlines. The black dot denotes the stagnation point located at $(X_c, Y_c) = (0, \Gamma/2\pi U_b)$; the fluid velocity vanishes there. The thick solid curve denotes the dividing streamline that divides the flow into three distinct regions: a core region near the vortex, upper outside region and lower outside region. As the magnitude of the imposed flow increases, the distance from the vortex center to the separatrix decreases and the amount of fluid isolated within the core region decreases.

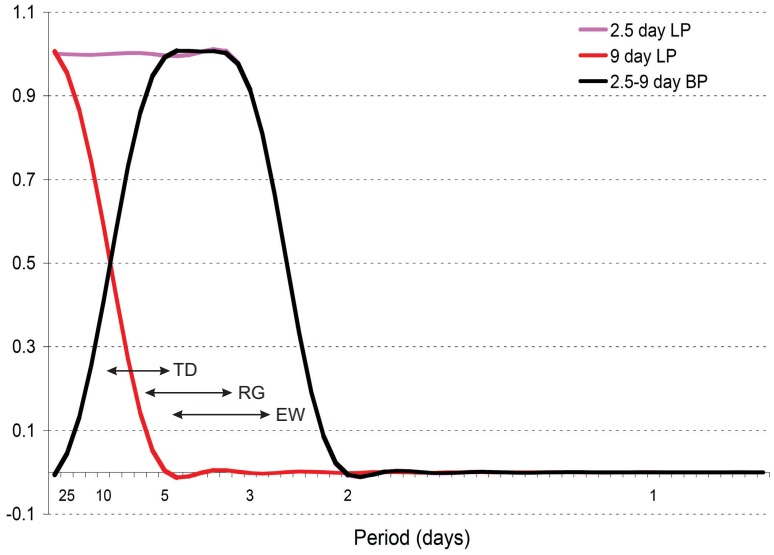

Fig. 4. Frequency response of temporal filters used in this study. A low-pass filter (purple curve; periods longer than ~2.5 days) describes the total flow evolution sans high-frequency component. A band-pass filter (black curve; periods between ~2.5 and 9 days) captures tropical waves in this frequency range for the purpose of estimating their propagation speed in Hovmöller diagrams: easterly waves (EW), Rossby-gravity waves (RG) and tropical depression disturbances (TD). A low-frequency filter (red curve; periods longer than 9 days) provides an informal estimate of critical latitudes as seen by the waves.

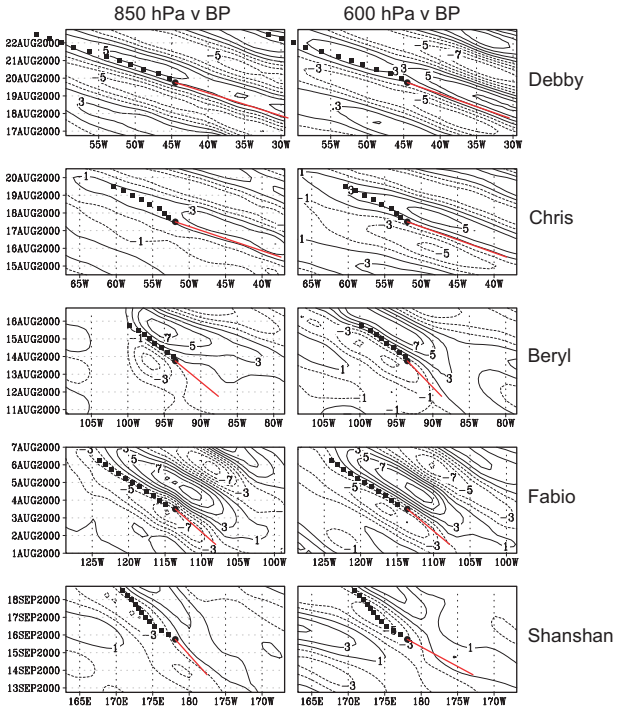

Fig. 5. Hovmöller plots of band-pass meridional velocity component at 850 hPa (left column) and 600 hPa (right column) in a longitude-time plane for the five cases of summer 2000 highlighted in the text: **(a)** Hurricane Debby; **(b)** Tropical Storm Chris; **(c)** Tropical Storm Beryl; **(d)** Tropical Storm Fabio; **(e)** Super Typhoon Shanshan. Black circles indicate the best-track longitude and time of genesis, while black squares indicate subsequent best track locations at 6-h intervals. Red line denotes the Hovmöller estimate of zonal translation speed C_p.

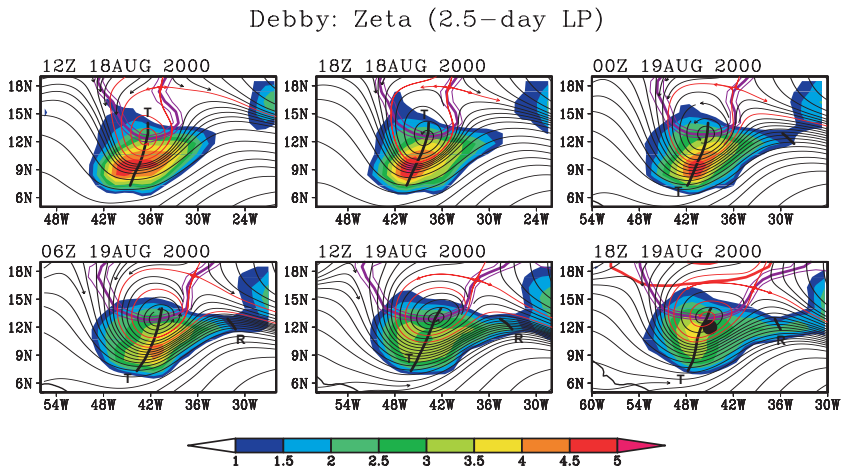

Fig. 6. Streamlines of horizontal (rotational + divergent) flow at 850 hPa, as seen in ERA-40 data, for six consecutive analyses leading up to the best-track genesis time of Hurricane Debby (2000). Streamlines passing near a separatrix are shown in red. Shading indicates relative vorticity (units: $10^{-5}\,s^{-1}$). The sequence of frames translates westward at the zonal propagation speed of the parent wave at 850 hPa as estimated from the Hovmöller method ($-10.0\pm0.6\,ms^{-1}$) and streamlines are displayed in this gauge; note that relative vorticity itself is invariant with respect to the translation. Isopleths of zero relative zonal flow are shown (purple) together with their uncertainty. In the final panel of the sequence the critical latitude of the parent wave is also indicated (red) corresponding to isopleths of zero relative zonal flow in low-frequency data with periods longer than 9 days. The wave's trough axis is shown for reference (black, "T"). The genesis location is indicated by the black dot in the final panel.

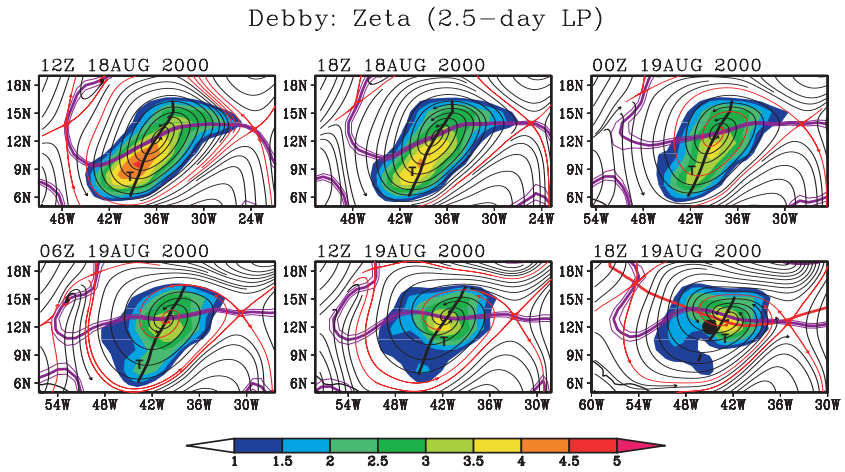

Fig. 7. Streamlines of horizontal flow for the genesis sequence of Hurricane Debby as in Fig. 6, but at 600 hPa. Shading indicates relative vorticity (units: $10^{-5}\,s^{-1}$). The sequence of frames translates westward at the zonal propagation speed of the parent wave at 600 hPa ($-9.1\pm0.3\,ms^{-1}$) and streamlines are displayed in this gauge.

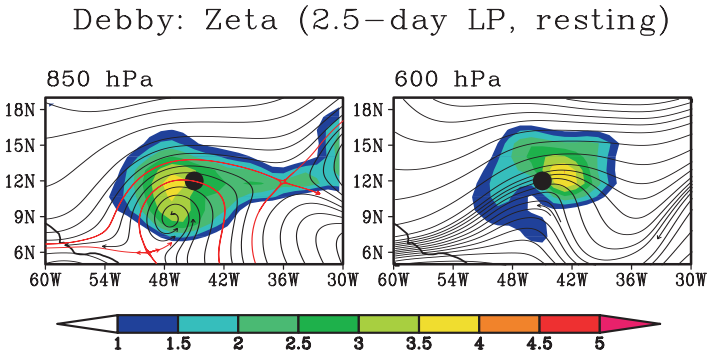

Fig. 8. Streamlines of horizontal flow at **(a)** 850 hPa and **(b)** 600 hPa at the genesis time of Hurricane Debby, in the *resting* frame. Shading indicates relative vorticity (units: $10^{-5}\,s^{-1}$) which is invariant with respect to translation, therefore identical in translating and resting frames (cp. final panels of Figs. 6 and 7).

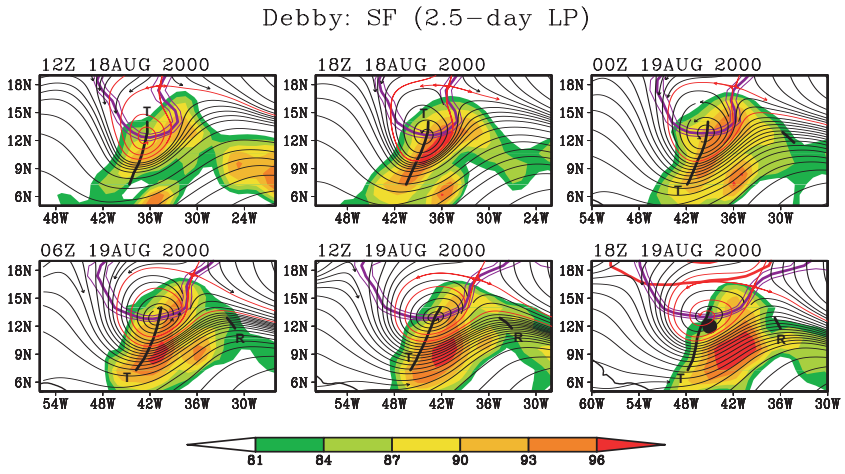

Fig. 9. Streamlines of horizontal flow at 850 hPa for the genesis sequence of Hurricane Debby as in Fig. 6, with high values of ERA-40 saturation fraction indicated by shading (units: percent). The sequence of frames translates westward at the zonal propagation speed of the parent wave at 850 hPa ($-10.0\pm0.6\,ms^{-1}$) and streamlines are displayed in this gauge.

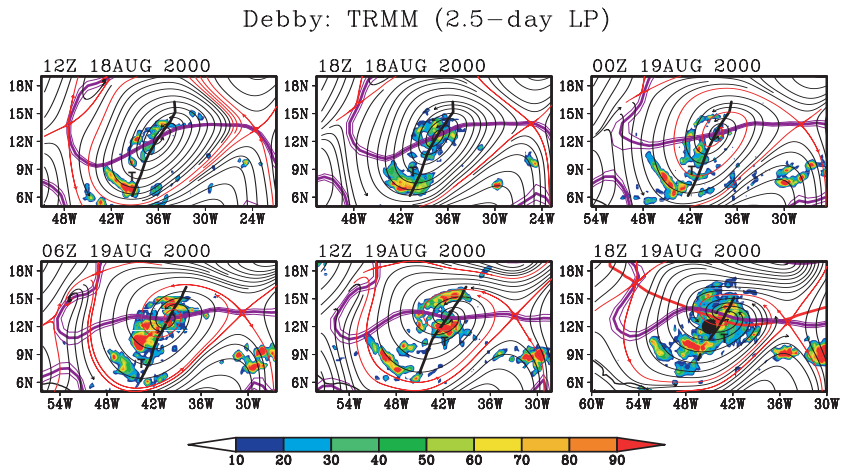

Fig. 10. Streamlines of horizontal flow at 600 hPa for the genesis sequence of Hurricane Debby as in Fig. 7, with high values of TRMM 3-h accumulated precipitation indicated by shading (units: mm/day). The sequence of frames translates westward at the zonal propagation speed of the parent wave at 600 hPa ($-9.1\pm0.3\,\mathrm{ms}^{-1}$) and streamlines are displayed in this gauge.

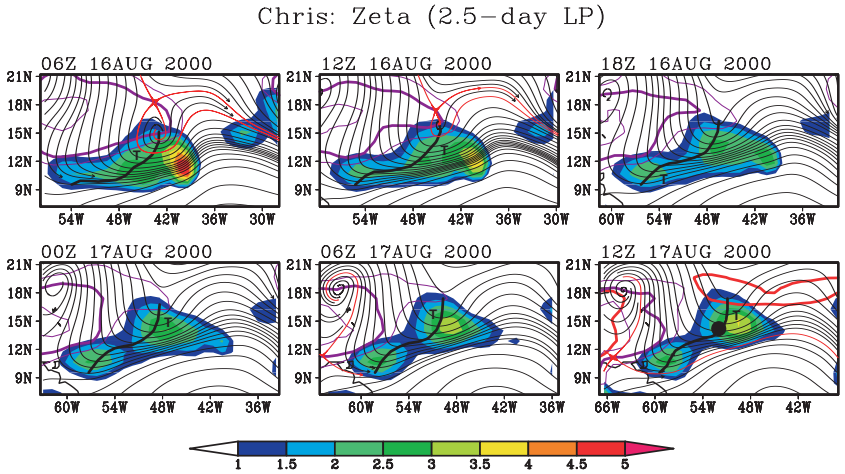

Fig. 11. Streamlines of horizontal (rotational + divergent) flow at 850 hPa, as seen in ERA-40 data, for six consecutive analyses leading up to the best-track genesis time of Tropical Storm Chris (2000). Streamlines passing near a separatrix are shown in red. Shading indicates relative vorticity (units: $10^{-5}\,\mathrm{s}^{-1}$). The sequence of frames translates westward at the zonal propagation speed of the parent wave at 850 hPa as estimated from the Hovmöller method ($-9.1\pm1.1\,\mathrm{ms}^{-1}$) and streamlines are displayed in this gauge; note that relative vorticity itself is invariant with respect to the translation. Isopleths of zero relative zonal flow are shown (purple) together with their uncertainty. In the final panel of the sequence the critical latitude of the parent wave is also indicated (red) corresponding to isopleths of zero relative zonal flow in low-frequency data with periods longer than 9 days. The wave's trough axis is shown for reference (black). The genesis location is indicated by the black dot in the final panel.

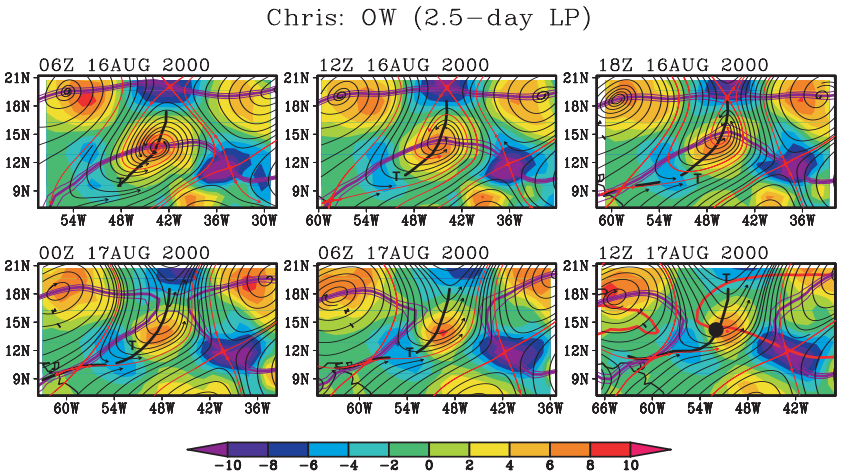

Fig. 12. Streamlines of horizontal flow for the genesis sequence of Tropical Storm Chris as in Fig. 11, but at 600 hPa. Shading indicates the Okubo-Weiss parameter (units: $10^{-10}s^{-2}$) as defined in Eq. (1). This quantity, like vorticity, is invariant with respect to translation, therefore identical in translating and resting frames. The sequence of frames translates westward at the zonal propagation speed of the parent wave at 600 hPa ($-8.5\pm0.5\,ms^{-1}$) and streamlines are displayed in this gauge.

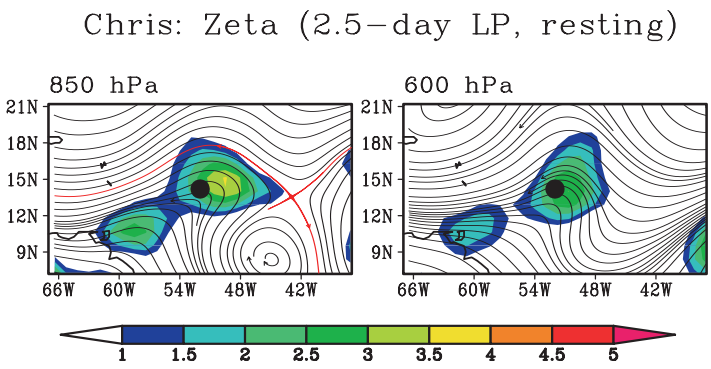

Fig. 13. Streamlines of horizontal flow at **(a)** 850 hPa and **(b)** 600 hPa at the genesis time of Tropical Storm Chris, in the *resting* frame. Shading indicates relative vorticity (units: $10^{-5}\,s^{-1}$) which is invariant with respect to translation, therefore identical in translating and resting frames (cp. final panel of Fig. 11).

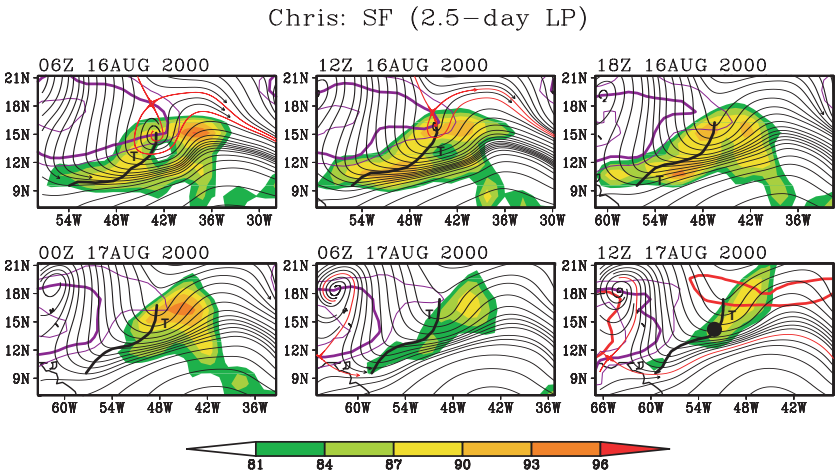

Fig. 14. Streamlines of horizontal flow at 850 hPa for the genesis sequence of Tropical Storm Chris as in Fig. 11, with high values of ERA-40 saturation fraction indicated by shading (units: percent).The sequence of frames translates westward at the zonal propagation speed of the parent wave at 850 hPa (-9.1 ± 1.1 ms^{-1}) and streamlines are displayed in this gauge.

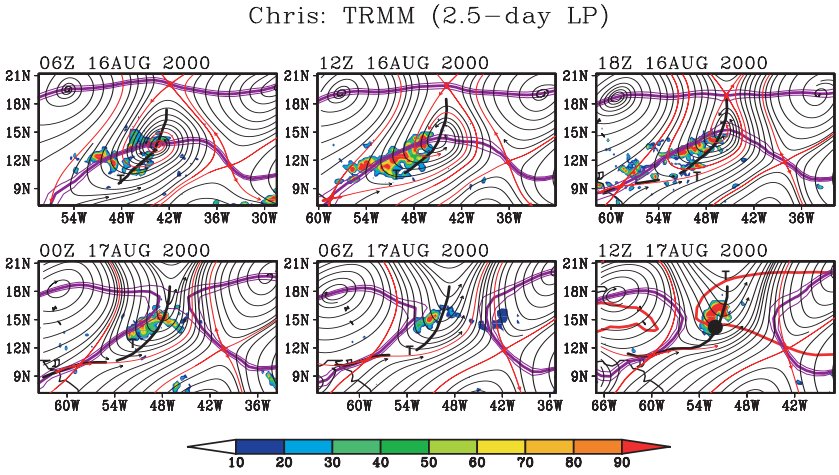

Fig. 15. Streamlines of horizontal flow at 600 hPa for the genesis sequence of Tropical Storm Chris as in Fig. 12, with high values of TRMM 3-h accumulated precipitation indicated by shading (units: mm/day). The sequence of frames translates westward at the zonal propagation speed of the parent wave at 600 hPa (-8.5 ± 0.5 ms^{-1}) and streamlines are displayed in this gauge.

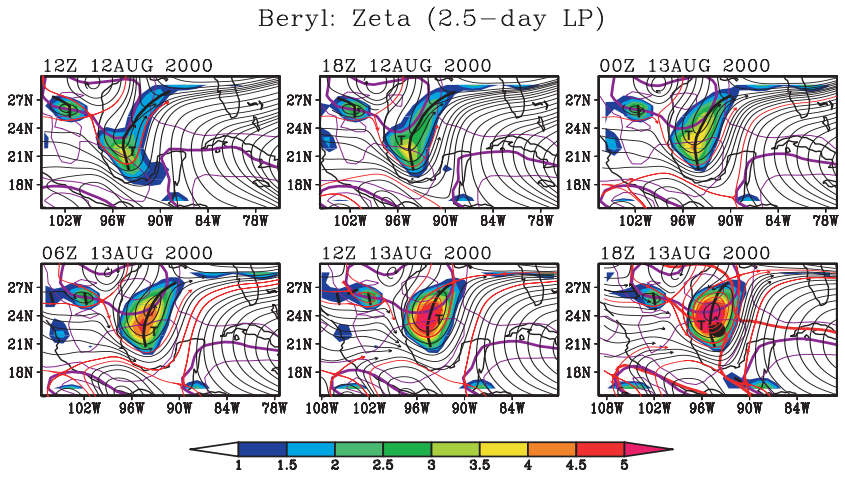

Fig. 16. Streamlines of horizontal (rotational + divergent) flow at 850 hPa, as seen in ERA-40 data, for six consecutive analyses leading up to the best-track genesis time of Tropical Storm Beryl (2000). Streamlines passing near a separatrix are shown in red. Shading indicates relative vorticity (units: $10^{-5}\,s^{-1}$). The sequence of frames translates westward at the zonal propagation speed of the parent wave at 850 hPa as estimated from the Hovmöller method ($-3.8\pm2.8\,ms^{-1}$) and streamlines are displayed in this gauge; note that relative vorticity itself is invariant with respect to the translation. Isopleths of zero relative zonal flow are shown (purple) together with their uncertainty. In the final panel of the sequence the critical latitude of the parent wave is also indicated (red) corresponding to isopleths of zero relative zonal flow in low-frequency data with periods longer than 9 days. The wave's trough axis is shown for reference (black). The genesis location is indicated by the black dot in the final panel.

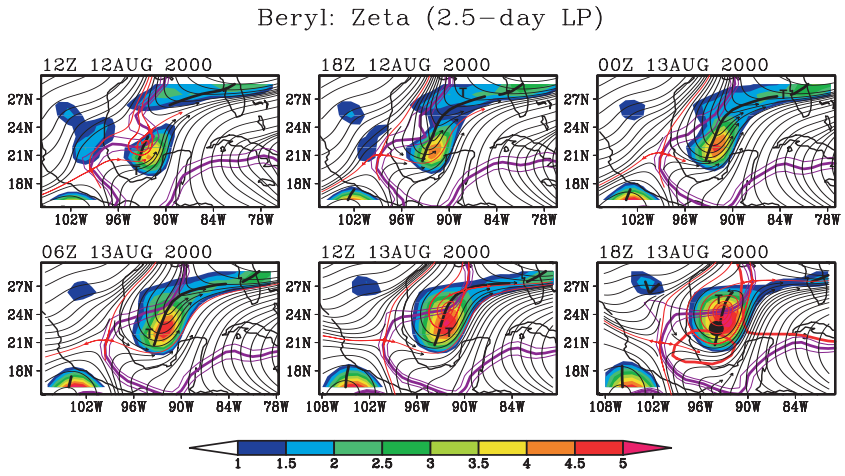

Fig. 17. Streamlines of horizontal flow for the genesis sequence of Tropical Storm Beryl as in Fig. 16, but at 600 hPa. Shading indicates relative vorticity (units: $10^{-5}\,s^{-1}$). The sequence of frames translates westward at the zonal propagation speed of the parent wave at 600 hPa ($-3.1\pm0.8\,ms^{-1}$) and streamlines are displayed in this gauge.

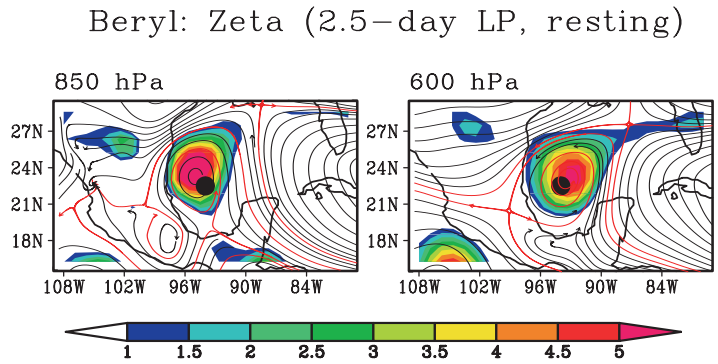

Fig. 18. Streamlines of horizontal flow at **(a)** 850 hPa and **(b)** 600 hPa at the genesis time of Tropical Storm Beryl, in the *resting* frame. Shading indicates relative vorticity (units: $10^{-5}\,s^{-1}$) which is invariant with respect to translation, therefore identical in translating and resting frames (cp. final panels of Figs. 16 and 17).

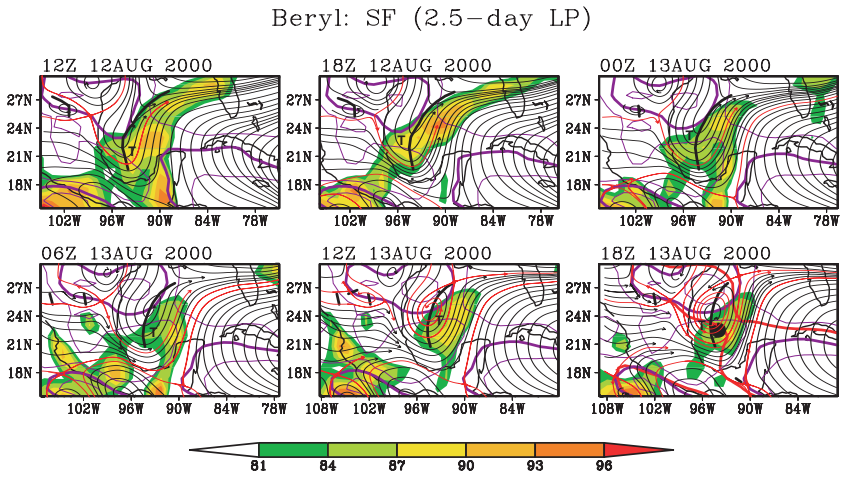

Fig. 19. Streamlines of horizontal flow at 850 hPa for the genesis sequence of Tropical Storm Beryl as in Fig. 16, with high values of ERA-40 saturation fraction indicated by shading (units: percent).The sequence of frames translates westward at the zonal propagation speed of the parent wave at 850 hPa ($-3.8\pm2.8\,ms^{-1}$) and streamlines are displayed in this gauge.

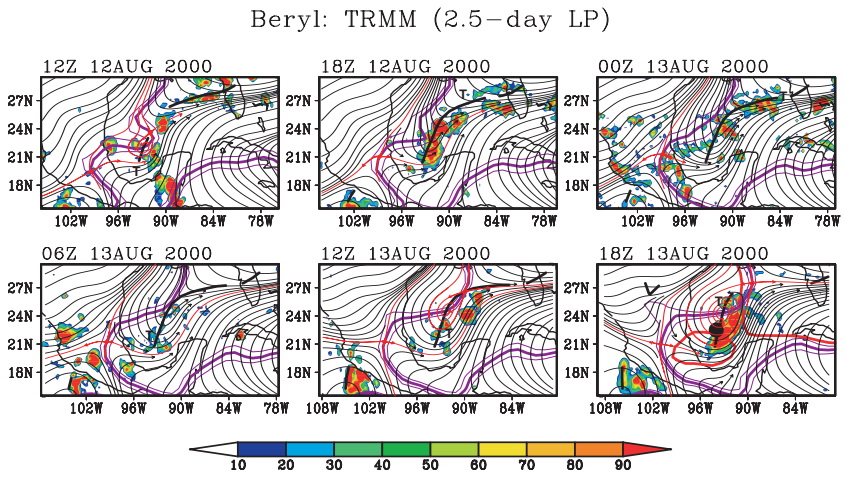

Fig. 20. Streamlines of horizontal flow at 600 hPa for the genesis sequence of Tropical Storm Beryl as in Fig. 17, with high values of TRMM 3-h accumulated precipitation indicated by shading (units: mm/day). The sequence of frames translates westward at the zonal propagation speed of the parent wave at 600 hPa ($-3.1\pm0.8\,\mathrm{ms}^{-1}$) and streamlines are displayed in this gauge.

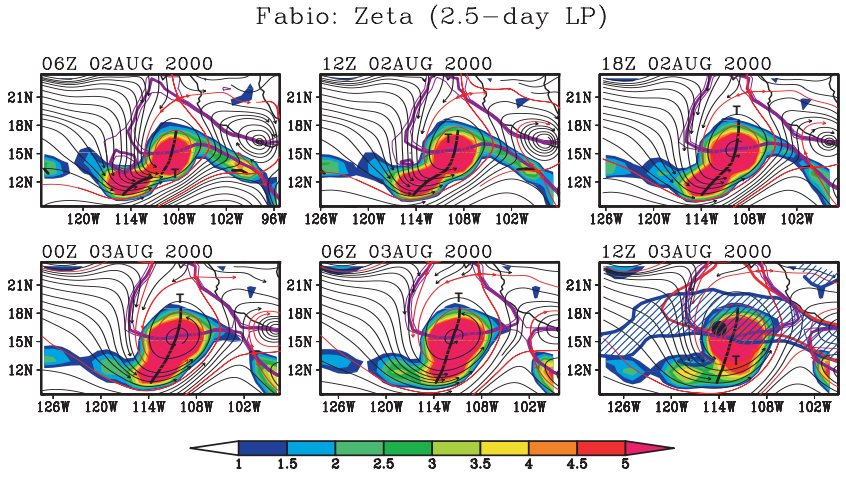

Fig. 21. Streamlines of horizontal (rotational + divergent) flow at 850 hPa, as seen in ERA-40 data, for six consecutive analyses leading up to the best-track genesis time of Tropical Storm Fabio (2000). Streamlines passing near a separatrix are shown in red. Shading indicates relative vorticity (units: $10^{-5}\,\mathrm{s}^{-1}$). The sequence of frames translates westward at the zonal propagation speed of the parent wave at 850 hPa as estimated from the Hovmöller method ($-3.7\pm0.5\,\mathrm{ms}^{-1}$) and streamlines are displayed in this gauge; note that relative vorticity itself is invariant with respect to the translation. Isopleths of zero relative zonal flow are shown (purple) together with their uncertainty. In the final panel of the sequence the critical latitude of the parent wave is also indicated (red) corresponding to isopleths of zero relative zonal flow in low-frequency data with periods longer than 9 days. These data were also used to estimate the zero contour of absolute vorticity gradient or "effective β" (blue). This quantity is negative in the zone just north of the genesis latitude, bracketed by the blue curves (diagonal hatching). The wave's trough axis is shown for reference (black). The genesis location is indicated by the black dot in the final panel.

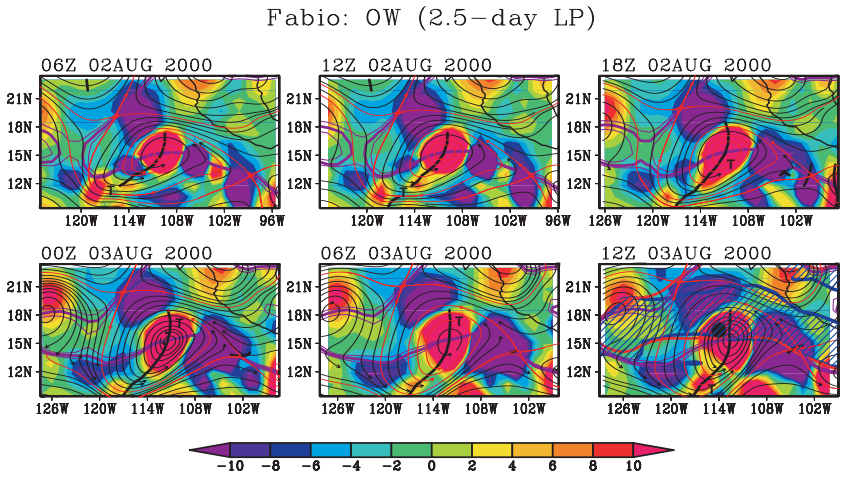

Fig. 22. Streamlines of horizontal flow for the genesis sequence of Tropical Storm Fabio as in Fig. 21, but at 600 hPa. Shading indicates the Okubo-Weiss parameter (units: $10^{-10}\,s^{-2}$) as defined in Eq. (1). This quantity, like vorticity, is invariant with respect to translation, therefore identical in translating and resting frames. The sequence of frames translates westward at the zonal propagation speed of the parent wave at 600 hPa ($-3.1\pm0.8\,ms^{-1}$) and streamlines are displayed in this gauge. Red and blue lines in the final panel show the wave's critical latitude and isopleth of zero effective β as estimated from low-frequency data with periods longer than 9 days.

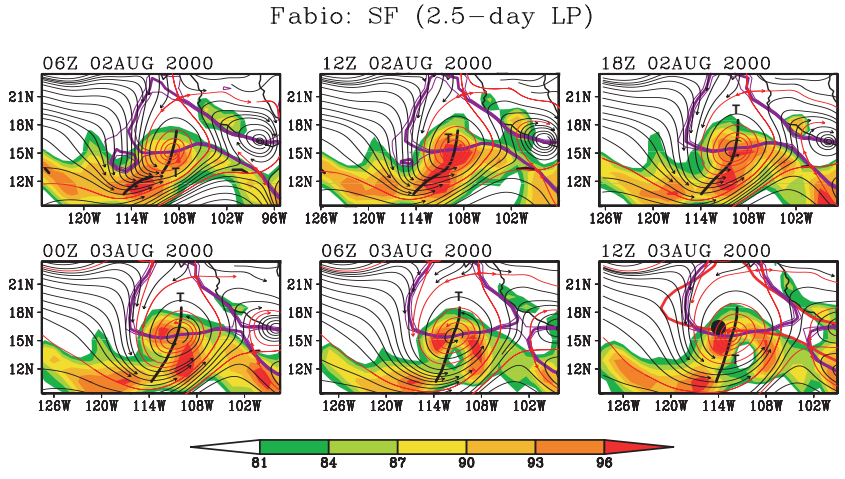

Fig. 23. Streamlines of horizontal flow at 850 hPa for the genesis sequence of Tropical Storm Fabio as in Fig. 21, with high values of ERA-40 saturation fraction indicated by shading (units: percent). The sequence of frames translates westward at the zonal propagation speed of the parent wave at 850 hPa ($-3.7\pm0.5\,ms^{-1}$) and streamlines are displayed in this gauge.

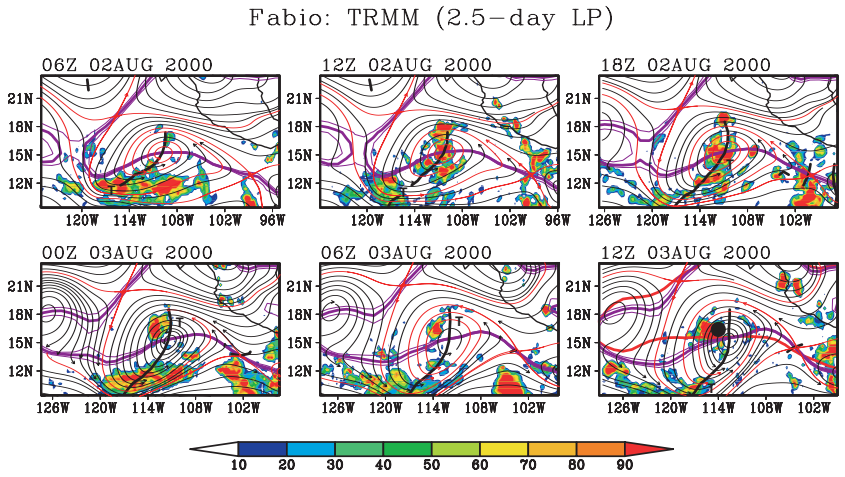

Fig. 24. Streamlines of horizontal flow at 600 hPa for the genesis sequence of Tropical Storm Fabio as in Fig. 22, with high values of TRMM 3-h accumulated precipitation indicated by shading (units: mm/day). The sequence of frames translates westward at the zonal propagation speed of the parent wave at 600 hPa ($-3.1\pm0.8\,\mathrm{ms}^{-1}$) and streamlines are displayed in this gauge.

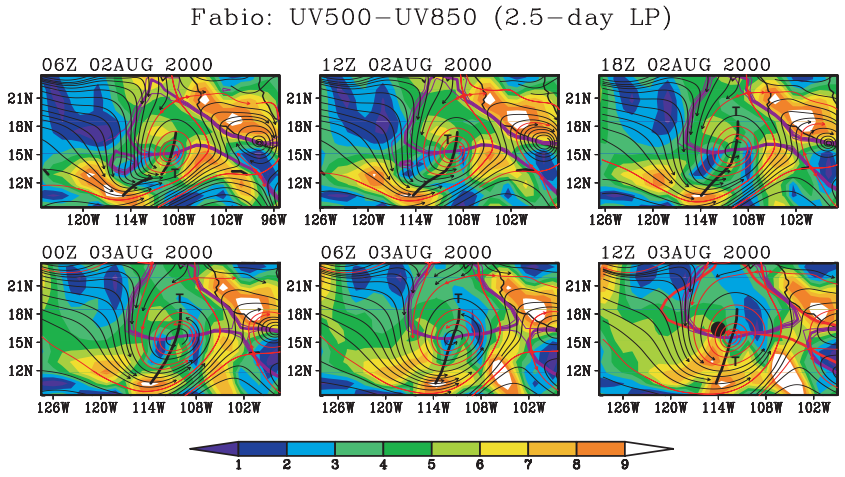

Fig. 25. Streamlines of horizontal flow at 850 hPa for the genesis sequence of Tropical Storm Fabio as in Fig. 21, with ERA-40 850–500 hPa vertical shear (magnitude of shear vector, units: ms^{-1}) indicated by shading. The sequence of frames translates westward at the zonal propagation speed of the parent wave at 850 hPa ($-3.7\pm0.5\,\mathrm{ms}^{-1}$) and streamlines are displayed in this gauge.

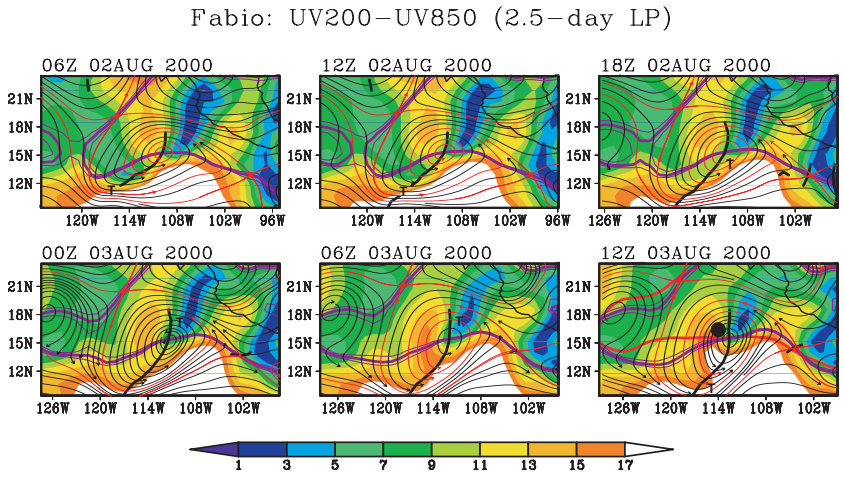

Fig. 26. Streamlines of horizontal flow at 600 hPa for the genesis sequence of Tropical Storm Fabio as in Fig. 22, with ERA-40 850–200 hPa vertical shear (magnitude of shear vector, units: ms^{-1}) indicated by shading. The sequence of frames translates westward at the zonal propagation speed of the parent wave at 600 hPa ($-3.1\pm0.8\,ms^{-1}$) and streamlines are displayed in this gauge.

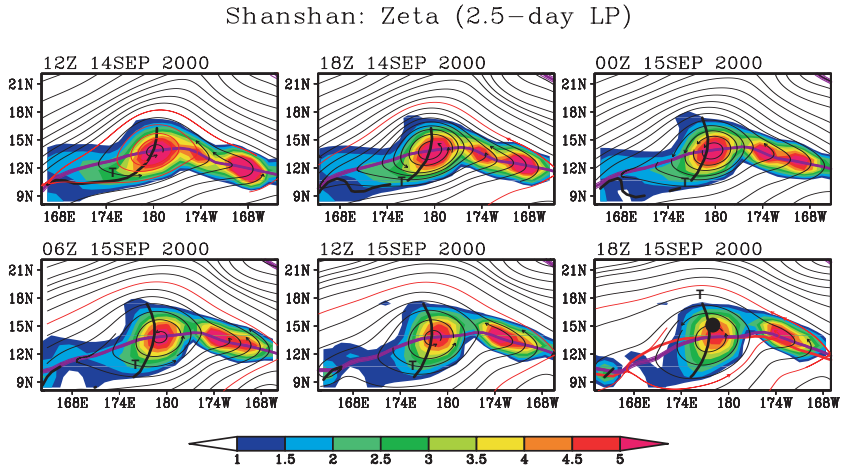

Fig. 27. Streamlines of horizontal (rotational + divergent) flow at 850 hPa, as seen in ERA-40 data, for six consecutive analyses leading up to the best-track genesis time of Super Typhoon Shanshan (2000). Streamlines passing near a separatrix are shown in red. Shading indicates relative vorticity (units: $10^{-5}\,s^{-1}$). The sequence of frames translates westward at the zonal propagation speed of the parent wave at 850 hPa as estimated from the Hovmöller method ($-2.8\pm0.3\,ms^{-1}$) and streamlines are displayed in this gauge; note that relative vorticity itself is invariant with respect to the translation. Isopleths of zero relative zonal flow are shown (purple) together with their uncertainty. In the final panel of the sequence the critical latitude of the parent wave is also indicated (red) corresponding to isopleths of zero relative zonal flow in low-frequency data with periods longer than 9 days. The wave's trough axis is shown for reference (black). The genesis location is indicated by the black dot in the final panel.

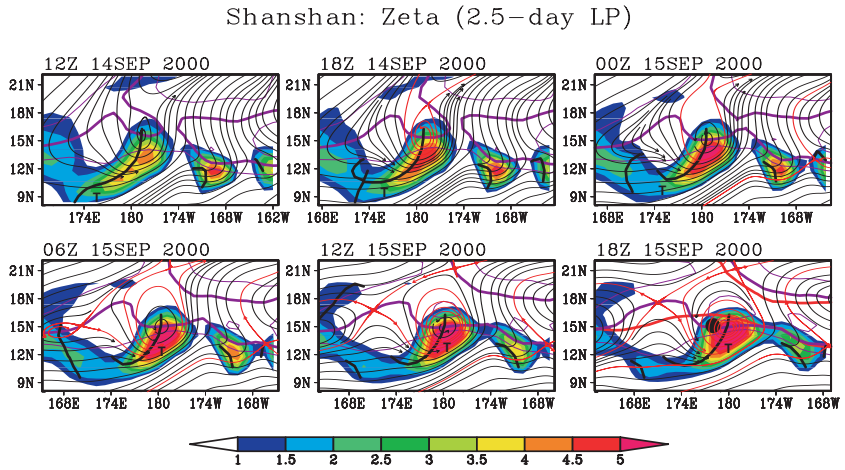

Fig. 28. Streamlines of horizontal flow for the genesis sequence of Super Typhoon Shanshan as in Fig. 27, but at 600 hPa. Shading indicates relative vorticity (units: $10^{-5}\,s^{-1}$). The sequence of frames translates westward at the zonal propagation speed of the parent wave at 600 hPa ($-5.7\pm2.8\,ms^{-1}$) and streamlines are displayed in this gauge.

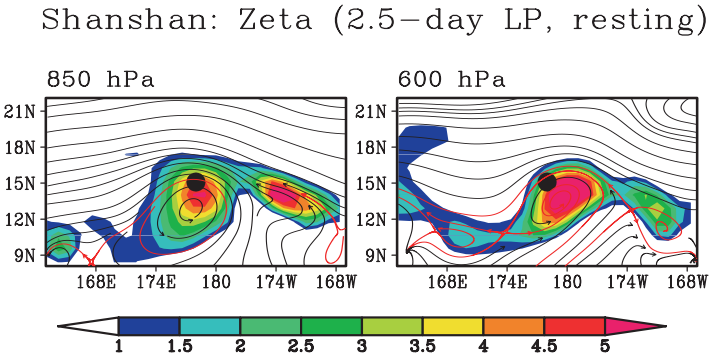

Fig. 29. Streamlines of horizontal flow at **(a)** 850 hPa and **(b)** 600 hPa at the genesis time of Super Typhoon Shanshan, in the *resting* frame. Shading indicates relative vorticity (units: $10^{-5}\,s^{-1}$) which is invariant with respect to translation, therefore identical in translating and resting frames (cp. final panels of Figs. 27 and 28).

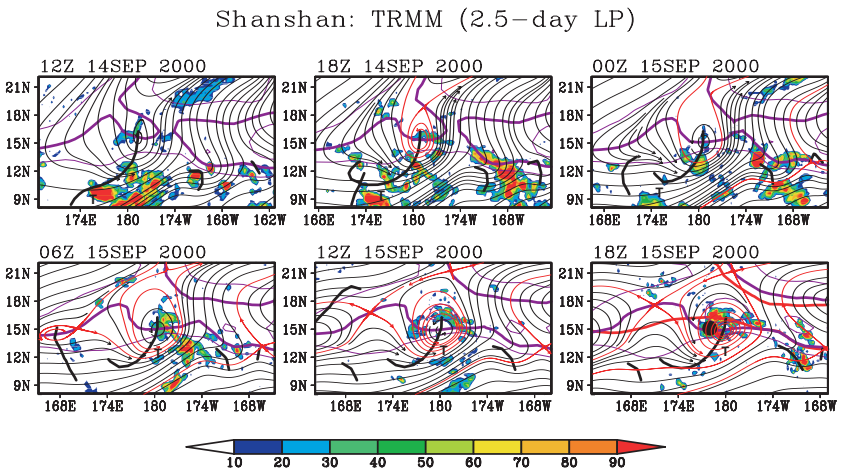

Fig. 30. Streamlines of horizontal flow at 600 hPa for the genesis sequence of Super Typhoon Shanshan as in Fig. 27, with high values of TRMM 3-h accumulated precipitation indicated by shading. Units: mm/day. The sequence of frames translates westward at the zonal propagation speed of the parent wave at 600 hPa ($-5.7\pm2.8\,\mathrm{ms}^{-1}$) and streamlines are displayed in this gauge.

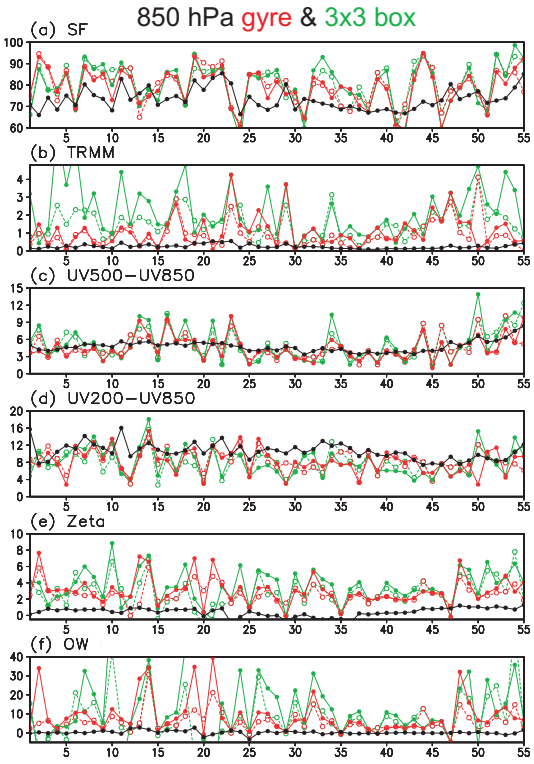

Fig. 31.

Fig. 31. Spatio-temporal average of dynamical and thermodynamical fields in the neighborhood of the best-track genesis location and time immediately preceding. The storms are arrayed west to east, from left to right, in the reverse of Table 1. The *spatial average* corresponds either to that of (i) the translating gyre (red) or (ii) a 3×3 matrix of ERA-40 grid points surrounding the point $x(t)=x_0-C_p\cdot(t-t_0)$ where x is longitude, t is time, C_p is the speed of translation and the subscript 0 refers to the location and time of genesis (green). The *temporal average* corresponds either to (i) the genesis time (single analysis, filled circles) or (ii) the 36-h interval preceding and slightly overlapping genesis time (average of six consecutive 6-hourly analyses ending at genesis time, open circles). Black circles denote "climatological" values for August-September 1998–2001 at the various gyre or grid box locations. The data shown in the figure were derived using gyre properties and translation speeds at 850 hPa: **(a)** saturation fraction averaged from 1000–500 hPa (units: percent), **(b)** TRMM deep convective precipitation (units: mm/day), **(c)** vertical shear from lower to mid-troposphere (850 to 500 hPa, units: ms^{-1}), **(d)** vertical shear from lower to upper troposphere (850 to 200 hPa, units: ms^{-1}), **(e)** relative vorticity at 850 hPa (units: $10^{-5}\,s^{-1}$), **(f)** Okubo-Weiss parameter at 850 hPa (units: $10^{-10}\,s^{-2}$). Please refer to footnote 31 for important information regarding the climatology of vertical shear and Okubo-Weiss.

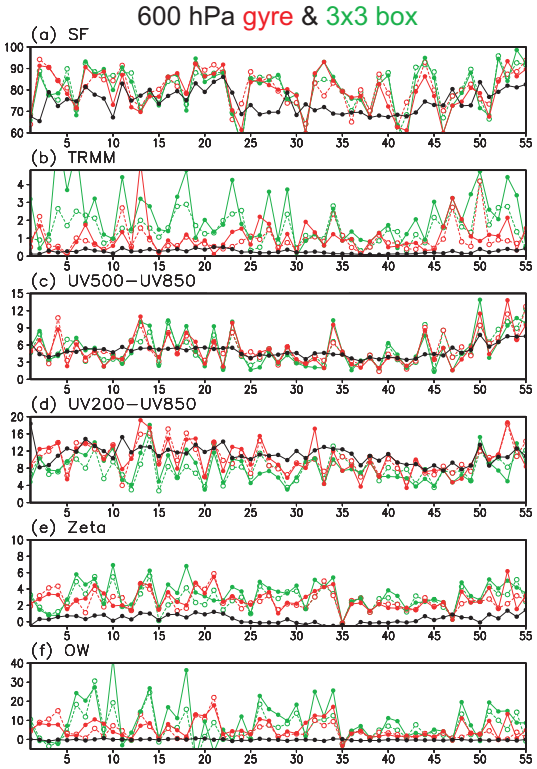

Fig. 32. Spatio-temporal average of dynamical and thermodynamical fields as in Fig. 31, but for 600 hPa gyres and translation speeds. Vorticity and Okubo-Weiss parameter from the 600, rather than 850 hPa level are shown in **(e, f)**.

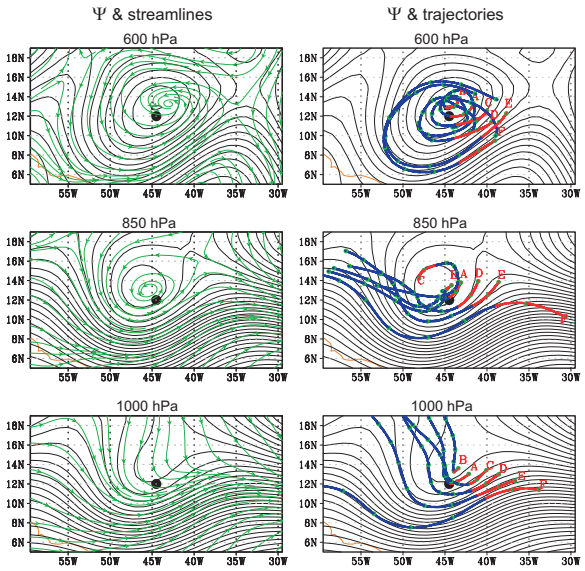

Fig. 33. Streamlines and trajectories of horizontal (rotational + divergent) flow at **(a, b)** 600 hPa, **(c, d)** 850 hPa, and **(e, f)** 1000 hPa as seen in ERA-40 data, for the average of six consecutive leading up to the best-track genesis time of Hurricane Debby (2000). As in Fig. 6, the streamlines (shown in panels a, c, and e) are calculated and displayed in a frame of reference moving westward with the parent wave. Translation speeds estimated from the Hovmöller method at the three levels are $-9.1\pm0.3\,\mathrm{ms}^{-1}$ (600 hPa), $-10.0\pm0.6\,\mathrm{ms}^{-1}$ (850 hPa) and $-10.1\pm0.6\,\mathrm{ms}^{-1}$ (1000 hPa). Likewise the stream function of non-divergent flow (thin solid) and trajectories (shown in panels b, d, and f) are calculated and is displayed in the translating frame. The contour interval for stream function is $0.5\times10^6\,\mathrm{m}^2\,\mathrm{s}^{-1}$. The genesis location is indicated by the black dot in each panel. Note that owing to the translation of sequential frames used to construct the time average when $C_p\neq0$, the longitude labels on the x-axis pertain to the final analysis time only.

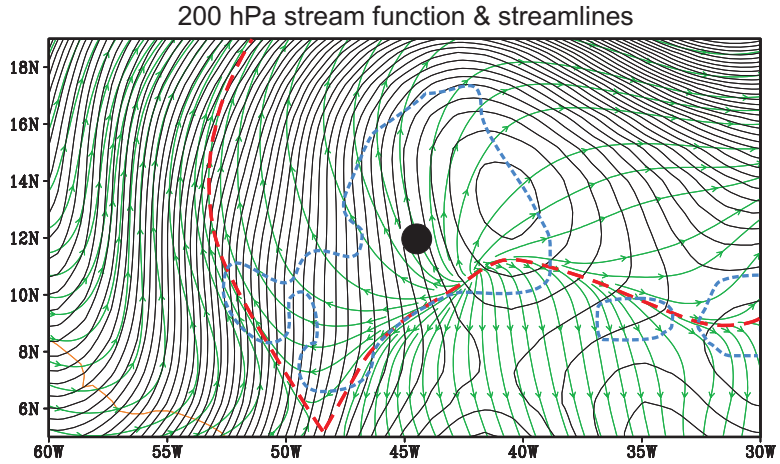

Fig. 34. Streamlines of horizontal flow and stream function of non-divergent flow at 200 hPa calculated and displayed in a frame of reference moving $5\,\mathrm{ms}^{-1}$ westward, at the genesis time of Hurricane Debby. Divergence contributing to anticyclonic outflow can be seen by comparing streamlines with stream function. Manifold boundaries are shown by red dashed lines; the peripheries of TRMM precipitation (Fig. 6f) are shown by blue dashed lines.The genesis location is indicated by the black dot. The contour interval for stream function is $0.2\times10^6\,\mathrm{m}^2\,\mathrm{s}^{-1}$.

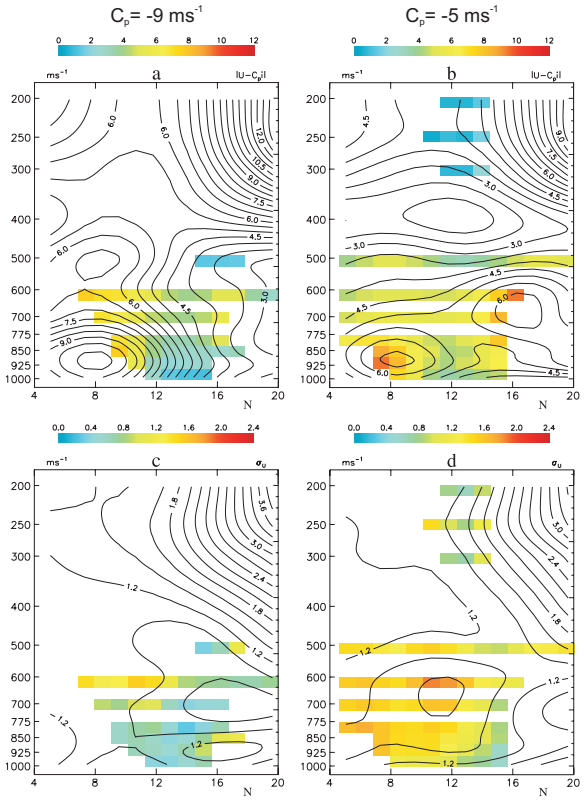

Fig. 35.

Fig. 35. Horizontal wind speed in the translating frame averaged over the six consecutive analyses leading up to the genesis time of Hurricane Debby. The range of longitudes x used to construct the average is given by the speed of translation beginning at the genesis longitude (x_0=44.5° W) and going eastward (backward) in longitude (time) from the genesis point according to the formula $x(t)=x_0-C_p\cdot(t-t_0)$ where t_0 is the best-track genesis time. The horizontal wind speed in the translating frame is given by $|\boldsymbol{U}-C_p\boldsymbol{i}|$ where $\boldsymbol{U}$ is the horizontal vector wind, C_p is translation speed and $\boldsymbol{i}$ is the unit vector in the x-direction. The quantity contoured represents a zonal average within ±15° longitude of the center longitude as given above, including regions inside *and* outside the gyre. **(a, c)** C_p=9 ms^{-1} westward; **(b, d)** C_p=5 ms^{-1} westward. These values correspond approximately to the zonal component of wave propagation in the lower and upper troposphere, respectively. The maximum extent of closed stream function gyre in each frame of reference is also shown by superposing (as shaded pixels) the gyre-average values of $|\boldsymbol{U}-C_p\boldsymbol{i}|$ where they exist. Here, "gyre average" refers to a zonal average over longitudes within a closed gyre as delimited by a bounding contour of stream function ψ intersecting the nearest (in ψ) separatrix. The lower panels show the temporal standard deviation of horizontal wind speed in the translating frame. The quantity contoured once again represents a zonal average over the entire domain, while shaded pixels indicate gyre-average values. For modulus and standard deviation, their zonal average was obtained by first summing the squares and then taking the square root of the sum.

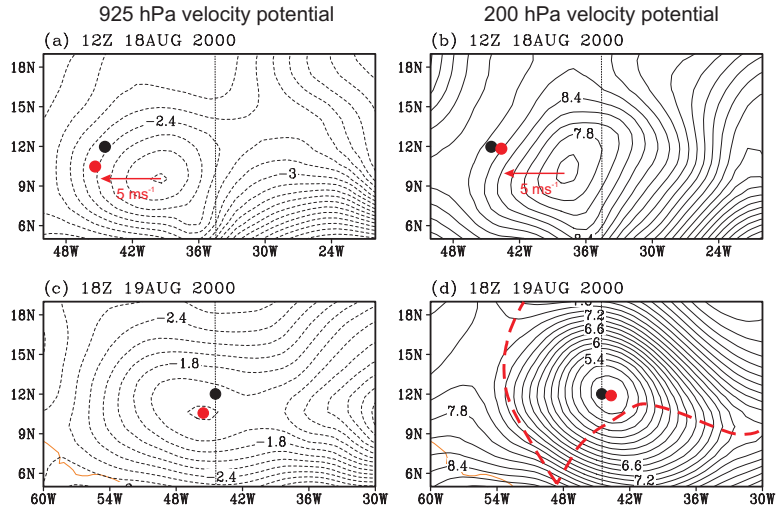

Fig. 36. Velocity potential of divergent flow, as seen in ERA-40 data, at **(a, c)** 925 hPa and **(b, d)** 200 hPa leading up to the genesis time of Hurricane Debby, at (a, b) 30 h before genesis and (c, d) genesis. The divergence center (red dot) propagates westward but at a slower pace ($-5\,\mathrm{ms}^{-1}$) than the primary wave ($-9\,\mathrm{ms}^{-1}$). The red dashed line in the final panel echoes the manifold boundaries of Fig. 34. The contour interval for velocity potential is $0.2\times10^{6}\,\mathrm{m}^{2}\,\mathrm{s}^{-1}$.

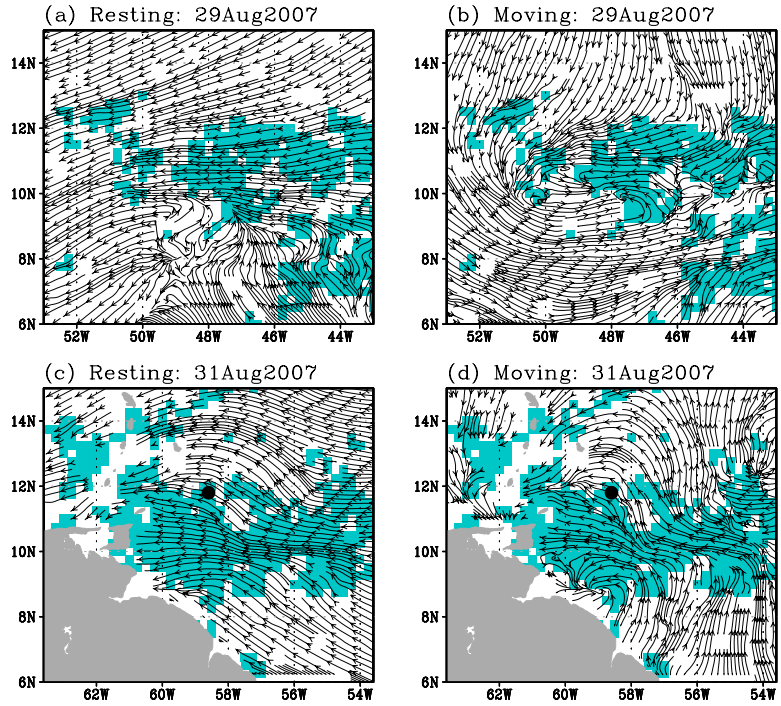

Fig. 37. Streamlines of surface flow obtained from QuikSCAT images of Hurricane Felix (2007) in late August 2007. **(a, c)** Resting frame; **(b, d)** translating frame (C_p=$-6.7\pm0.5\,\mathrm{ms}^{-1}$). Regions of possible rain contamination are indicated by cyan shading.